NASA MEMO 5-16-59A

NASA

MEMORANDUM

THE STATIC AND DYNAMIC ROTARY STABILITY DERIVATIVES AT SUBSONIC SPEEDS OF AN AIRPLANE MODEL HAVING WING AND TAIL SURFACES SWEPT BACK 45°

By Armando E. Lopez, Donald A. Buell,
and Bruce E. Tinling

Ames Research Center
Moffett Field, Calif.

NATIONAL AERONAUTICS AND SPACE ADMINISTRATION

WASHINGTON
May 1959
Declassified July 11, 1961

NATIONAL AERONAUTICS AND SPACE ADMINISTRATION

MEMORANDUM 5-16-59A

THE STATIC AND DYNAMIC ROTARY STABILITY DERIVATIVES AT SUBSONIC SPEEDS OF AN AIRPLANE MODEL HAVING WING AND TAIL SURFACES SWEPT BACK 45°

By Armando E. Lopez, Donald A. Buell,
and Bruce E. Tinling

SUMMARY

Wind-tunnel measurements were made of the static and dynamic rotary stability derivatives of an airplane model having sweptback wing and tail surfaces. The Mach number range of the tests was from 0.23 to 0.94.

The components of the model were tested in various combinations so that the separate contribution to the stability derivatives of the component parts and the interference effects could be determined.

Estimates of the dynamic rotary derivatives based on some of the simpler existing procedures which utilize static force data were found to be in reasonable agreement with the experimental results at low angles of attack.

The results of the static and dynamic measurements were used to compute the short-period oscillatory characteristics of an airplane geometrically similar to the test model. The results of these calculations are compared with military flying qualities requirements.

INTRODUCTION

A program of research on the dynamic rotary stability derivatives of various airplane models has been carried out in the Ames 12-foot pressure wind tunnel. The models were tested on an apparatus which forces a single-degree-of-freedom oscillation. (The apparatus is described in ref. 1.) One of the objectives of this research program was to determine the accuracy with which the dynamic rotary derivatives

can be estimated by methods which utilize the known static characteristics of the various model components. Accordingly, measurements of the static characteristics of various combinations of the model components were also made so that the forces on each surface could be isolated. The results of tests on a triangular-winged model and on a straight-winged model with a high horizontal tail have been reported in references 2 and 3.

This report presents the measured static and dynamic rotary stability derivatives of a model having 45° of sweepback of the wing and tail surfaces. Estimates of the rotary derivatives were made utilizing some of the simpler existing procedures to assess the accuracy with which these derivatives can be estimated from static force data. On the basis of the measured derivatives calculations were made of the period and time to damp of the longitudinal and lateral-directional short-period oscillations of an airplane geometrically similar to the model. Results of these calculations are presented.

SYMBOLS

A aspect ratio

B_b body base cross-sectional area

b wing span

C_D drag coefficient, $\frac{\text{drag}}{(1/2)\rho V^2 S}$

C_L lift coefficient, $\frac{\text{lift}}{(1/2)\rho V^2 S}$

C_l rolling-moment coefficient, $\frac{\text{rolling moment}}{(1/2)\rho V^2 S b}$

C_m pitching-moment coefficient, $\frac{\text{pitching moment}}{(1/2)\rho V^2 S \bar{c}}$

C_N normal-force coefficient, $\frac{\text{normal force}}{(1/2)\rho V^2 S}$

C_n yawing-moment coefficient, $\frac{\text{yawing moment}}{(1/2)\rho V^2 S b}$

C_Y side-force coefficient, $\frac{\text{side force}}{(1/2)\rho V^2 S}$

$C_{1/2}$ number of cycles to damp to half amplitude

c local chord, streamwise

$\bar{c}$ mean aerodynamic chord

I mass moment of inertia

i_t tail incidence, deg

l body length

l_t tail length

M Mach number

m mass

p rolling velocity

q pitching velocity

R Reynolds number

r yawing velocity

S wing area

$T_{1/2}$ time to damp to half amplitude

V velocity

v_e equivalent sideslipping velocity, $\frac{V\sqrt{\sigma}|\beta|}{57.3}$

x distance of the axis of rotation behind nose of body

α angle of attack, deg

β angle of sideslip, deg

$\Delta\delta_a$ difference between the deflection of the right and left ailerons, positive to induce a positive rolling moment, deg

δ_a aileron deflection angle, deg

δ_r rudder deflection, positive to induce positive yawing moment, deg

ϵ effective angle of downwash at the horizontal tail, deg

ζ ratio of actual damping to critical damping

θ angle of pitch

Λ angle of sweepback

λ taper ratio

ρ air density

σ ratio of density at assumed altitude to density at sea level

φ angle of bank, deg

$\frac{|\varphi|}{|v_e|}$ ratio of bank angle amplitude to equivalent side velocity amplitude during a Dutch roll oscillation, $\frac{\text{deg}}{\text{ft/sec}}$

ψ angle of yaw, deg

ω circular frequency of oscillation, radians/sec

$( )'$ derivatives referred to the body system of axes in which X axis is coincident with the fuselage reference line

The stability system of axes used for the presentation of the data, together with an indication of the positive direction of forces, moments, and angles, is defined in figure 1. The various stability derivatives are defined as follows:

$C_{L_\alpha}, C_{m_\alpha}, C_{N_\alpha}, C_{l_\beta}, C_{n_\beta}, C_{Y_\beta}$ derivatives with respect to subscript, per deg

$C_{m_{\dot{\alpha}}}, C_{m_q}$ derivatives with respect to $\frac{\bar{c}}{2V} \times$ subscript, per radian

$C_{l_{\dot{\beta}}}, C_{l_p}, C_{l_r}, C_{n_{\dot{\beta}}}, C_{n_p}, C_{n_r}, C_{Y_p}, C_{Y_r}$ derivatives with respect to $\frac{b}{2V} \times$ subscript, per radian

$\frac{C_l}{\beta}, \frac{C_m}{\beta}, \frac{C_Y}{\beta}$ forces and moments measured at approximately 6° of sideslip divided by true sideslip angle

Subscripts

H horizontal tail

v vertical tail

MODEL

The complete model consisted of a wing of aspect ratio 3.56, a horizontal tail mounted below the wing chord plane, two interchangeable vertical tails, and a fuselage. The wing and tail surfaces were swept back 45°. Figure 2 is a drawing of the model showing pertinent dimensions. Some additional geometric and dimensional data are given in table I. A photograph of the model mounted on the oscillation apparatus in the wind tunnel is shown in figure 3. The two interchangeable vertical tails were used to evaluate the effects of tail size on the static and dynamic directional characteristics.

Low moments of inertia are desirable for dynamic stability tests to minimize certain design problems of the model support and oscillation apparatus. The wing and tail surfaces were machined from magnesium forgings and the body shell was formed from soft magnesium sheets in a drop-hammer die. These parts were attached to a magnesium case which enclosed the oscillation mechanism. The complete model weighed about 36 pounds.

APPARATUS

The static-force and -moment characteristics were measured with a 2-1/2-inch-diameter, six-component, strain-gage balance enclosed within the model case.

The dynamic stability derivatives were measured on a special oscillation apparatus having a single degree of freedom. The model was mounted on crossed-flexure restraining springs which permitted rotation about one axis. By various orientations of this axis, different combinations of rolling, pitching, and yawing motions were obtained. The moments about these axes were measured and separated into the various stability derivatives. The oscillation equipment, including the electronic feedback network which stabilizes the oscillation at the desired amplitude, and the analog computing circuit used to process the strain-gage measurements are described in detail in reference 1.

To insure that the model support system did not oscillate and thereby invalidate the readings, the sting was guyed rigidly to the tunnel walls throughout the dynamic stability tests.

TESTS

Tests were conducted at Mach numbers from 0.23 to 0.94 for a range of angles of attack from -8° to $+24^\circ$ or to a maximum angle limited by choking of the tunnel flow or erratic oscillation of the model. A further limitation on angle of attack was imposed by static deflection of the oscillation mechanism during the tests to measure damping in pitch. These tests were limited, therefore, to angles of attack where the static pitching moment was near zero. The Reynolds number for most of the tests was 1.0 million for Mach numbers greater than 0.23 and 1.8 million for a Mach number of 0.23. Static longitudinal characteristics at a Mach number of 0.23 were also measured for Reynolds numbers up to 8.0 million.

The variations of the static lateral characteristics with angle of attack were evaluated from tests at 0° and 6° of sideslip. In addition, measurements of the static characteristics were made in which the sideslip angle was varied from about -5° to $+20^\circ$ for angles of attack of 0°, 3°, 6°, and 9°.

In the lateral oscillation tests the frequency range was from about 5 cycles per second for the complete model to about 8 cycles per second for the body alone. This resulted in a range of reduced frequency $\omega b/2V$ from 0.22 at low speeds to about 0.06 at high speeds for the complete model and from about 0.37 to 0.15 for the body alone tests. The frequency for all the damping-in-pitch tests was about 5 cycles per second or a value of reduced frequency $\omega\bar{c}/2V$ of 0.066 at low speeds and 0.018 at the higher Mach numbers. The oscillation amplitude was about 2° for both the pitch and lateral oscillatory tests.

CORRECTIONS TO DATA

The drag coefficient and the angle of attack have been corrected by the method of reference 4 for the induced effects of the tunnel walls resulting from lift on the model. The following corrections were added to the measured values:

$$\Delta\alpha = 0.25\ C_L$$

$$\Delta C_D = 0.0043\ C_L^2$$

The induced effects of the wind-tunnel walls on the pitching moment were calculated and found to be negligible.

Corrections to the Mach number and dynamic pressure for the effects of constriction due to the wind-tunnel walls were calculated by the method of reference 5. At a Mach number of 0.94 this correction amounted to an increase of about 2 percent in the measured values of Mach number and dynamic pressure.

The drag data have been adjusted to correspond to a base pressure equal to free-stream static pressure.

Corrections to the measured values of the damping due to internal damping of the model and friction of the oscillation mechanism were determined from wind-off measurements of the damping with the tunnel evacuated. Measurements of the wind-off damping were made at various pressures below atmospheric and the extrapolated value at zero absolute pressure was assumed to be the correction.

The effects of aerodynamic resonance caused by the wind-tunnel walls, similar to that discussed in reference 6, cannot be determined accurately in this case. The relation used in reference 2 yields a minimum wind-tunnel resonant frequency of 17 cycles per second at a Mach number of 0.95 and higher frequencies for lower Mach numbers. Since the model oscillation frequency never exceeded 9 cycles per second, it is doubtful that aerodynamic resonance had any effect on the data.

RESULTS

The measured and estimated rotary stability derivatives and the measured static characteristics are referred to the stability system of axes (see fig. 1). Often, the calculation of airplane motions is simplified when a body system of axes, rather than the stability system, is used. For this reason, the measured values of those derivatives which change in transferring from one axes system to the other have also been presented referred to a body system of axes. The X axis of the body system of orthogonal axes to which the derivatives have been referred is coincident with the fuselage reference line. The equations for effecting the transfer of the lateral rotary derivatives are given in the appendix of reference 3.

An index of figures, presenting the results and the calculated short-period oscillatory characteristics of a fighter-type airplane geometrically similar to the model, is given in the following table:

Except where otherwise noted the Reynolds number for the tests was 1.8 million for a Mach number of 0.23 and 1.0 million for higher Mach numbers.

DISCUSSION

Longitudinal Characteristics

Static characteristics.- The results of the low-speed tests to evaluate the longitudinal characteristics are similar to those of tests of a similar model reported in reference 7. Typical of these results, and of those of reference 7, is a region of reduced stability above a lift

coefficient of about 0.5 as shown in figure 4. This decrease in stability is associated with separation of the flow near the tips of the wings. In the tests reported herein, the region of reduced stability existed at all Mach numbers below 0.94.

At a Mach number of 0.23 an increase in Reynolds number from 1.8 to 4.0 million (fig. 5) resulted in an increase in the angle of attack at which the reduction in stability occurred. This increase in Reynolds number also resulted in a decrease in drag up to a lift coefficient of 1.0 (see fig. 6). A further increase in Reynolds number to 8.0 million resulted in only a slight additional decrease in drag and no significant changes in lift or pitching-moment coefficients.

Measured damping in pitch.- The variation of the measured damping-in-pitch derivative with angle of attack is shown in figure 7. The damping in pitch increased markedly at approximately the same angle of attack at which a reduction in static stability occurred (see fig. 4). A damping decrease occurred at higher angles of attack and can be correlated with an increase in static stability. Similar correlation between the static longitudinal stability and the damping in pitch has been observed on a straight-wing model and on a triangular-wing model (see refs. 2 and 3).

At Mach numbers between 0.90 and 0.94 a sizable reduction of damping occurred for the complete model as the angle of attack was increased from 0° to 2° (fig. 7). It was not possible to measure the damping for the wing-body combination in this angle-of-attack range; however, data obtained with the wing-body combination at corresponding negative angles of attack indicated no similar reduction in damping with the horizontal tail removed. It is probable therefore that the reduction in damping between 0° and 2° angle of attack at high subsonic speeds was caused by wing-tail interference.

Comparison of measured and estimated damping in pitch.- The contributions of the components of the model to the damping-in-pitch coefficient have been calculated by some of the simpler theoretical methods and have been compared in figure 7 with the measured values.

The damping of the body was estimated by the method of reference 8 which contends that the damping contribution of the body is only a function of the base area and its distance from the axis of rotation, so that

$$(C_{m_q} + C_{m_{\dot{\alpha}}})_{body} = \frac{-4B_b}{Sc^2}(l - x)^2$$

This equation yields a value of damping coefficient of -0.42 which is in good agreement with the measured values throughout the Mach number range.

The contribution of the wing was calculated by the method outlined in reference 8 but certain terms were expanded to apply this method to wings of plan form other than triangular. The formula then became

$$(C_{m_q})_{wing} = \frac{-9\pi}{32} \frac{1+\lambda^2}{[1+\lambda-(\lambda/1+\lambda)]^2} + \left(\frac{C_{m_b}}{\epsilon}\right) \frac{b}{\bar{c}} \tan \Lambda_{0.75c}$$

The first term on the right-hand side of the equation is damping due to apparent camber and the second term is damping due to apparent twist. The values of (C_{m_b}/ϵ), the pitching moment per unit twist, were obtained from reference 9. The acceleration derivative, $C_{m_{\dot{\alpha}}}$ due to the wing, was estimated to be small with respect to C_{m_q} and was neglected.

The predicted and measured values of damping in pitch for the wing-body combination (a simple summation of the damping of the body and the damping of the wing) agreed reasonably well up to a Mach number of 0.90 at low angles of attack as shown in figure 7. The theory did not predict the reduction in damping above this Mach number so that at a Mach number of 0.94 the estimated values were considerably larger than the measured values.

The contribution of the tail to damping was computed by the method of reference 10 where it was shown that

$$(C_{m_q} + C_{m_{\dot{\alpha}}})_{tail} = 114.6 \left(\frac{l_t}{\bar{c}}\right) \left(\frac{dC_m}{di_t}\right) \left(1 + \frac{d\epsilon}{d\alpha}\right)$$

It is noted from figure 7 that for Mach numbers to 0.90 the tail contribution to damping was underestimated by this method. As was the case for the wing-body combination the method failed to predict the reduction at a Mach number of 0.94.

Lateral-Directional Characteristics

Static characteristics.- The variations of C_l, C_Y, and C_n with sideslip angle for several angles of attack are presented in figures 9, 10, and 11. The variations of the lateral coefficients per unit sideslip with angle of attack as evaluated from data obtained at 6° of sideslip are presented in figure 12. As can be seen from the data of figures 9 through 11, the variations of the lateral coefficients with sideslip are approximately linear to 6° of sideslip so that the unit coefficients presented in figure 16 are representative of the lateral characteristics for small angles of sideslip.

The results presented in figure 12 indicate large variations in the dihedral effect. The departure of C_l/β from a linear variation with angle of attack occurs in the same angle-of-attack range as the previously mentioned changes in longitudinal stability. Presumably, then, this change in the variation of dihedral effect is associated with stalling near the tips of the sweptback wing. The directional stability, however, remained relatively constant up to an angle of attack of about 15°.

Measured lateral-directional rotary stability derivatives.- The results of the measurements of the lateral-directional rotary stability derivatives from the oscillatory tests are presented in figure 17. Examination of these results reveals that fairly large changes in the magnitudes of C_{l_p}, $C_{l_r} - C_{l_{\dot{\beta}}}$, and, to a lesser extent, C_{n_p} occur within the range of angles of attack for which stalling near the wing tips had large effects on the static characteristics. The damping-in-yaw derivative, $C_{n_r} - C_{n_{\dot{\beta}}}$, arising mostly from forces on the vertical tail, was little affected by these changes in wing load distribution. Measurements of the values of these derivatives on a similar model in steady rolling and in steady yawing flow are presented in reference 7. Comparison of these measurements with those of the present investigation indicates agreement at low angles of attack, and sizable differences at the higher angles of attack.

There are two reasons evident for the disparity in the results at high angles of attack. In the case of the yawing derivatives, the measurements obtained in the oscillatory tests include contributions resulting from both sideslipping acceleration $\dot{\beta}$ and yawing velocity r, while the measurements obtained in steady yawing flow include the effects of yawing velocity only. It is not possible to separate the effects of sideslipping acceleration and yawing velocity by the oscillatory measurements employed. Results presented in reference 11 show the sideslipping acceleration derivatives, $C_{n_{\dot{\beta}}}$ and $C_{l_{\dot{\beta}}}$, to be small at low angles of attack. At the higher angles of attack, however, these derivatives are not small and can become a significant part of the quantities, $C_{n_r} - C_{n_{\dot{\beta}}}$ and $C_{l_r} - C_{l_{\dot{\beta}}}$, measured during an oscillatory test. In addition, it has been shown in reference 12 that, at the higher angles of attack, the derivatives due to yawing velocity alone can be quite different in value, depending upon whether the yawing motion is steady or oscillatory. It is further shown in reference 13 that the derivatives due to yawing velocity during an oscillatory test are not independent of oscillation frequency at the higher angles of attack.

From the foregoing, it would appear that, at the higher angles of attack, the data on the lateral dynamic rotary derivatives presented in this report may not represent appropriate values if the reduced frequency of interest is very different from the reduced frequency for which the results were obtained. Further, in this range of angles of attack,

separation of the derivatives due to sideslipping acceleration and yawing velocity is desirable if the coefficients are to be utilized in the calculation of airplane motions.

Estimates of the lateral rotary derivatives.- The values of the lateral rotary derivatives were estimated utilizing, for the most part, the methods outlined in reference 14. In these methods, the results of measurements of the static characteristics are used to obtain the effective lift-curve slopes and centers of pressure of the lifting surfaces. Unfortunately, the method does not evaluate the derivatives due to sideslipping acceleration. In the estimates of the contributions of the wings and tail surfaces to the rotary derivatives, the acceleration derivatives have been considered to be zero. Some of the disparity between the estimated and measured yawing derivatives, therefore, may be caused by the presence of acceleration derivatives of significant magnitude.

Damping in roll, C_{l_p}: The damping in roll contributed by the wing was estimated by a method presented in reference 14 which relates the damping to the wing lift-curve slope and drag characteristics. As can be seen from the data presented in figure 18(a), this method predicted a reduction in roll damping with increasing angle of attack but underestimated the magnitude of this reduction at the higher Mach numbers.

Since the horizontal tail had the same plan form as the wing, the tail damping was assumed to be equal to the wing damping multiplied by the fourth power of the ratio of tail span to wing span. The horizontal tail damping was estimated, therefore, to be about 7 percent of the total. The damping of the vertical tail would be expected to be considerably smaller and was neglected in estimating the total roll damping of the model.

Yawing moment due to rolling, C_{n_p}: The estimate of C_{n_p} of the wing was based on the method of reference 15 with one modification. The value of $(2C_L/3A^2)$ which represents the value of C_{n_p} for potential flow over a triangular wing was replaced by $(\Delta C_{n_p}/C_L)C_L$ where the bracketed quantity was obtained from charts in reference 14. The complete equation then reads

$$(C_{n_p})_{wing} = [-C_{l_p} \tan \alpha] - K\left[-C_{l_p} \tan \alpha - \left(\frac{\Delta C_{n_p}}{C_L}\right)C_L\right]$$

where

$$K = \frac{(\partial/\partial\alpha)(C_L \tan \alpha) - (\partial/\partial\alpha)\left[C_D - (C_D)_{C_L=0}\right]}{(\partial/\partial\alpha)(C_L \tan \alpha) - (\partial/\partial\alpha)(C_L^2/\pi A)}$$

In the equation K is the ratio of leading-edge suction obtained to that existing on an elliptically loaded wing in potential flow. The estimated values of C_{l_p} were used in the estimation of C_{n_p}.

The contribution of the vertical tail to C_{n_p} was estimated by the method outlined in reference 14. However, in place of the theoretical center of pressure, the center of pressure calculated from the static-force measurements was used.

Calculations were made of the short-period lateral oscillatory characteristics of an airplane geometrically similar to the model. When the value of C_{n_p} was varied in these calculations by 0.1, large changes in the calculated damping occurred. In view of the sensitivity of the lateral damping of this configuration to changes in C_{n_p}, it can be seen from figure 18(b) that the estimation procedure is inadequate for Mach numbers of 0.80 and greater.

Damping in yaw, $C_{n_r} - C_{n_{\dot{\beta}}}$: The method of estimating the damping of the body in yaw was identical to that for damping in pitch so that

$$(C_{n_r} - C_{n_{\dot{\beta}}})_{body} = (C_{m_q} + C_{m_{\dot{\alpha}}})_{body}\left(\frac{\bar{c}}{b}\right)^2$$

The wing and tail contributions to C_{n_r} were estimated by the method of reference 14. A comparison of the estimated and measured values of damping in yaw presented in figure 18(c) shows that the damping of the wing-body combination was predicted quite well. At a Mach number of 0.23, the estimated contribution of each vertical tail was about 80 percent of the measured tail damping. At the higher Mach numbers, the measured damping contributions of both the large and small tails were nearly the same and approximately equal to the estimated damping of the large tail. The prediction method, of course, merely reflects the static test results. It is not understood why the same difference in the effectiveness of the large and small tails which was observed in the static test results was not observed in the measurements of the yaw damping at Mach numbers greater than 0.23.

Rolling moment due to yawing, $C_{l_r} - C_{l_{\dot{\beta}}}$: At low angles of attack, the estimates of C_{l_r} for both the wing-body combination and the contribution of the tail surfaces agreed reasonably well with the measurements of $C_{l_r} - C_{l_{\dot{\beta}}}$ (fig. 18(d)). At the larger angles of attack, where stalling of the outer wing sections was evident from the static test results, no agreement was obtained. As previously mentioned, this lack of agreement might be caused by the presence of large values of the acceleration derivative $C_{l_{\dot{\beta}}}$. Further, the estimation procedure yields the steady-state values of the rotary derivatives and therefore takes no account of frequency effects which can be important in this angle-of-attack range.

Dynamic Stability Calculations

The measured stability derivatives have been used in the calculation of the short-period longitudinal and lateral characteristics of a representative airplane goemetrically similar to the model. The mass and inertia characteristics of the representative airplane are given in table II. The minimum requirements for damping of the short-period oscillations for military airplanes from reference 16 have been included for reference in the figures presenting the results of these calculations. Failure to meet these requirements does not necessarily indicate dangerous or divergent motions, but merely that the airplane may not be able to perform its intended maneuvers satisfactorily.

Longitudinal stability.- The frequency of the short-period longitudinal oscillation was computed by the method presented in the appendix of reference 2. The damping ratio ζ was calculated using the formula presented in reference 17, from which the equation is repeated for convenience.

$$\zeta = \sqrt{\frac{\bar{c}^3 S}{32 I_{Y_O}}} \sqrt{\frac{\rho}{-C_{m_\alpha}}} \left[\frac{2 I_{Y_O} C_{L_\alpha}}{m \bar{c}^2} - (C_{m_q} + C_{m_{\dot{\alpha}}}) \right]$$

The flying qualities as specified in reference 16 state that the short-period longitudinal oscillation shall decrease to 1/10 amplitude in one cycle. It is obvious in figure 20 that only at a few selected Mach numbers and altitudes would the damping be sufficient to fulfill this requirement without an artifical damping device. Reference 16 further states that for a nontactical mission the requirements may be relaxed to 1/2 amplitude in one cycle for operations at altitudes above 30,000 feet. This criterion was fulfilled throughout the Mach number range at both 30,000 and 40,000 feet.

Inspection of the equation for damping ratio shows that this ratio is proportional to the damping-in-pitch coefficient and lift-curve slope and inversely proportional to the square root of the aerodynamic spring constant C_{m_α}. The decrease in damping ratio at the higher Mach numbers is not only caused by a decrease in damping but also by an increase in C_{m_α} (fig. 8).

Lateral-directional stability.- The period and time to damp to half amplitude of the short-period lateral oscillations were calculated by the method outlined in reference 14 and the results are presented in figure 21. Two derivatives encountered in these calculations which were not measured in this investigation are C_{Y_p} and C_{Y_r}. Estimates of these derivatives were made by the method of reference 14 and it was found

that any reasonable variation in these derivatives caused insignificant changes in the dynamic stability of the airplane. They were therefore assumed to be zero for all stability estimates presented.

The equations of motion presented in reference 14 do not consider separately the derivatives due to sideslipping acceleration $C_{n_{\dot{\beta}}}$ and $C_{l_{\dot{\beta}}}$. The measured values of $C_{n_r} - C_{n_{\dot{\beta}}}$ and $C_{l_r} - C_{l_{\dot{\beta}}}$ were used in place of C_{n_r} and C_{l_r} in the equations. In the absence of separate measurements of all the derivatives, this is believed to be the most accurate way to take into account the effects of sideslipping acceleration derivatives at the low angles of attack involved in these computations.

The period and time to damp to half amplitude are not sufficient indications of whether the airplane will be able to perform its required maneuvers satisfactorily. An additional criterion is ratio of bank angle amplitude to equivalent side velocity amplitude, $|\varphi|/|v_e|$ (fig. 21). The values of $|\varphi|/|v_e|$ were calculated by the method outlined in reference 18.

For the range of values of $|\varphi|/|v_e|$ encountered for this configuration the boundaries shown in figure 21, as pointed out in reference 16, are constant values for each condition. Boundary B represents the minimum value of damping for a configuration which normally employs an artificial stabilizing device. Boundary A represents the minimum for an airplane not normally using a stability augmenter. It can be seen that at all flight conditions and altitudes investigated the configuration fulfilled the requirements without use of artificial damping.

The additional boundary at a value of $1/C_{1/2}$ of 1.73 is a requirement for an airplane on a tactical mission. This criterion was not met at any condition investigated, indicating a need for artificial stability for the represented airplane if it is to be used as a gun platform or bomber.

CONCLUDING REMARKS

The results of this investigation have shown that the rotary stability derivatives of an airplane model having 45° of sweepback can be estimated reasonably well at low angles of attack if the details of the static characteristics are known. Once the angle of attack is reached at which separation of the flow near the tips of the sweptback wing occurs, the estimation method fails to predict variations in the damping in pitch, damping in roll, yawing moment due to rolling, and rolling

moment due to yawing. Calculations of the longitudinal and lateral-directional short-period oscillations of a representative airplane geometrically similar to the model indicated the damping to be adequate for a nontactical mission.

Ames Research Center
National Aeronautics and Space Administration
Moffett Field, Calif., Feb. 16, 1959

REFERENCES

1. Beam, Benjamin H.: A Wind-Tunnel Test Technique for Measuring the Dynamic Rotary Stability Derivatives at Subsonic and Supersonic Speeds. NACA Rep. 1258, 1956. (Supersedes NACA TN 3347)

2. Beam, Benjamin H., Reed, Verlin D., and Lopez, Armando E.: Wind-Tunnel Measurements at Subsonic Speeds of the Static and Dynamic-Rotary Stability Derivatives of a Triangular-Wing Airplane Model Having a Triangular Vertical Tail. NACA RM A55A28, 1955.

3. Buell, Donald A., Reed, Verlin D., and Lopez, Armando E.: The Static and Dynamic-Rotary Stability Derivatives at Subsonic Speeds of an Airplane Model With an Unswept Wing and a High Horizontal Tail. NACA RM A56I04, 1956.

4. Glauert, Hermann: The Elements of Aerofoil and Airscrew Theory. Ch. XIV, The University Press, Cambridge, England, 1926.

5. Herriot, John G.: Blockage Corrections for Three-Dimensional-Flow Closed-Throat Wind Tunnels, With Considerations of the Effects of Compressibility. NACA Rep. 995, 1950. (Supersedes NACA RM A7B28)

6. Runyan, Harry L., Woolston, Donald S., and Rainey, A. Gerald: Theoretical and Experimental Investigation of the Effect of Tunnel Walls on the Forces on an Oscillating Airfoil in Two-Dimensional Subsonic Compressible Flow. NACA Rep. 1262, 1956. (Supersedes NACA TN 3416)

7. Jaquet, Byron M., and Fletcher, H. S.: Wind-Tunnel Investigation at Low Speed of Sideslipping, Rolling, Yawing, and Pitching Characteristics for a Model of a 45° Swept-Wing Fighter-Type Airplane. NACA RM L55F21, 1955.

8. Tobak, Murray, Reese, David E., Jr., and Beam, Benjamin H.: Experimental Damping in Pitch of a 45° Triangular Wing. NACA RM A50J26, 1950.

9. Stevens, Victor I.: Theoretical Basic Span Loading Characteristics of Wings With Arbitrary Sweep, Aspect Ratio, and Taper Ratio. NACA TN 1772, 1948.

10. Perkins, Courtland D., and Hage, Robert E.: Airplane Performance Stability and Control. John Wiley and Sons, Inc., N. Y., 1949.

11. Riley, Donald R., Bird, John D., and Fisher, Lewis R.: Experimental Determination of the Aerodynamic Derivatives Arising From Acceleration in Sideslip for a Triangular, a Swept, and an Unswept Wing. NACA RM L55A07, 1955.

12. Queijo, M. J., Fletcher, Herman S., Marple, C. G., and Hughes, F. M.: Preliminary Measurements of the Aerodynamic Yawing Derivatives of a Triangular, a Swept, and an Unswept Wing Performing Pure Yawing Oscillations, With a Description of the Instrumentation Employed. NACA RM L55L14, 1956.

13. Campbell, John P., Johnson, Joseph L., Jr., and Hewes, Donald E.: Low-Speed Study of the Effect of Frequency on the Stability Derivatives of Wings Oscillating in Yaw With Particular Reference to High Angle-of-Attack Conditions. NACA RM L55H05, 1955.

14. Campbell, John P., and McKinney, Marion O.: Summary of Methods for Calculating Dynamic Lateral Stability and Response and for Estimating Lateral Stability Derivatives. NACA Rep. 1098, 1952. (Supersedes NACA TN 2409)

15. Wiggins, James W.: Wind-Tunnel Investigation at High Subsonic Speeds to Determine the Rolling Derivatives of Two Wing-Fuselage Combinations Having Triangular Wings, Including a Semiempirical Method of Estimating the Rolling Derivatives. NACA RM L53L18a, 1954.

16. Anon.: Military Specification - Flying Qualities of Piloted Airplanes. MIL-F-8785 (ASG), Sept. 1, 1954. Amendment no. 1, Oct. 19, 1954; Amendment no. 2, Oct. 17, 1955.

17. Wolowicz, Chester H.: Dynamic Longitudinal Stability Characteristics of a Swept-Wing Fighter-Type Airplane at Mach Numbers Between 0.36 and 1.45. NACA RM H56H03, 1957.

18. McNeill, Walter E., and Creer, Brent Y.: A Summary of Results Obtained During Flight Simulation of Several Aircraft Prototypes With Variable-Stability Airplanes. NACA RM A56C08, 1956.

TABLE I.- DIMENSIONS OF THE MODEL

Wing	
Area, sq ft	3.760
Span, ft	3.658
Mean aerodynamic chord, $\bar{c}$, ft	1.133
Aspect ratio	3.56
Taper ratio	0.3
Dihedral, deg	0
Incidence, deg	0
Sweepback of a quarter-chord line, deg	45
Section (streamwise)	64A007
Location of moment center	$0.346\bar{c}$
Aileron	
Area, (each), sq ft	0.193
Span, ft	0.981
Hinge line location, percent chord	75
Spanwise location, percent semispan	32.3 to 75
Horizontal tail	
Area, sq ft	0.989
Span, ft	1.878
Mean aerodynamic chord, $\bar{c}_H$, ft	0.577
Aspect ratio	3.56
Taper ratio	0.3
Dihedral, deg	0
Sweepback of quarter chord line, deg	45
Section (streamwise)	65A003.5
Distance from moment center to $\bar{c}_H/4$	$1.311\bar{c}$
Vertical tail (leading and trailing edges extended to fuselage reference line)	
Area	
Small, sq ft	0.566
Large, sq ft	0.665
Span	
Small, ft	0.873
Large, ft	1.052
Mean aerodynamic chord, $\bar{c}_V$	
Small, ft	0.700
Large, ft	0.710
Aspect ratio	
Small	2.692
Large	3.325
Taper ratio	
Small	0.345
Large	0.244
Sweepback of quarter chord line	
Small, deg	45
Large	45°10'

TABLE I.- DIMENSIONS OF THE MODEL - Concluded

Length (moment center to $\bar{c}_v/4$)	
Small, ft	1.317
Large, ft	1.333
Vertical location (center line to $\bar{c}_v/4$)	
Small, ft	0.366
Large, ft	0.420
Section (streamwise)	65A003.5
Rudder	
Area, sq ft	0.0623
Chordwise hinge line location (percent of chord)	
Small	70
Large	72
Spanwise location (percent of semispan)	
Small	33 to 70
Large	27 to 58
Rudder area, percent of tail area	
Small	11.00
Large	9.35

TABLE II.- ASSUMED GEOMETRIC AND MASS DATA FOR REPRESENTATIVE AIRPLANE

Geometric data	
Model scale (wing area 376 sq ft)	0.10
Mass data	
Weight, lb	24,800
I_{X_O}, slug-ft^2	11,103
I_{Y_O}, slug-ft^2	59,248
I_{Z_O}, slug-ft^2	67,279
Inclination of the principal longitudinal axis below the fuselage reference line, deg	0.5
Center of gravity position, percent $\bar{c}$	34.6
where: I_{X_O}, I_{Y_O}, I_{Z_O} are moments of inertia about the principal axes.	

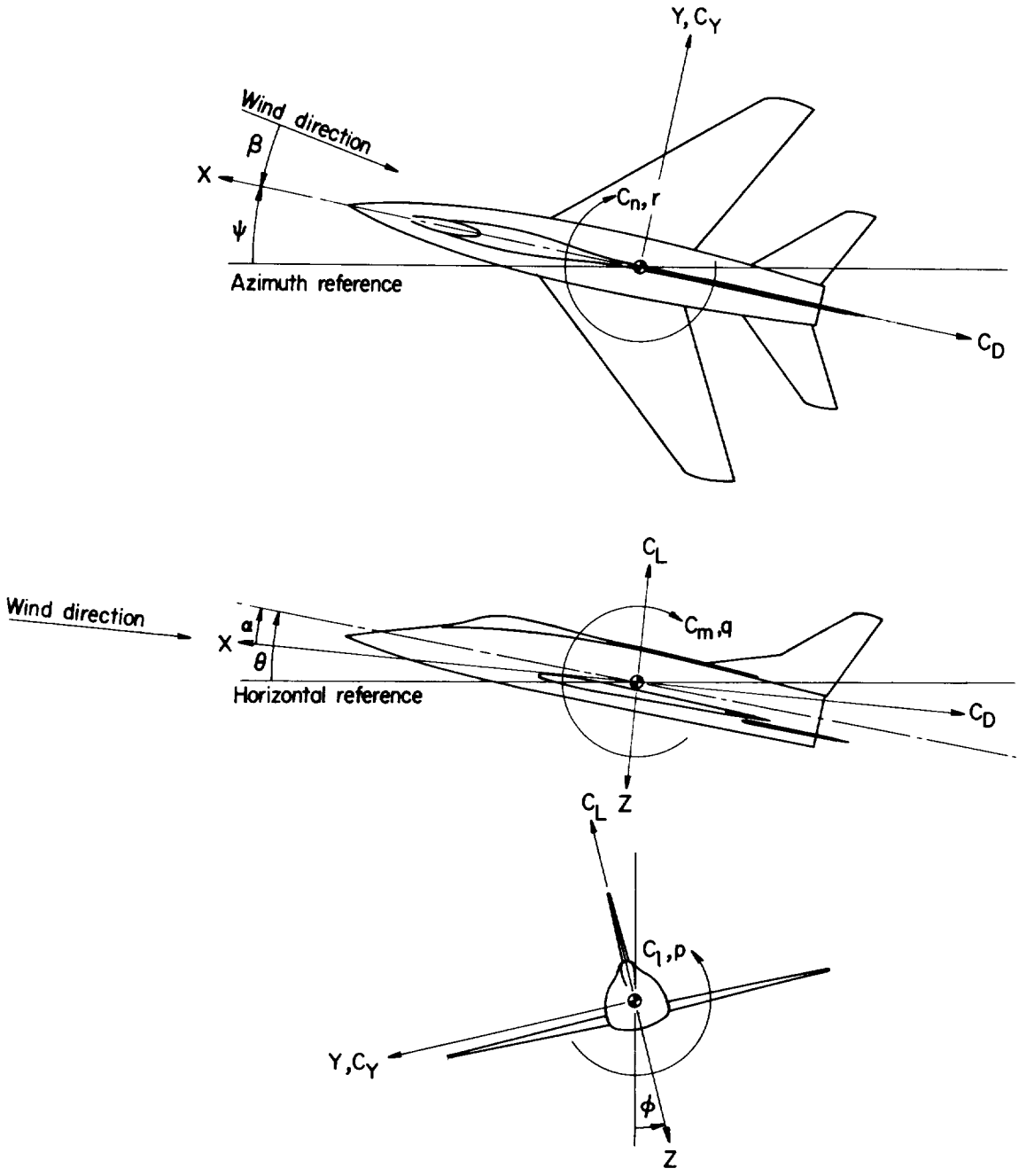

Figure 1.- The stability system of axes. Arrows indicate positive directions.

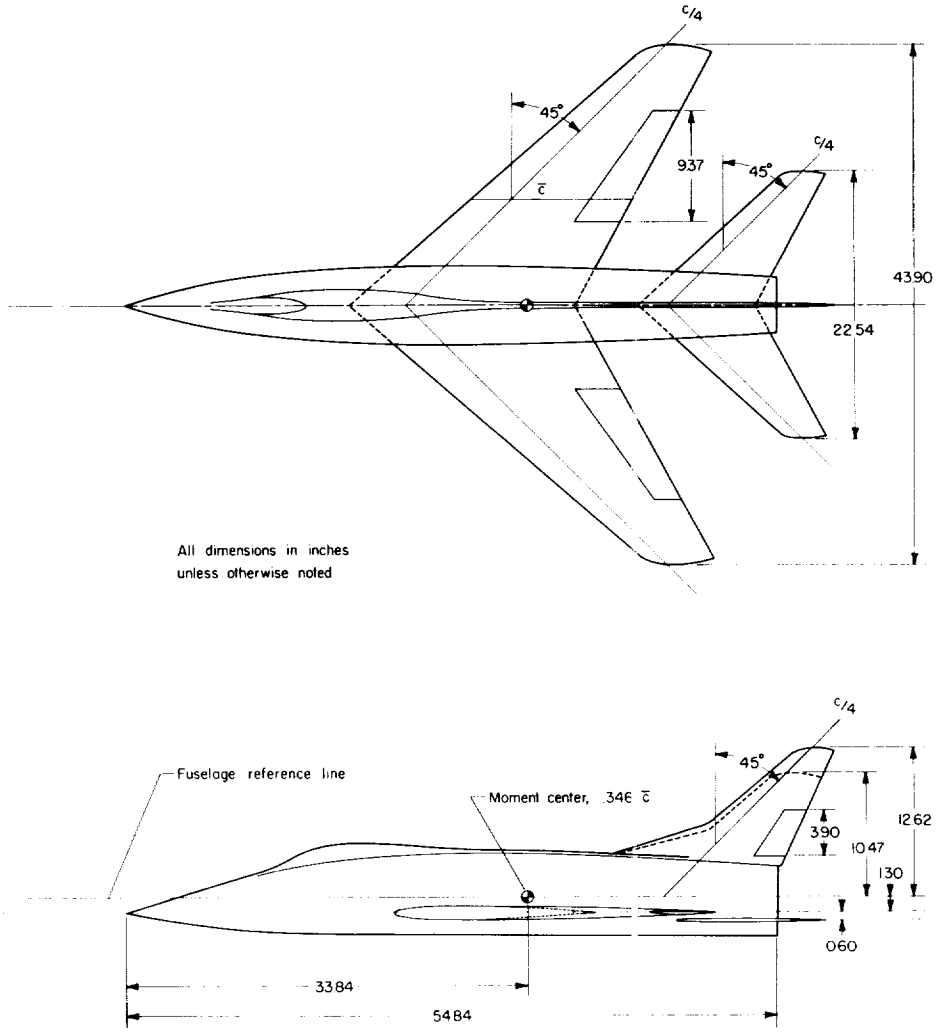

Figure 2.- Geometry of the model.

A-21200

(a) Top view.

Figure 3.- Photographs of the model in the wind tunnel.

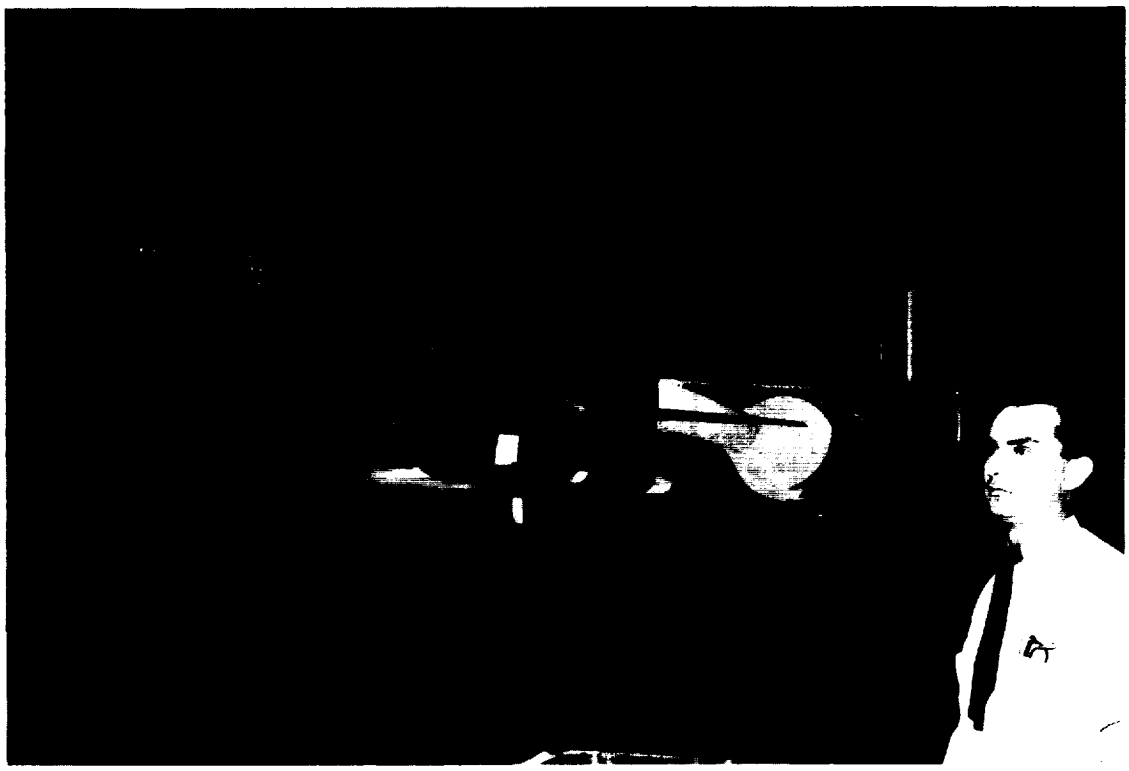

A-21199

(b) Three-quarter front view.

Figure 3.- Concluded.

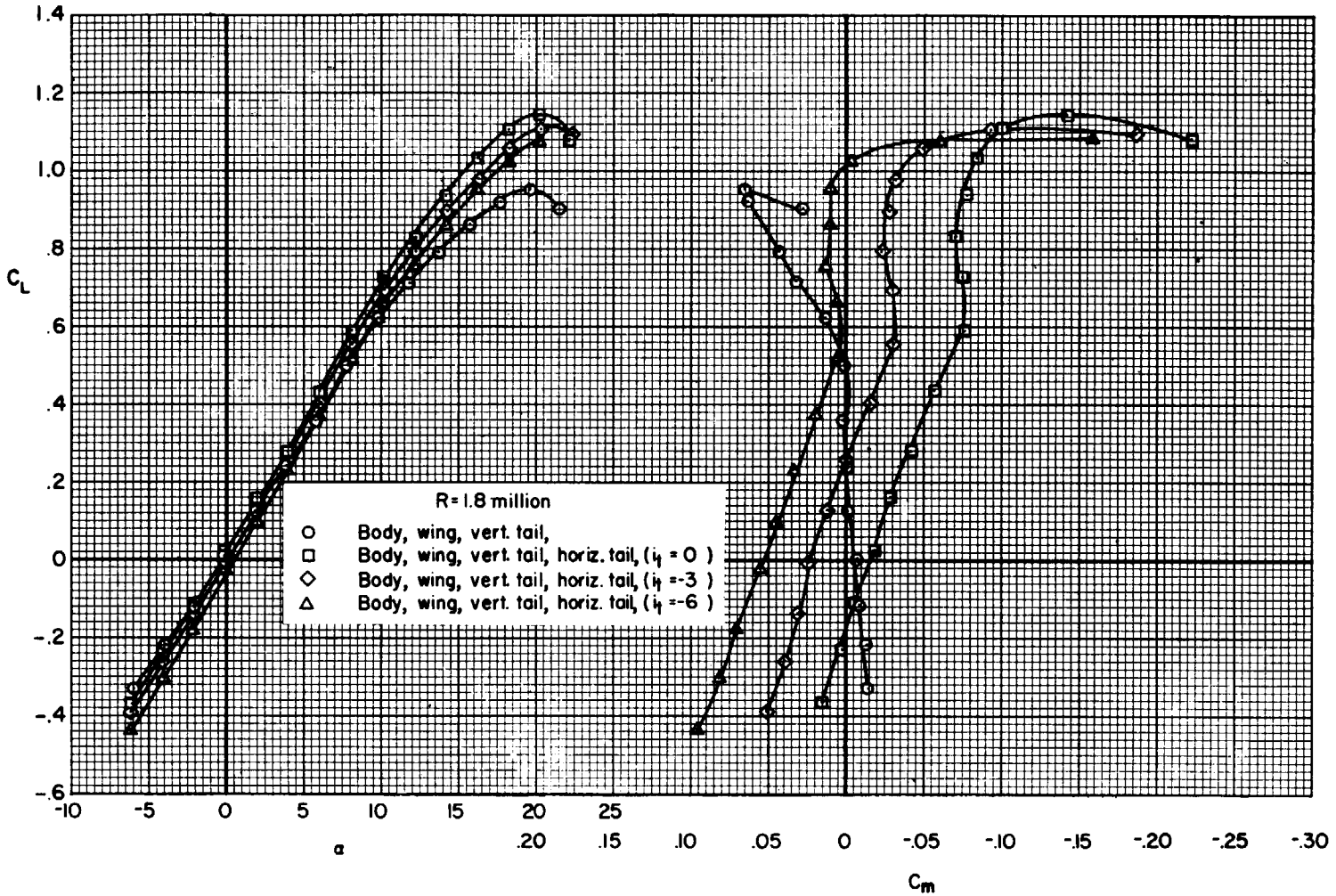

(a) M = 0.23

Figure 4.- Lift and pitching-moment data for the complete model for several tail incidences and for the model with the horizontal tail removed.

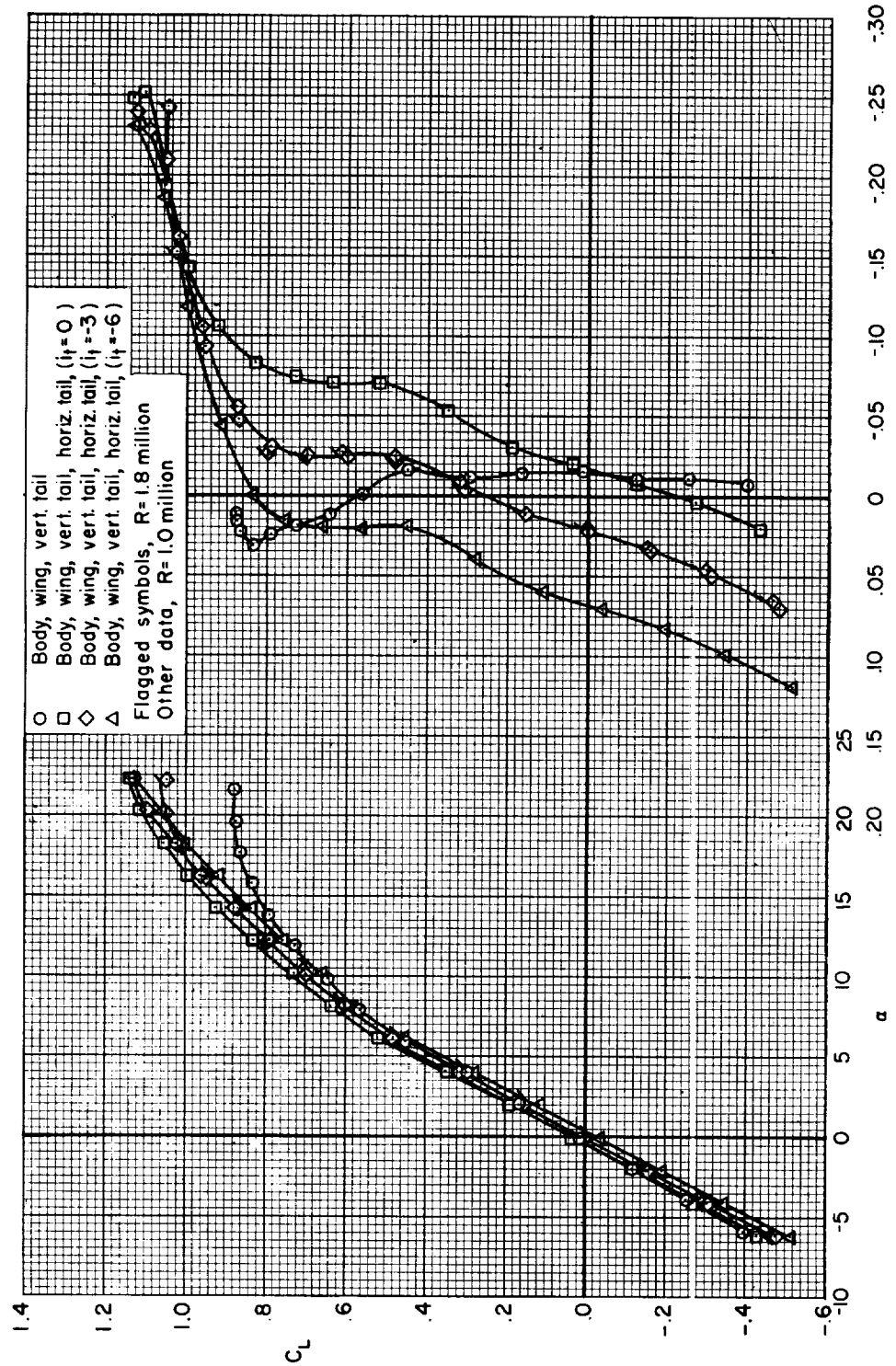

(b) M = 0.80

Figure 4.- Continued.

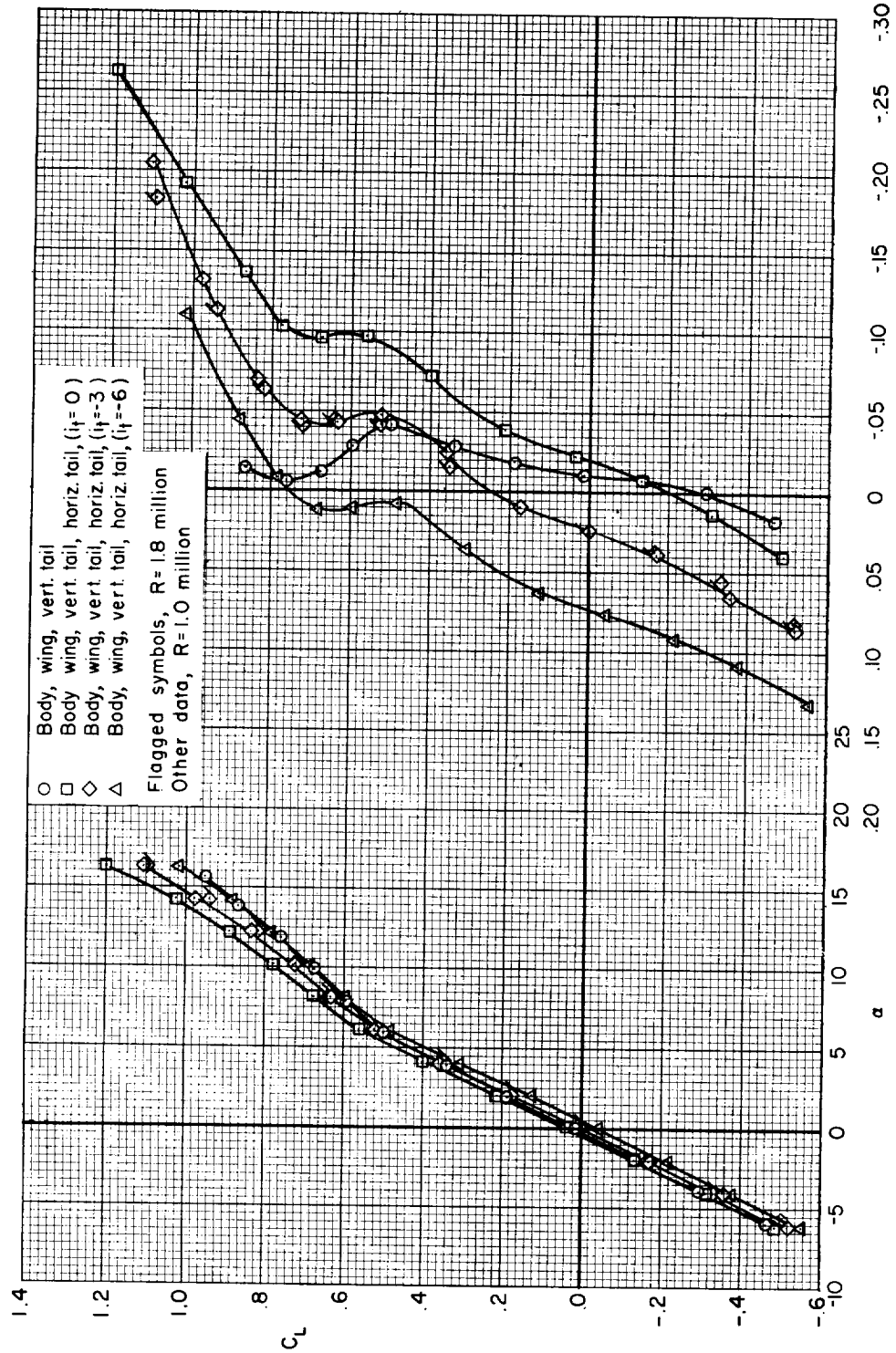

(c) M = 0.90

Figure 4.- Continued.

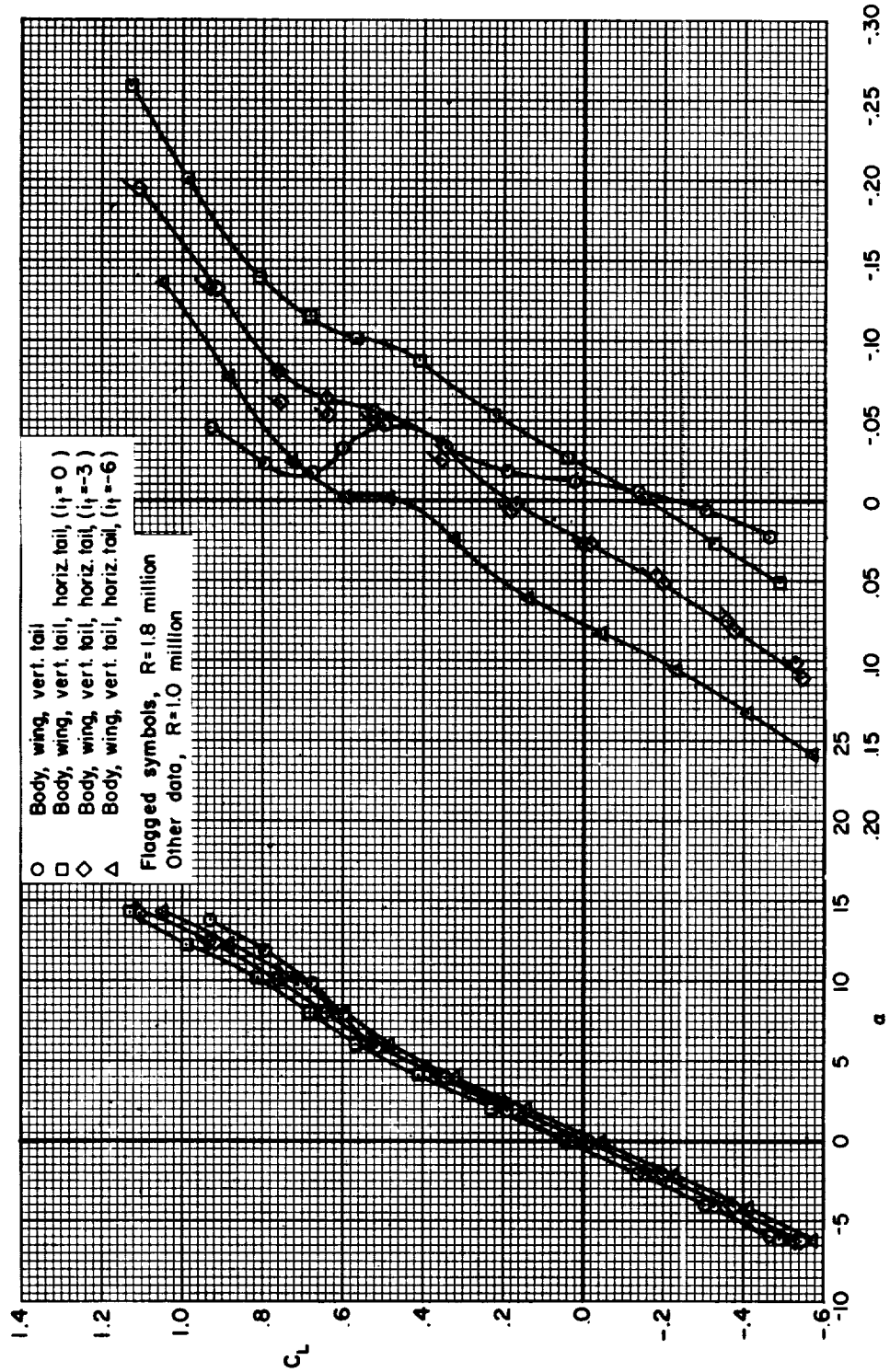

(d) M = 0.92

Figure 4.- Continued.

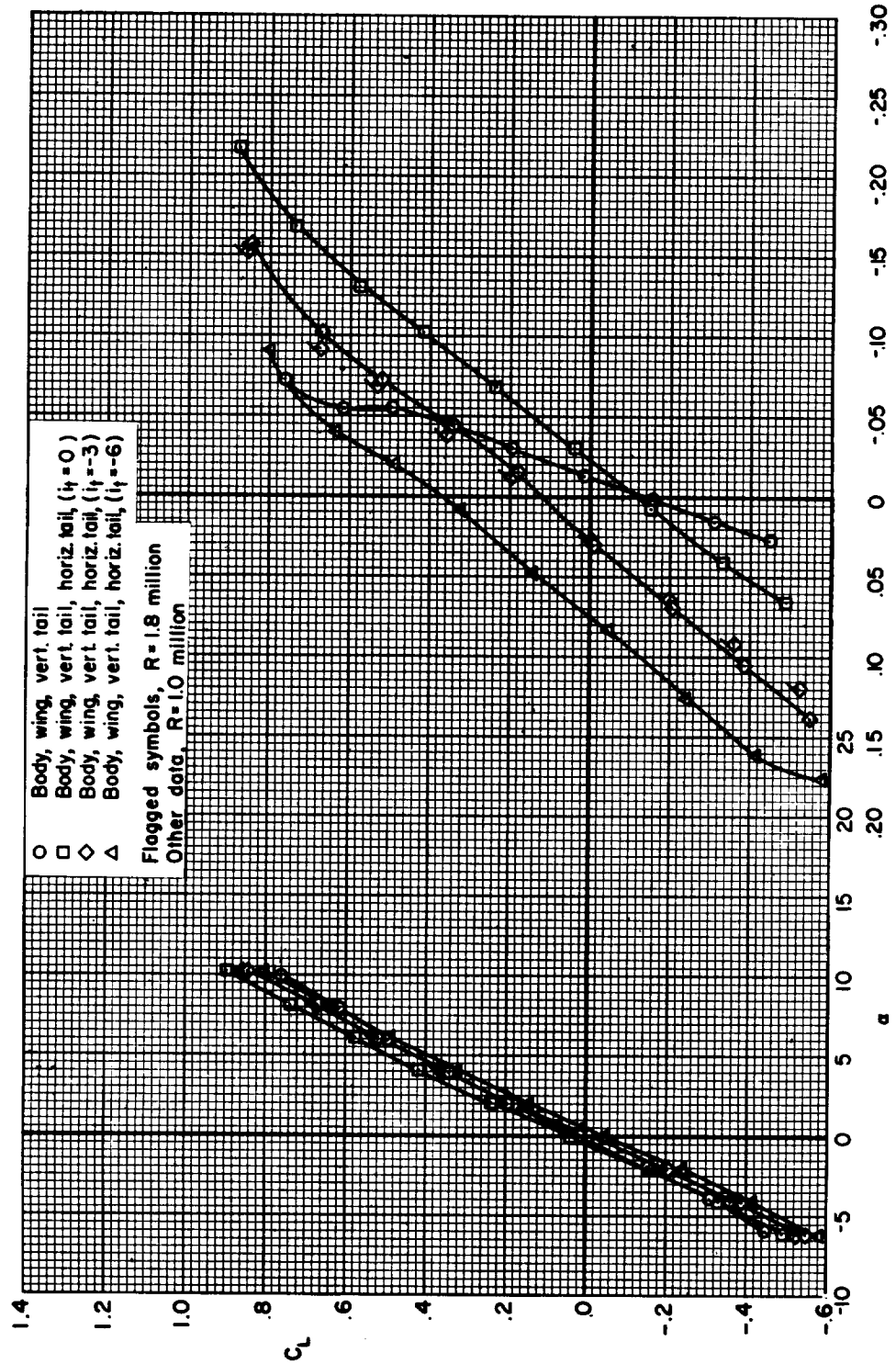

(e) M = 0.94

Figure 4.- Concluded.

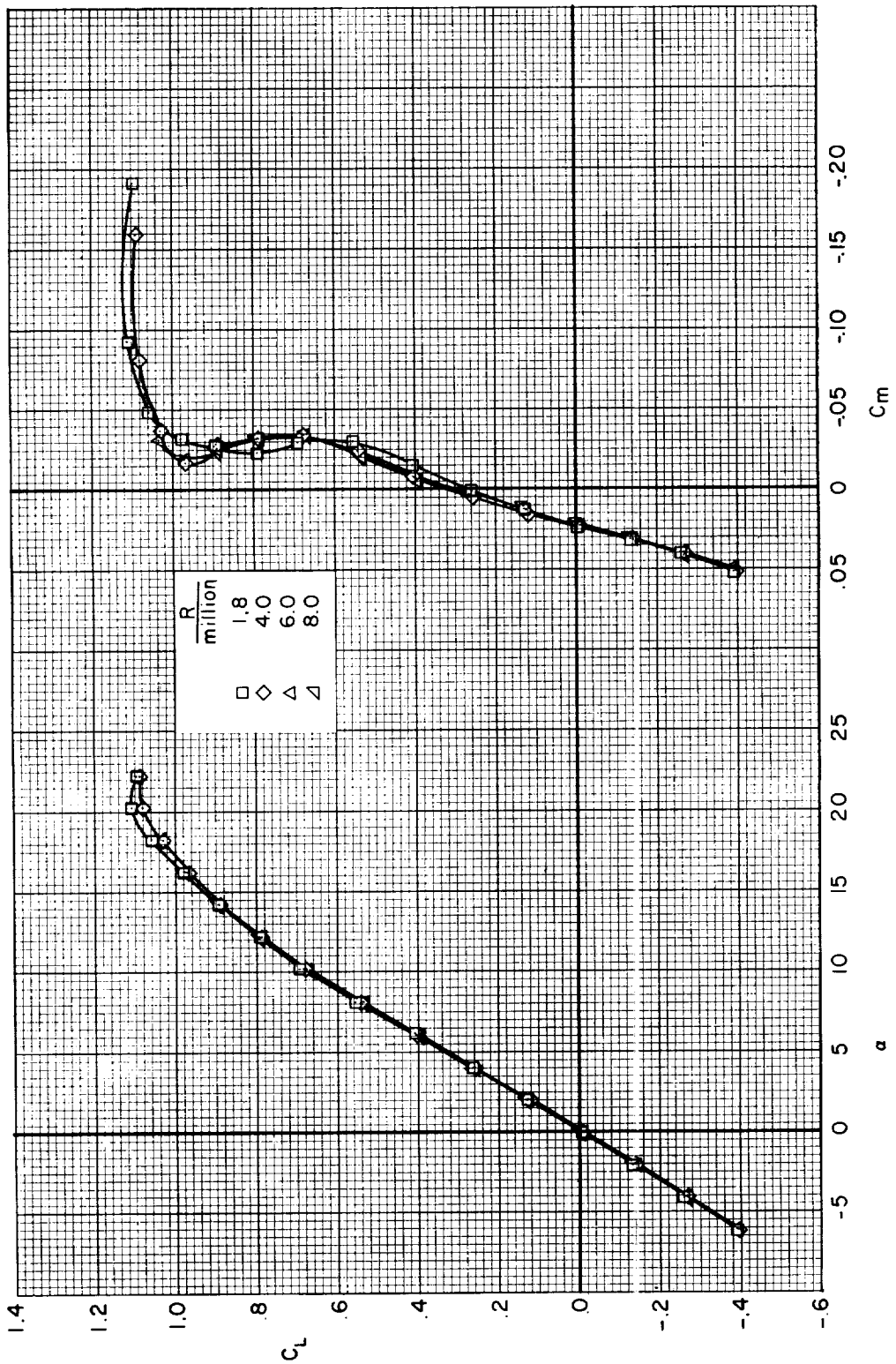

Figure 5.- Effects of Reynolds number on lift and pitching-moment coefficients for the complete model; $i_t = -3^\circ$, M = 0.23.

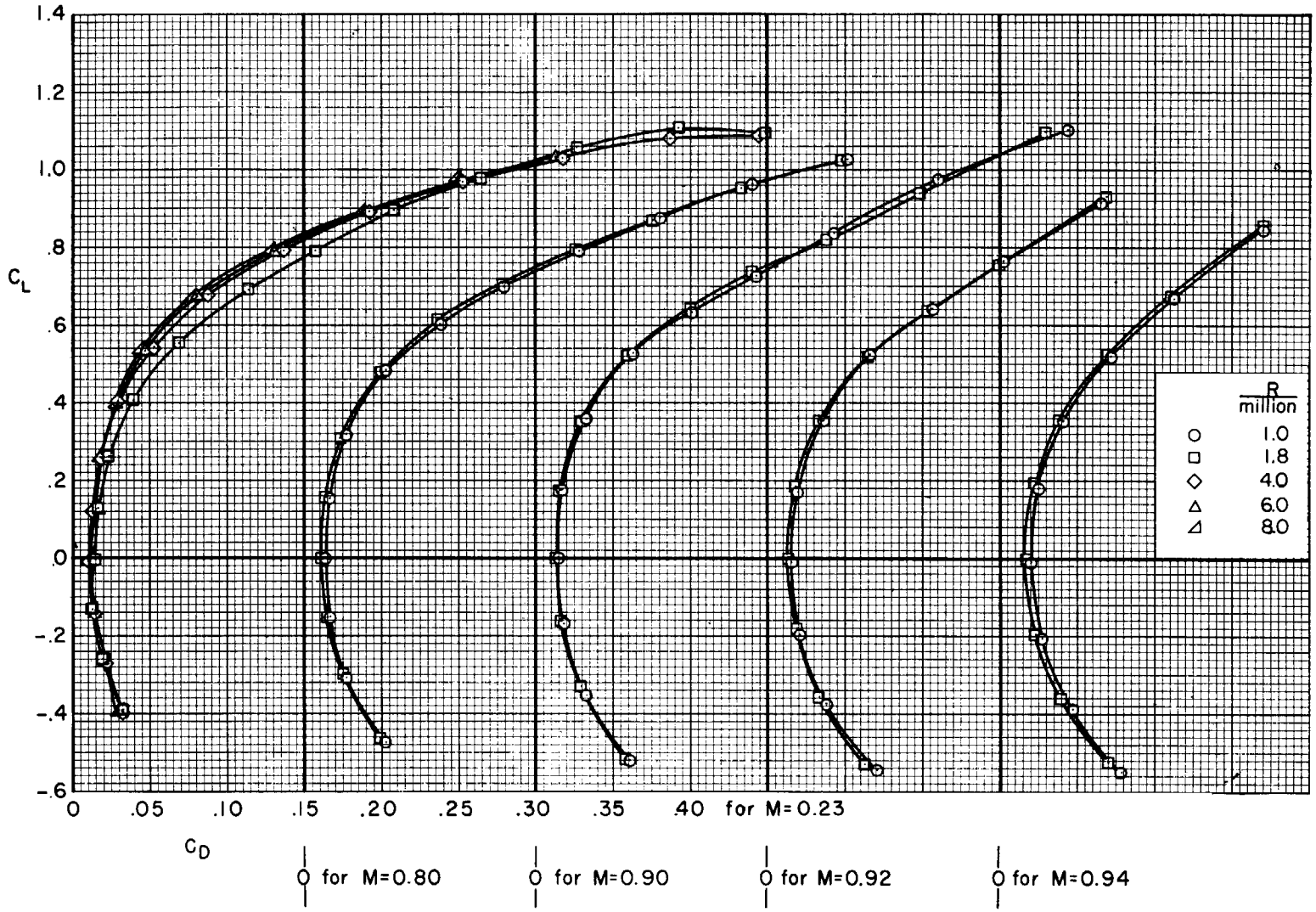

Figure 6.- Variation of drag coefficient with lift coefficient for the complete model; $i_t = -3^o$.

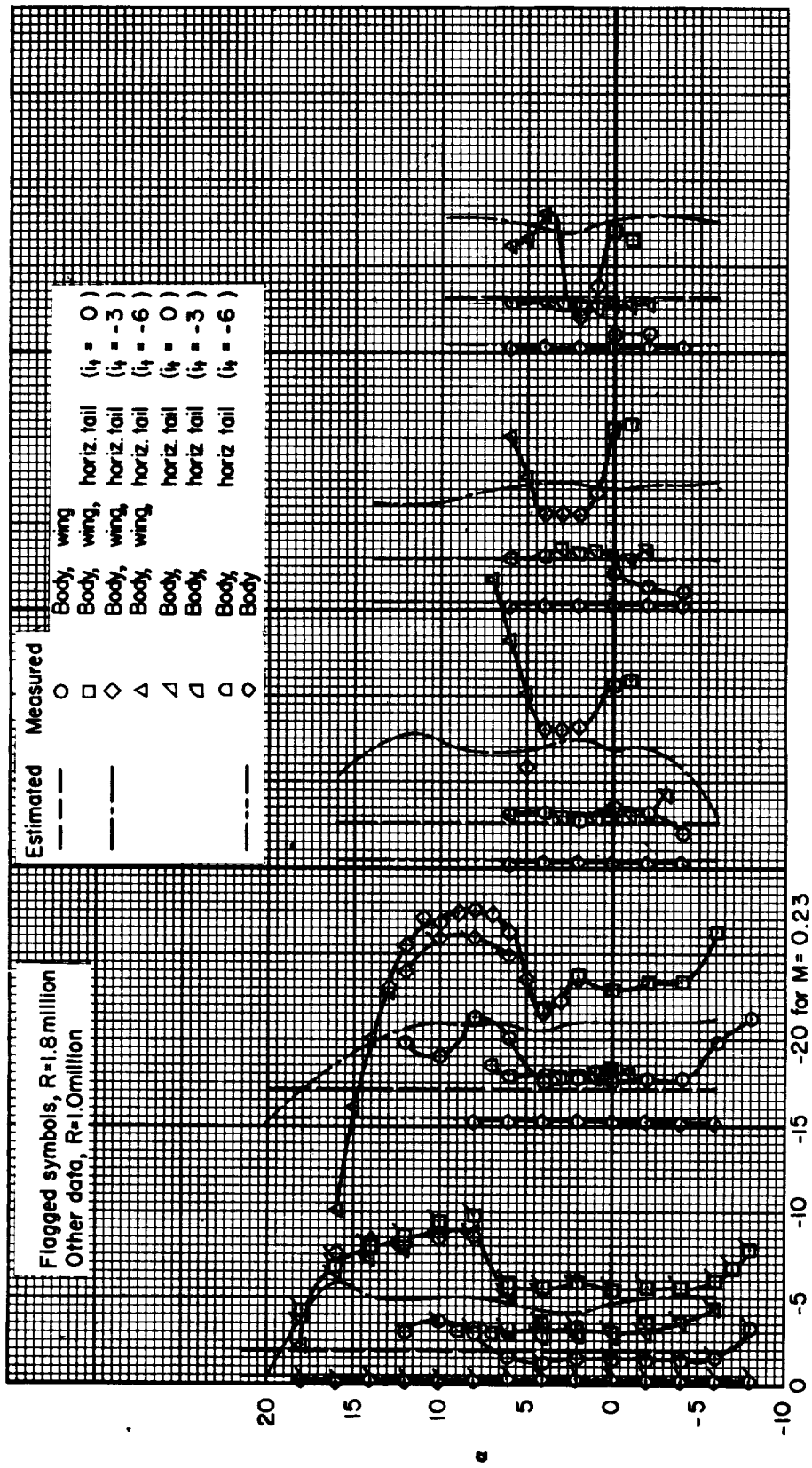

Figure 7.- Variation of damping-in-pitch coefficient with angle of attack.

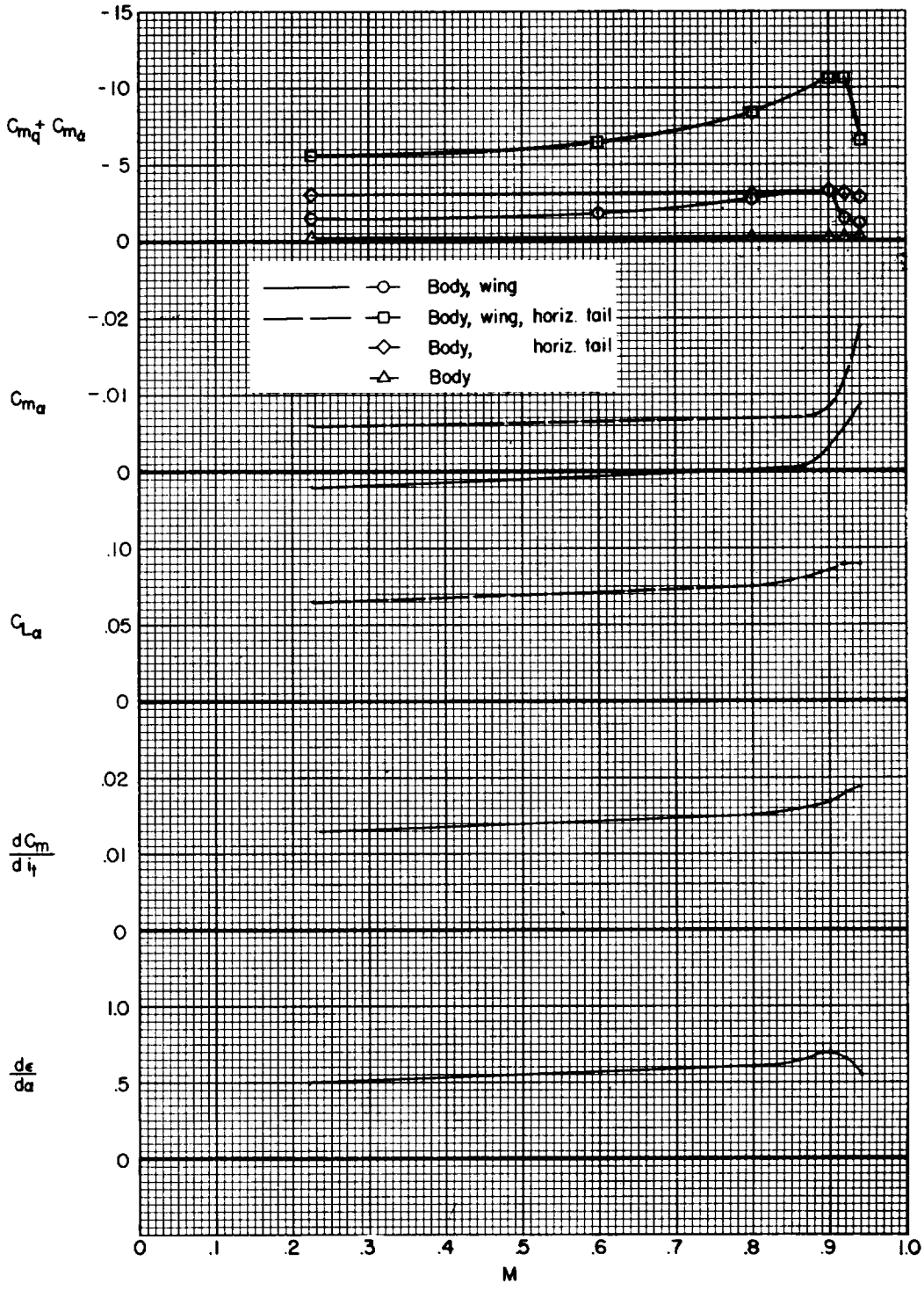

Figure 8.- Variation with Mach number of the measured longitudinal stability parameters; $\alpha = 0^{\circ}$.

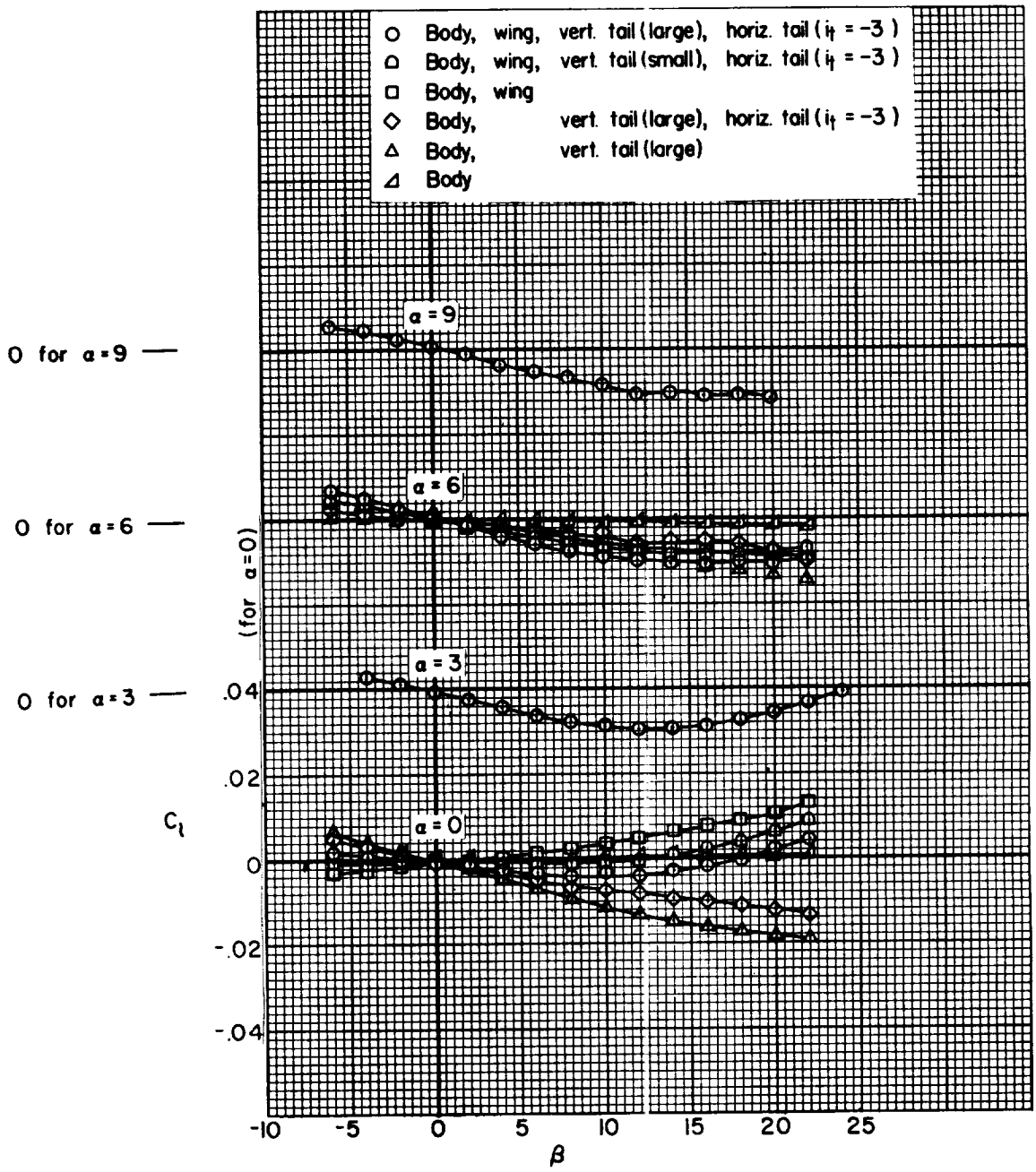

(a) M = 0.23

Figure 9.- Variation of rolling-moment coefficient with sideslip angle.

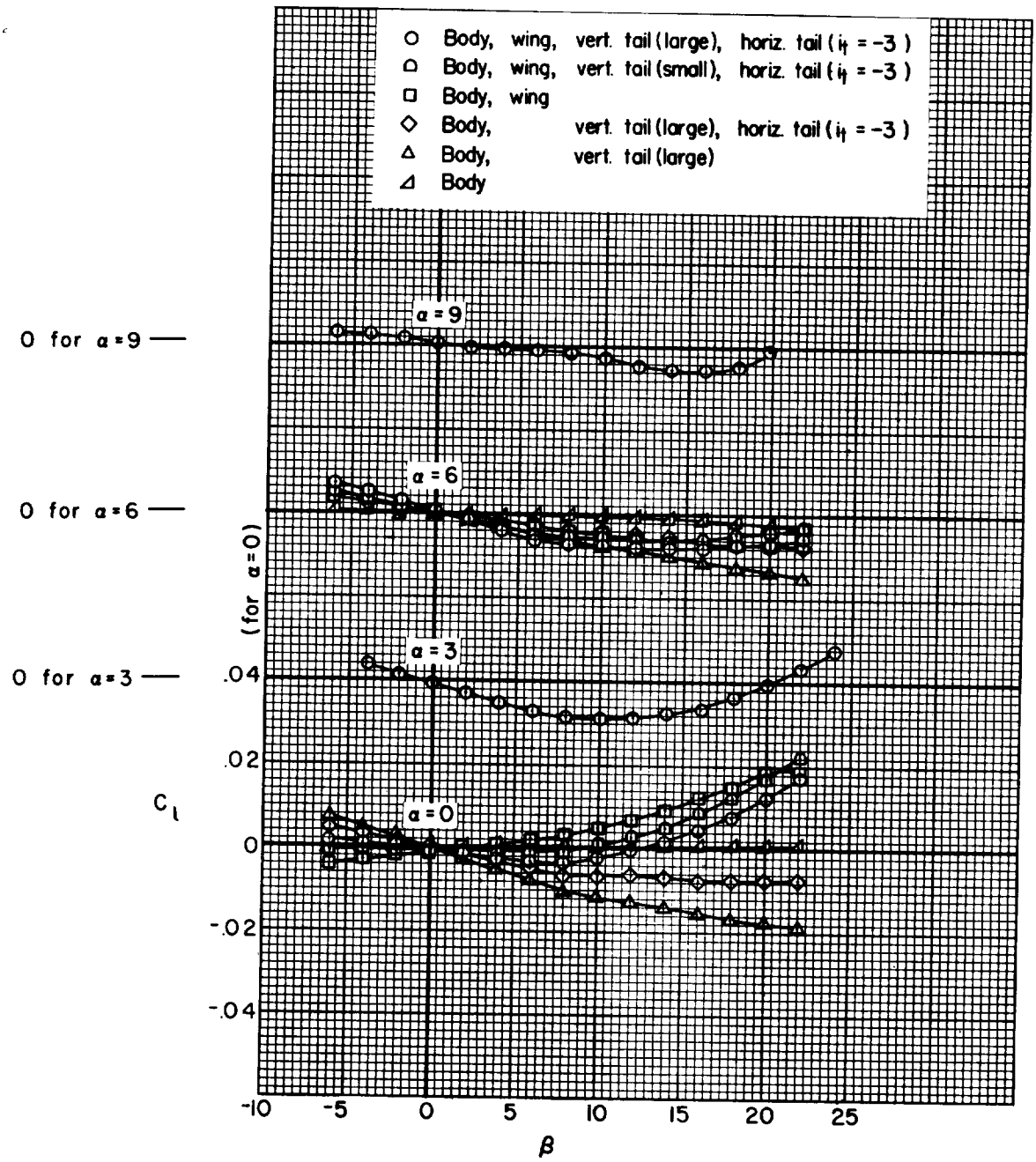

(b) M = 0.80

Figure 9.- Continued.

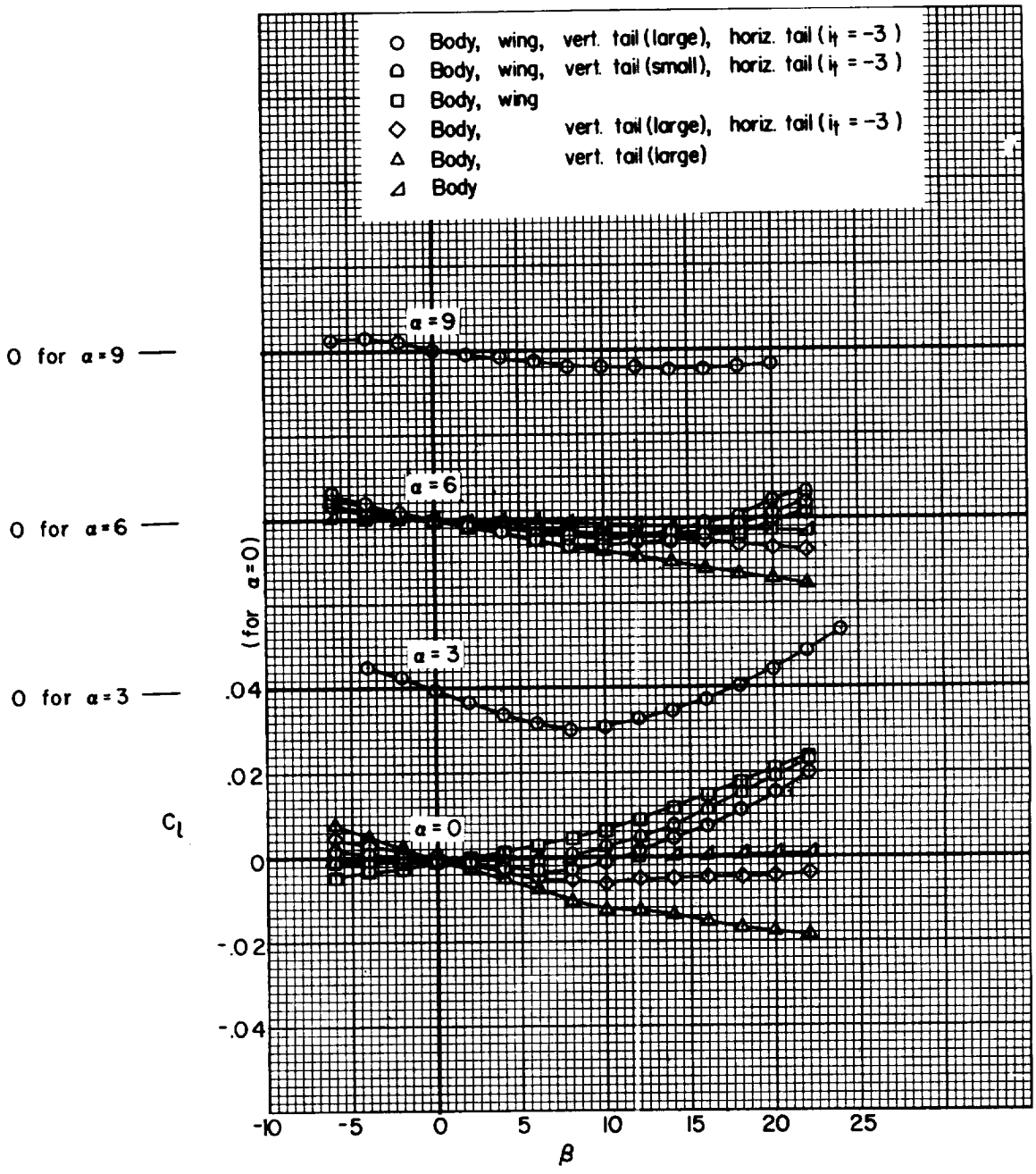

(c) M = 0.90

Figure 9.- Continued.

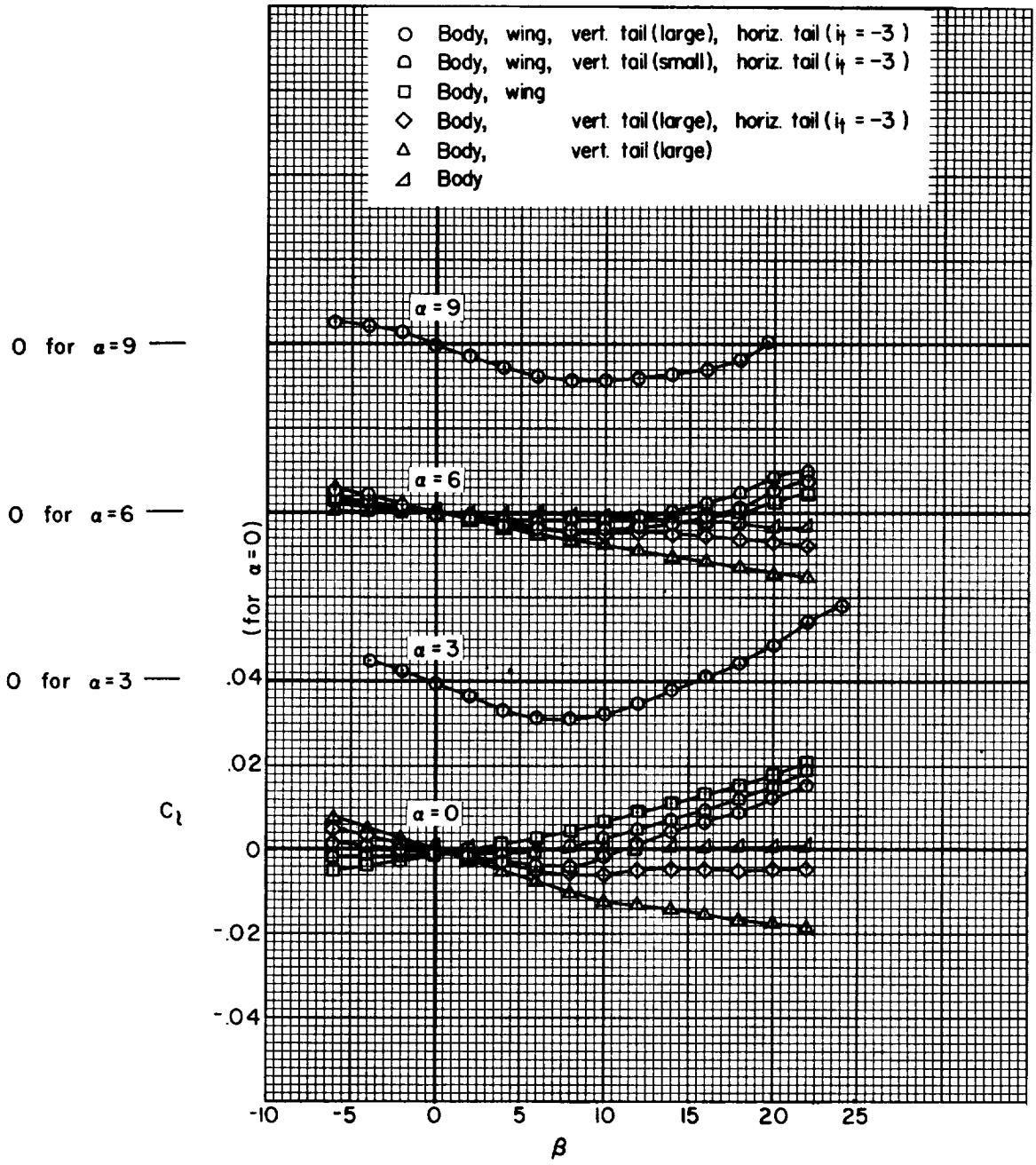

(d) M = 0.92

Figure 9.- Continued.

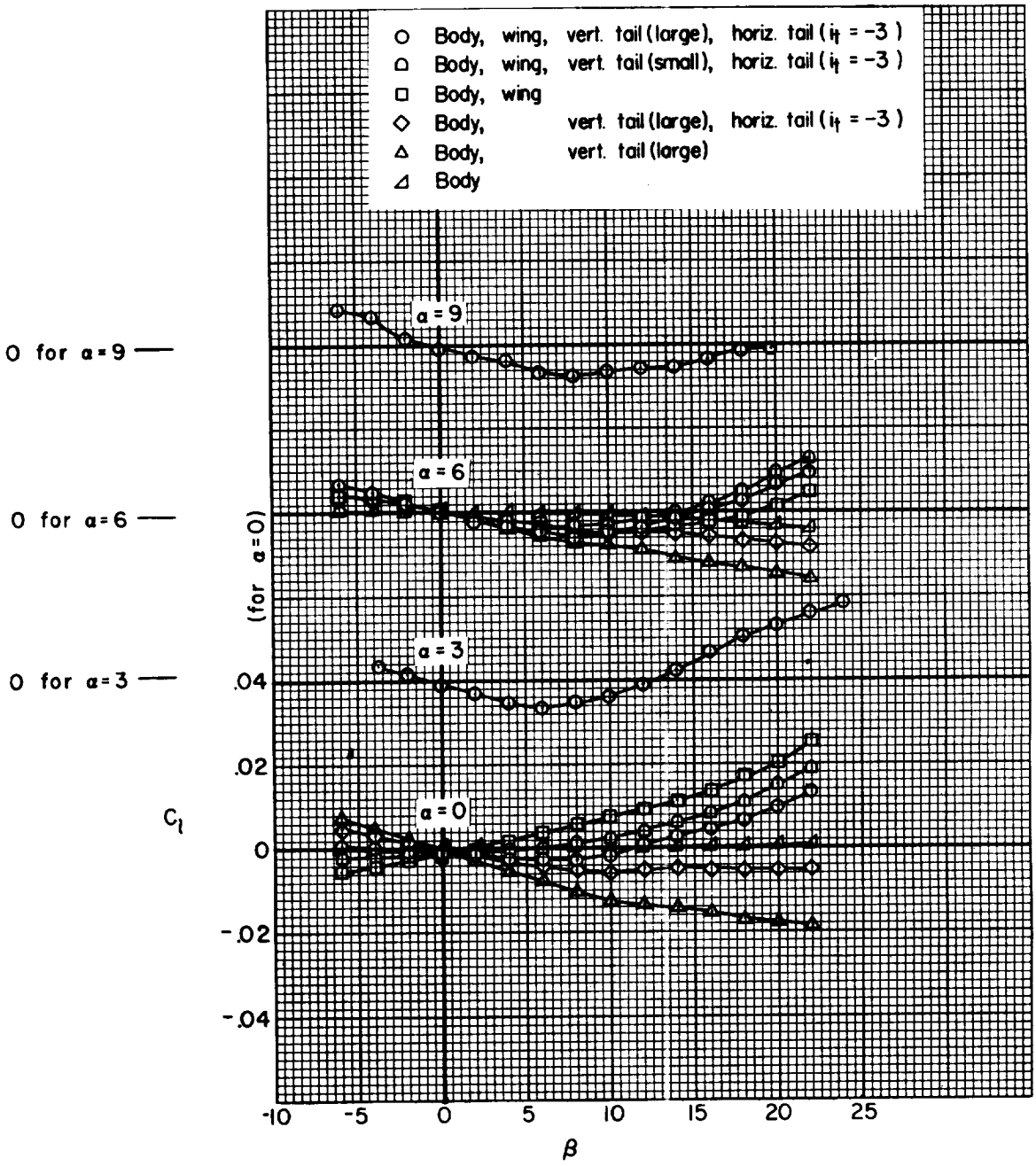

(e) M = 0.94

Figure 9.- Concluded.

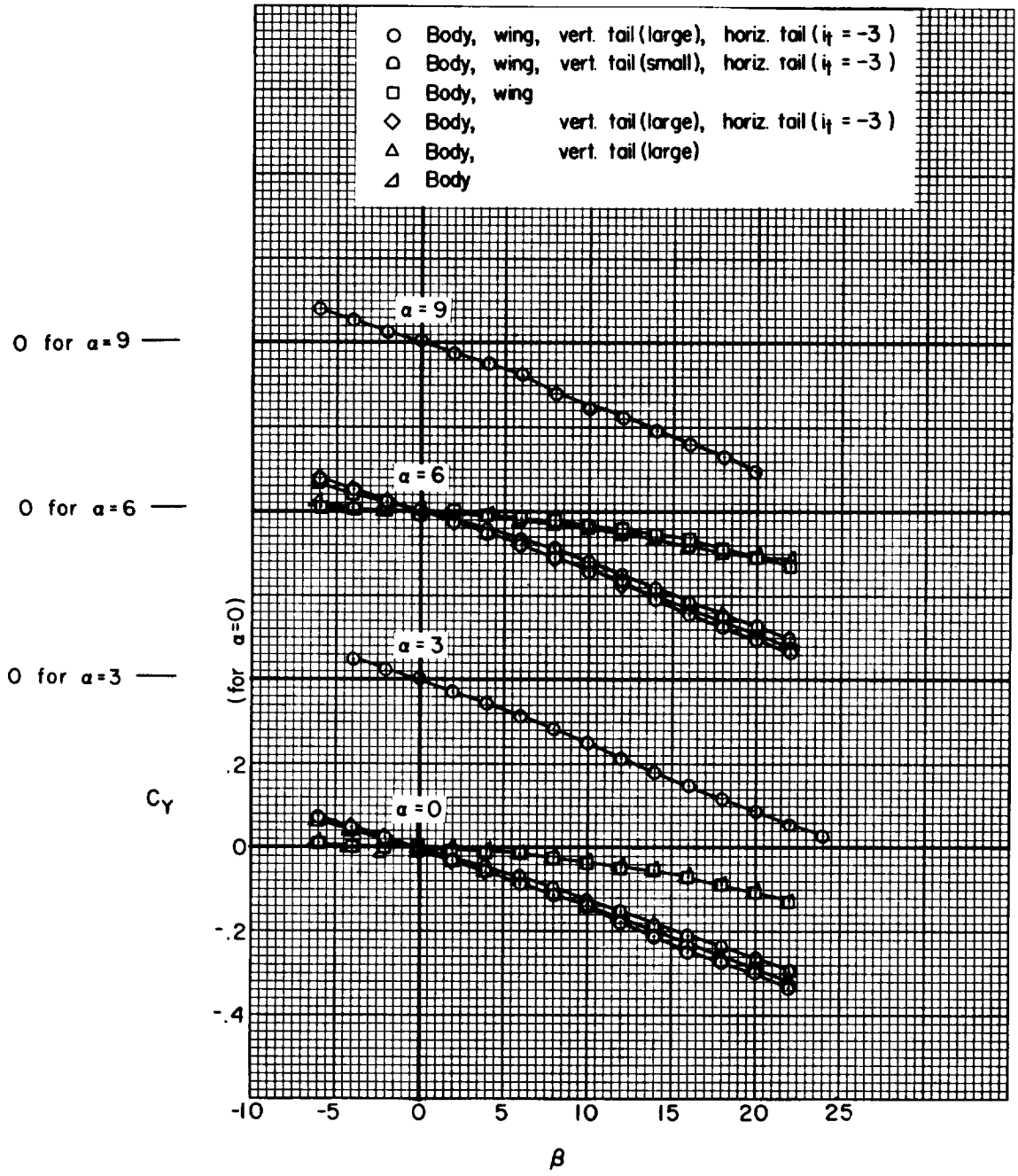

(a) M = 0.23

Figure 10.- Variation of side-force coefficient with sideslip angle.

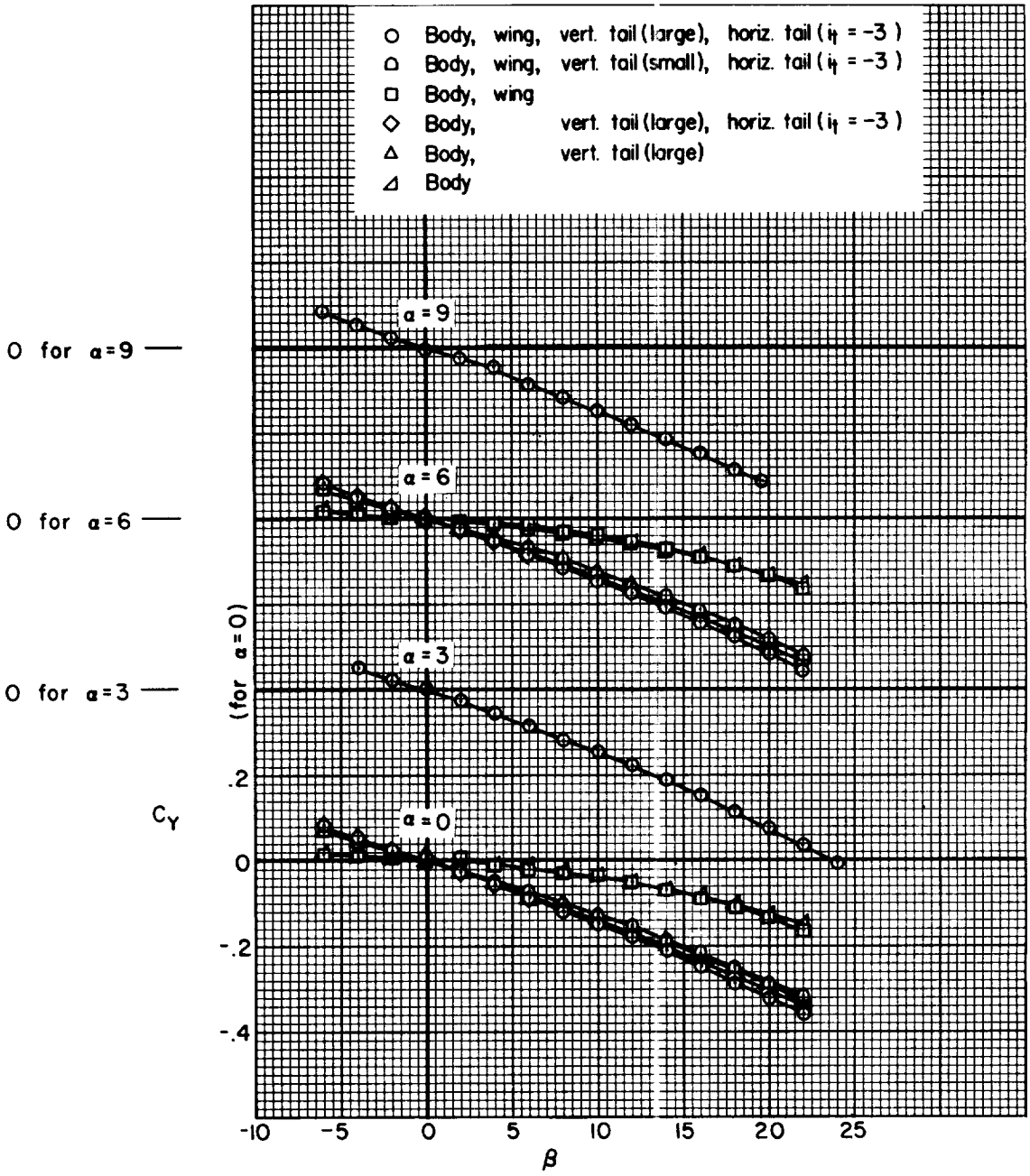

(b) M = 0.80

Figure 10.- Continued.

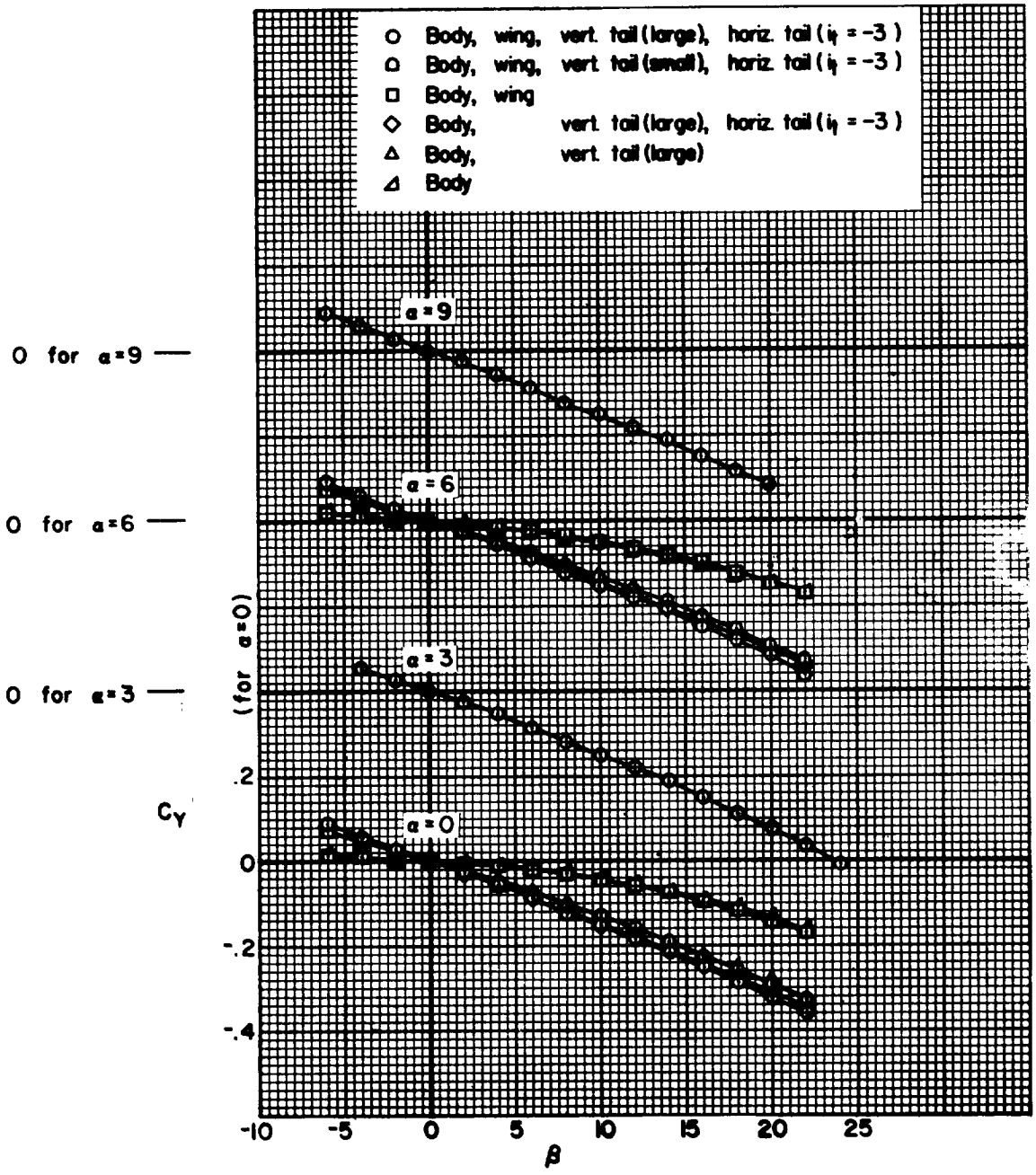

(c) M = 0.90

Figure 10.- Continued.

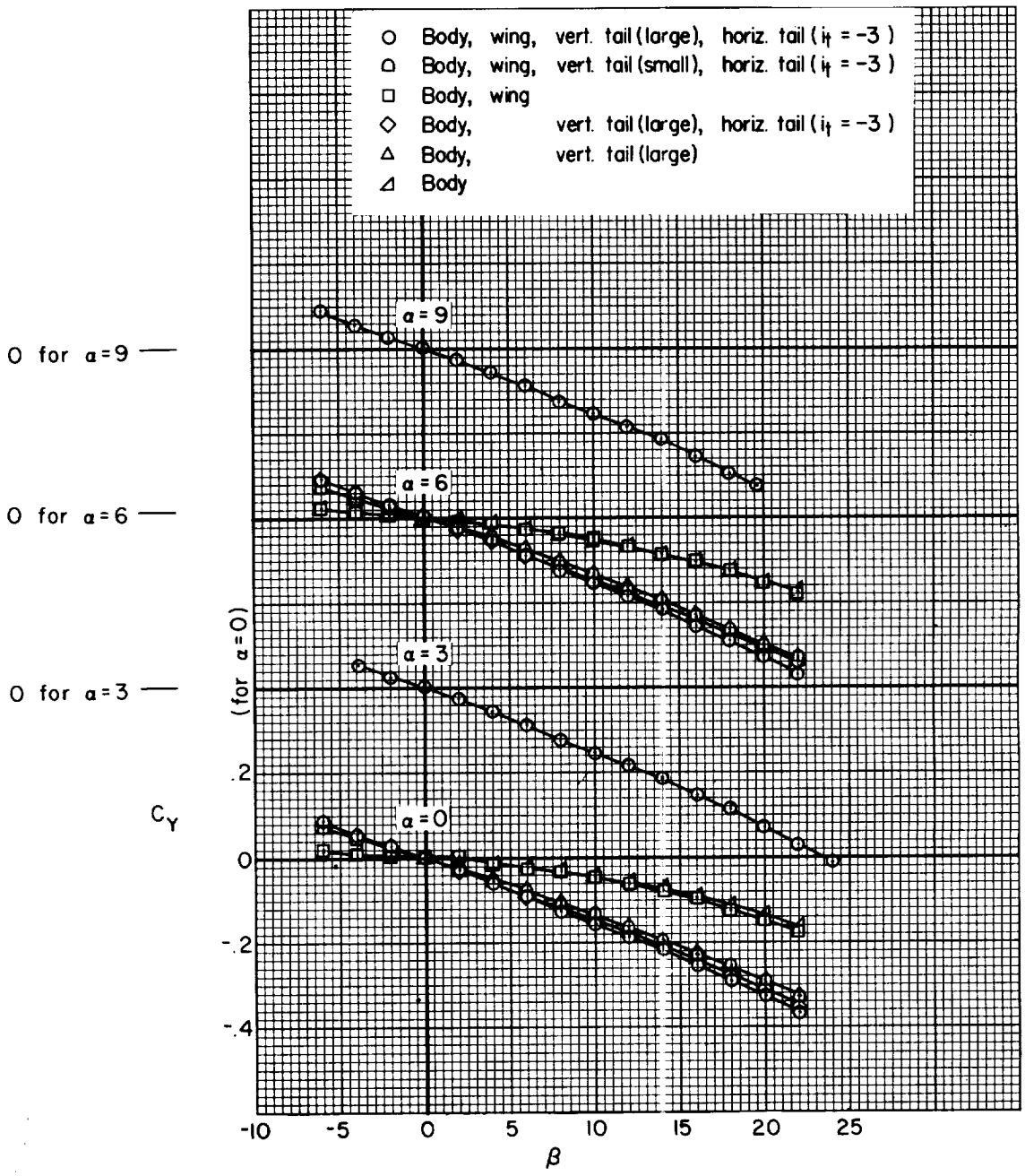

(d) M = 0.92

Figure 10.- Continued.

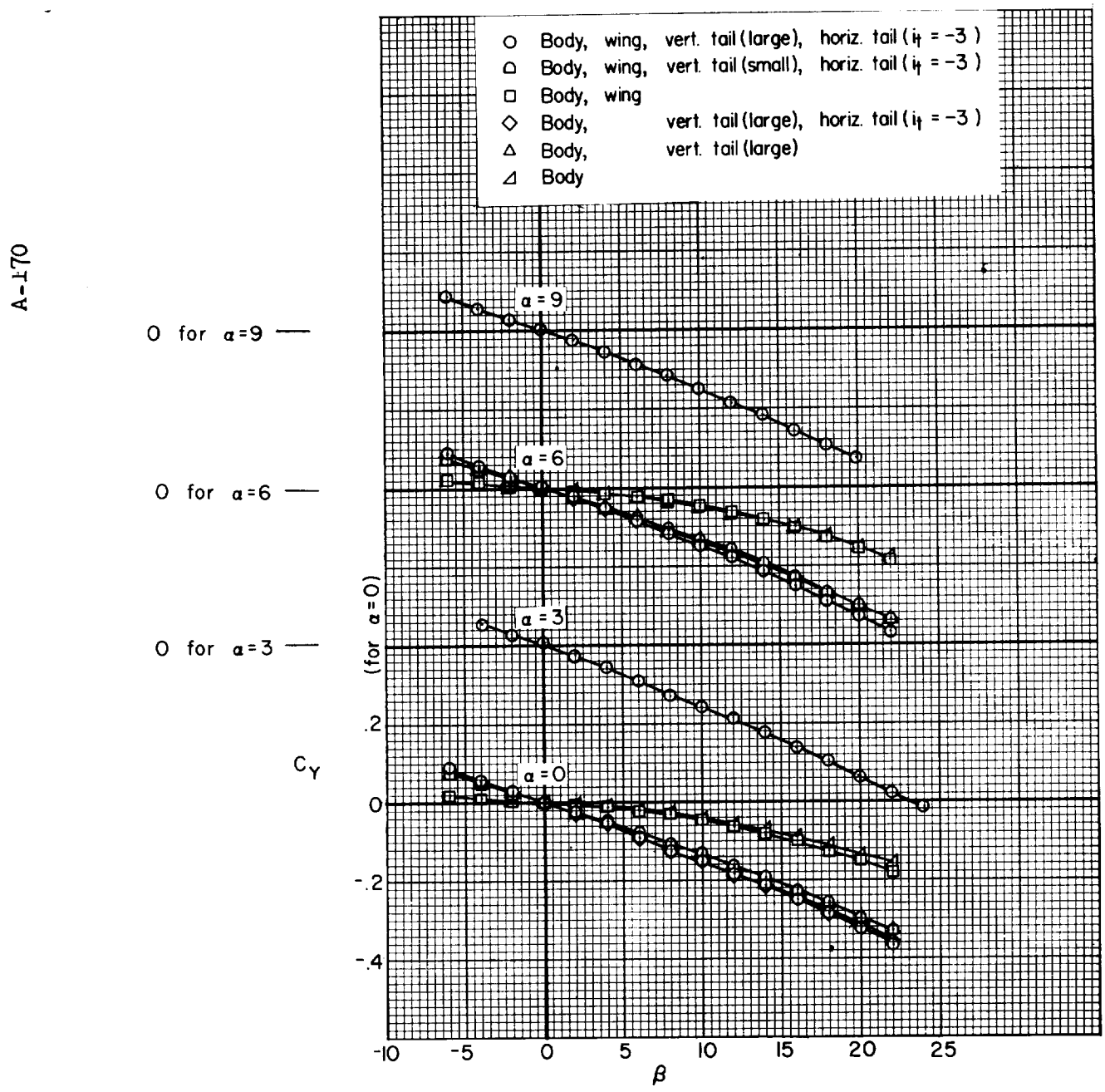

(e) M = 0.94

Figure 10.- Concluded.

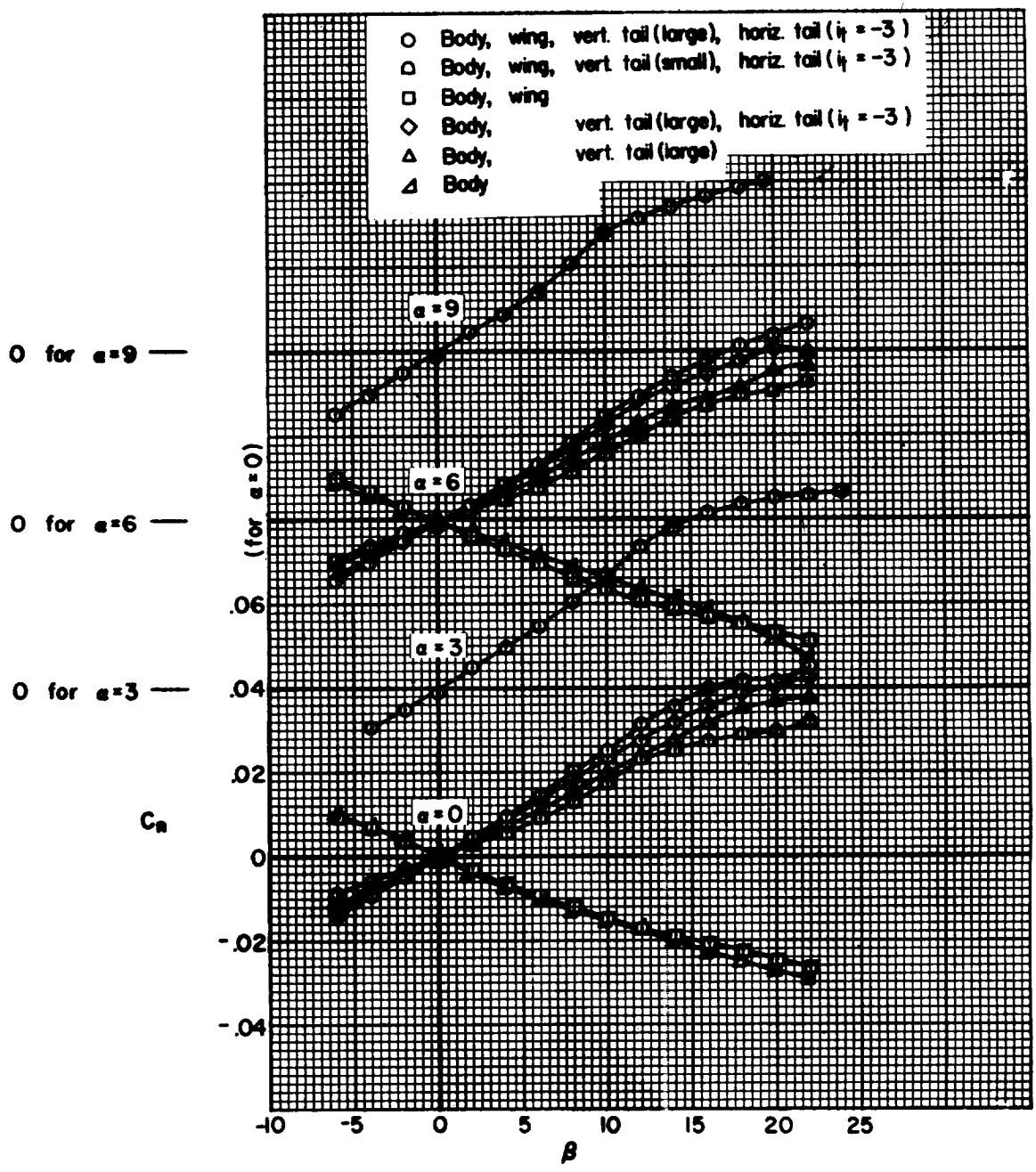

(a) M = 0.23

Figure 11.- Variation of yawing-moment coefficient with sideslip angle.

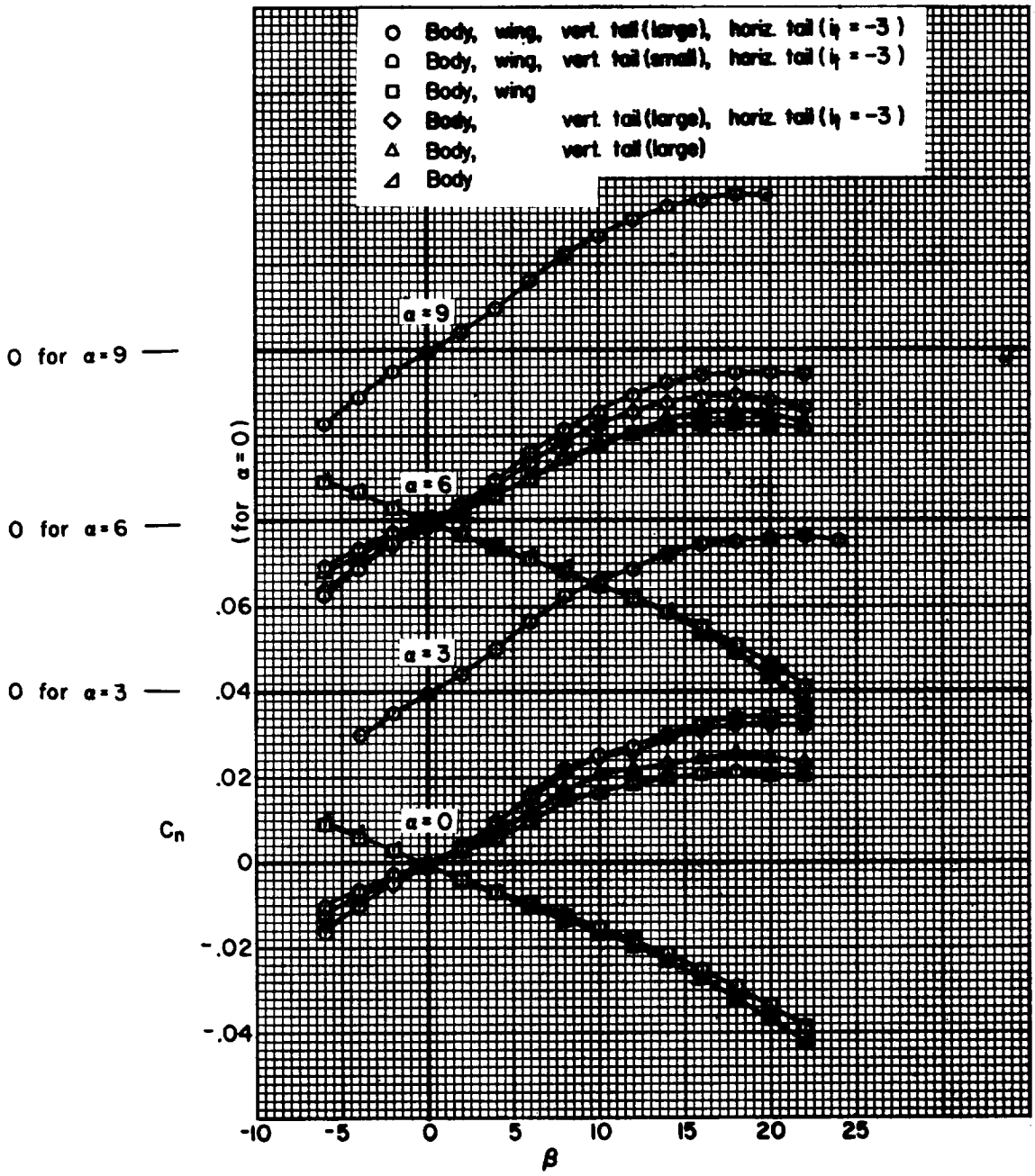

(b) M = 0.80

Figure 11.- Continued.

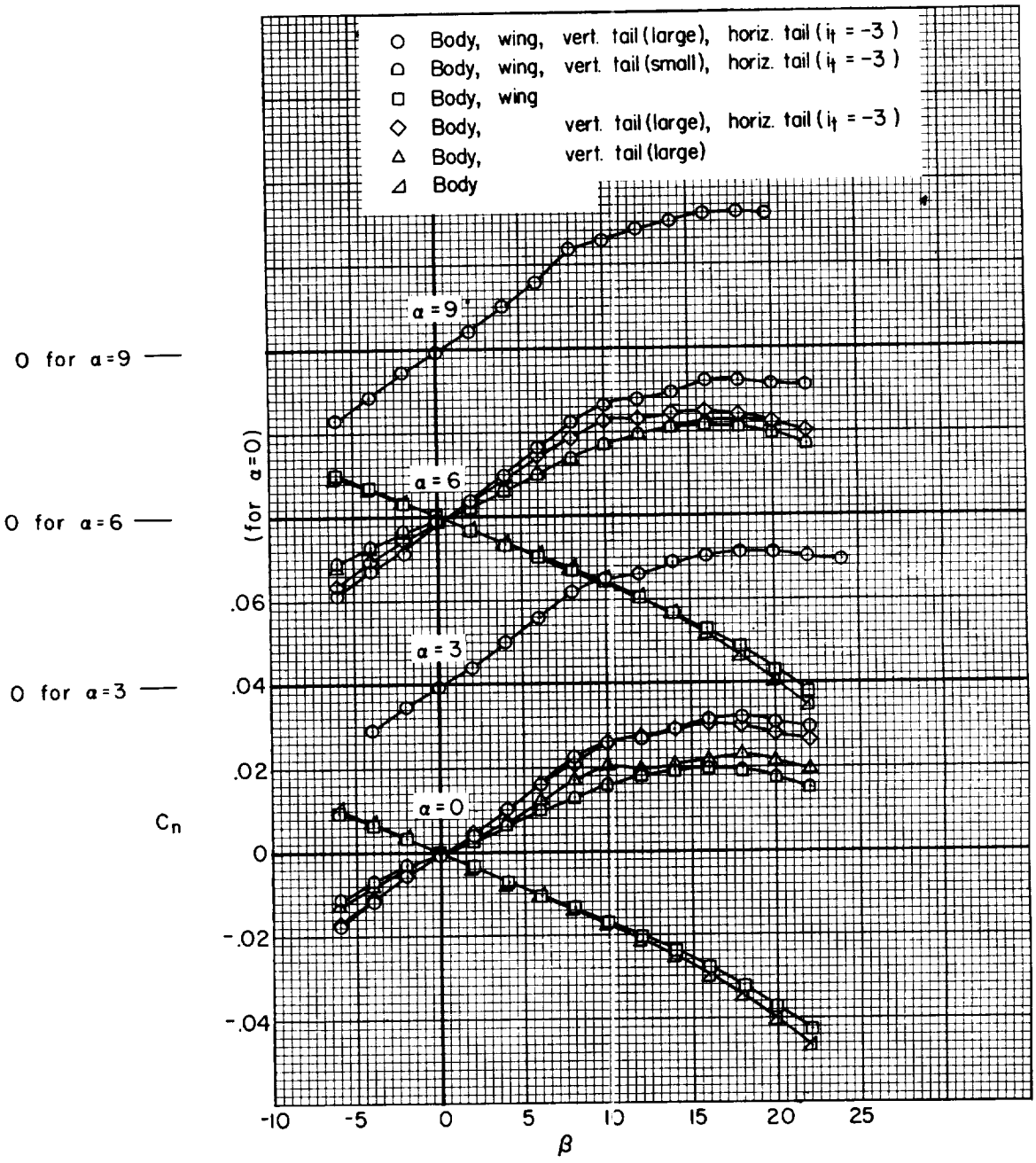

(c) M = 0.90

Figure 11.- Continued.

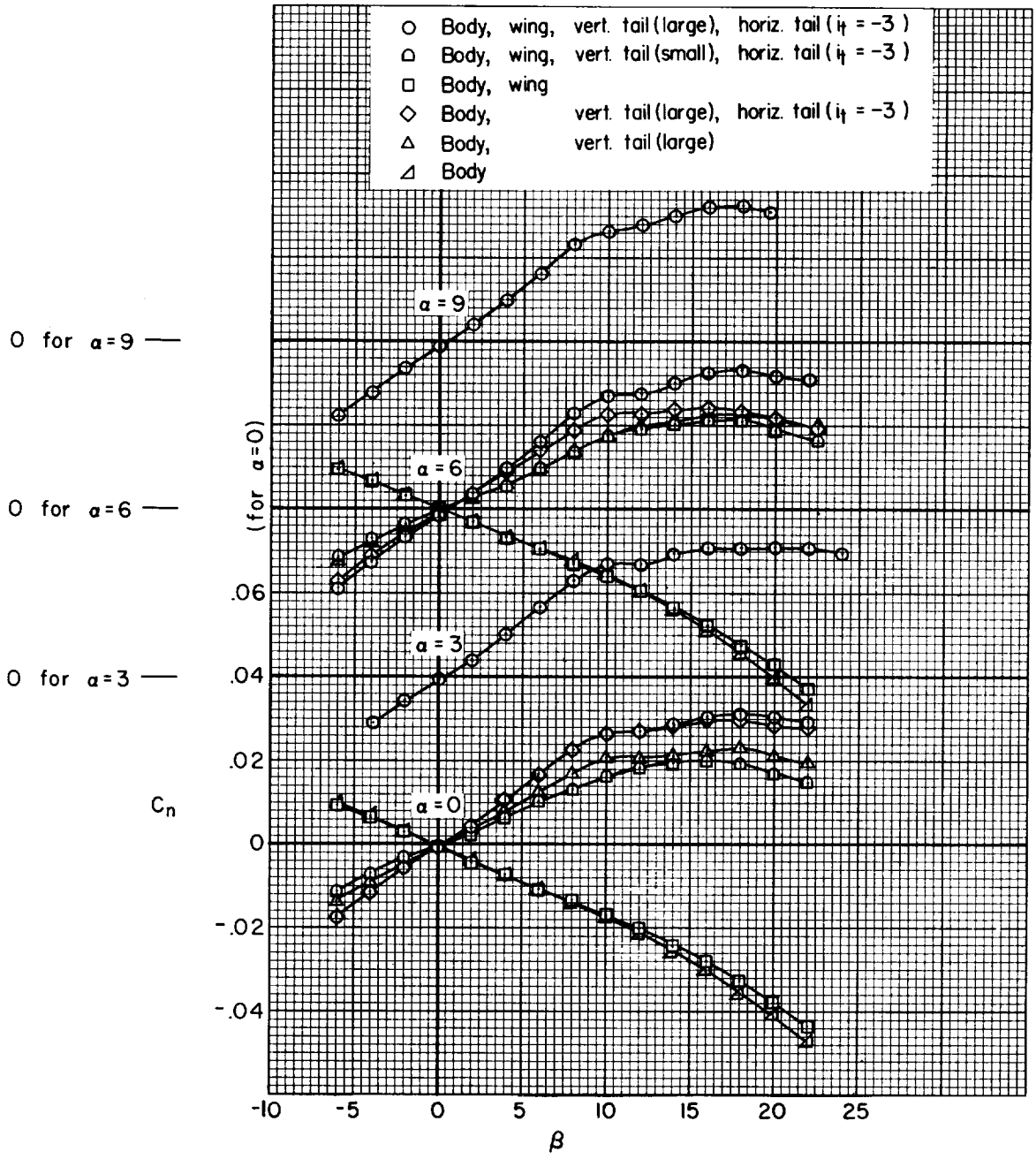

(d) M = 0.92

Figure 11.- Continued.

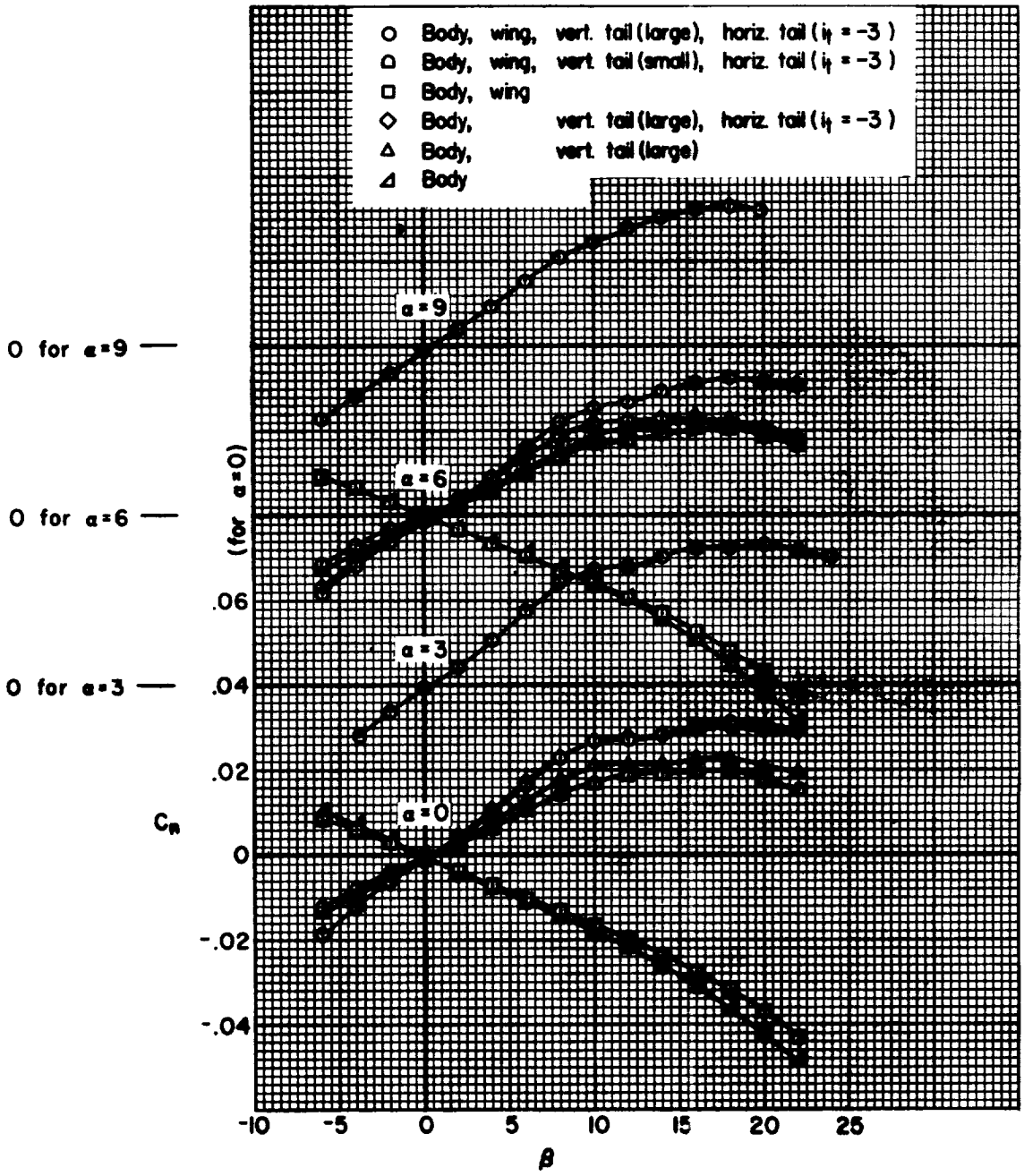

(e) M = 0.94

Figure 11.- Concluded.

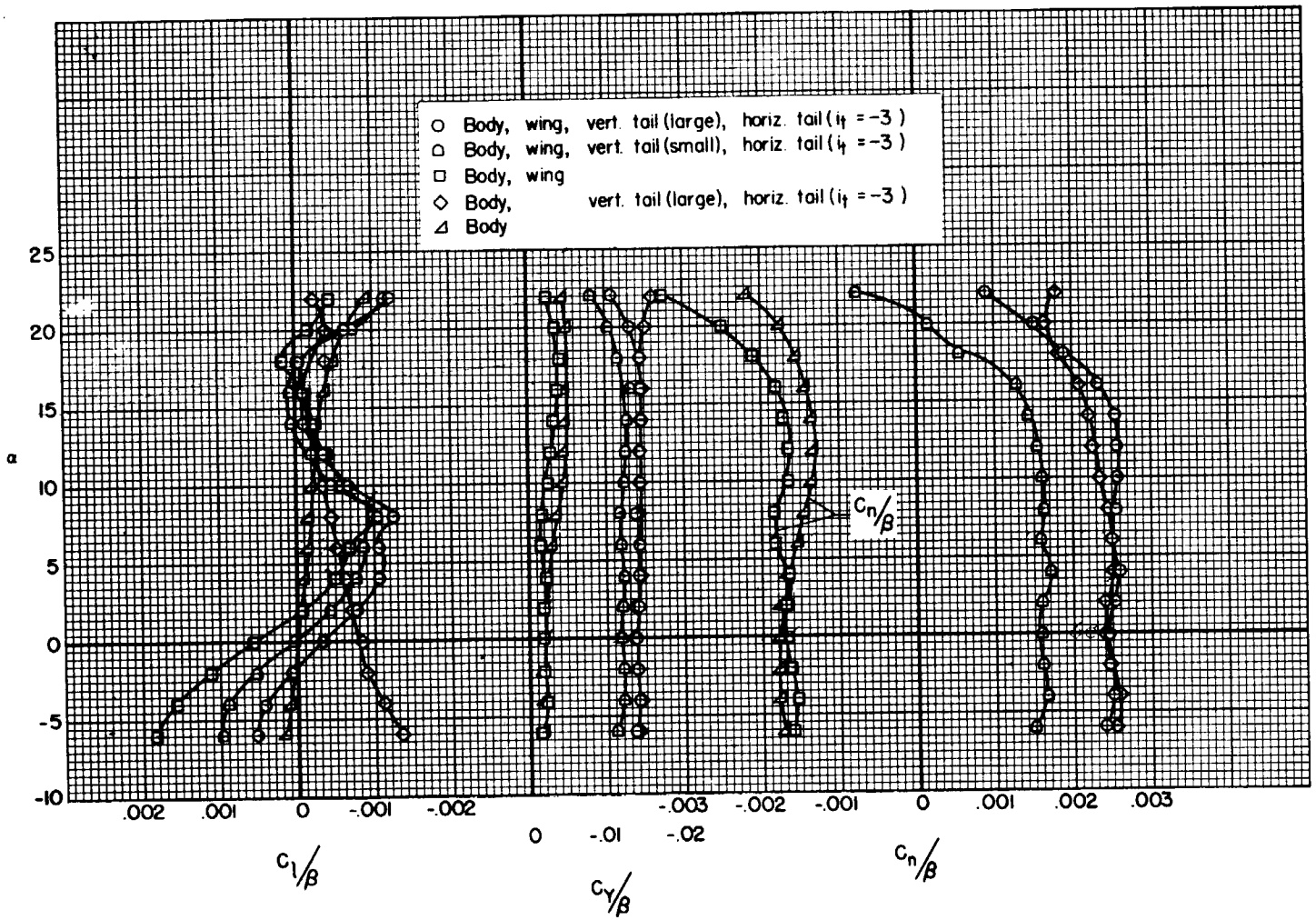

(a) M = 0.23

Figure 12.- The variation with angle of attack of the lateral-directional static derivatives evaluated from data obtained at 6° of sideslip.

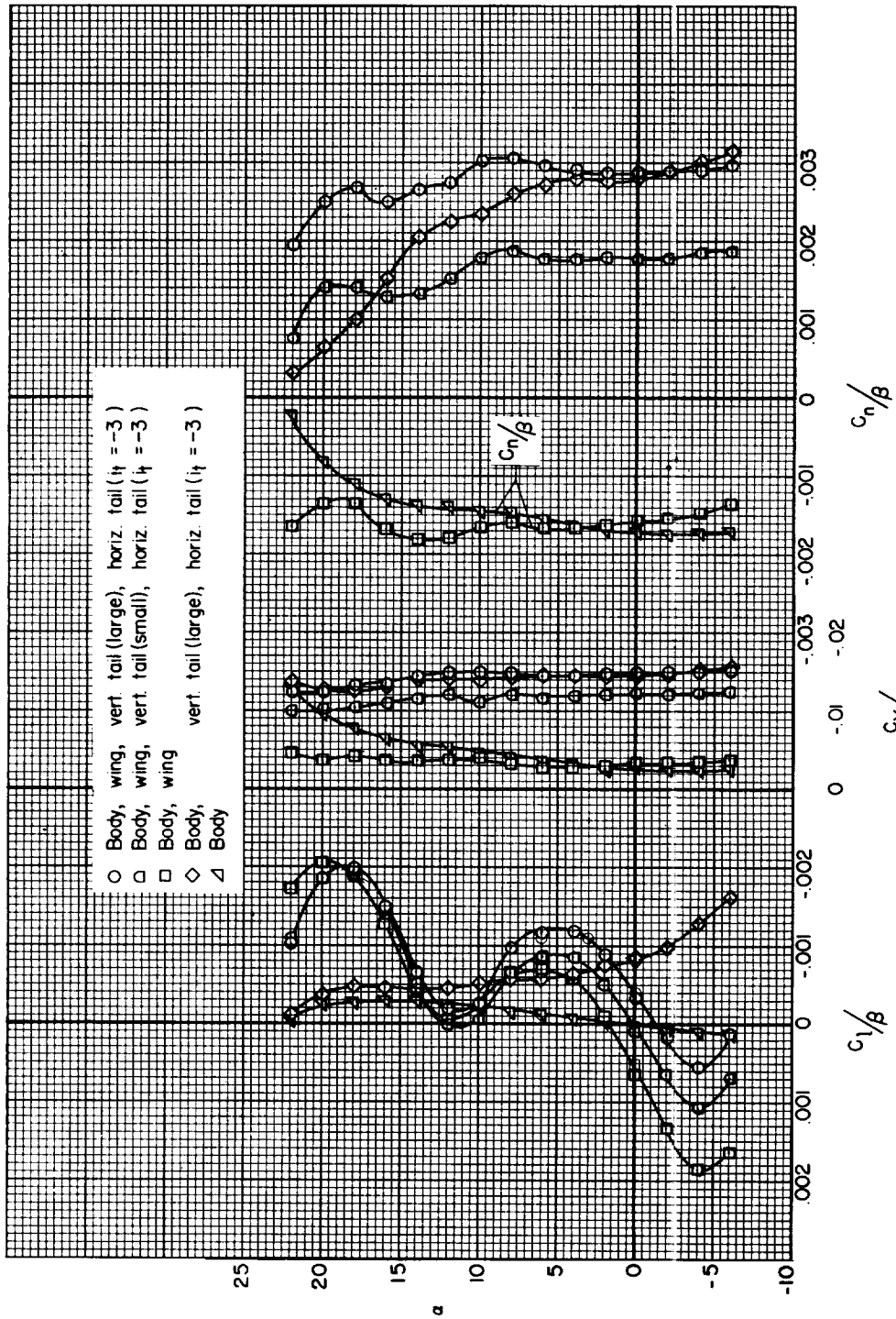

(b) M = 0.80

Figure 12.- Continued.

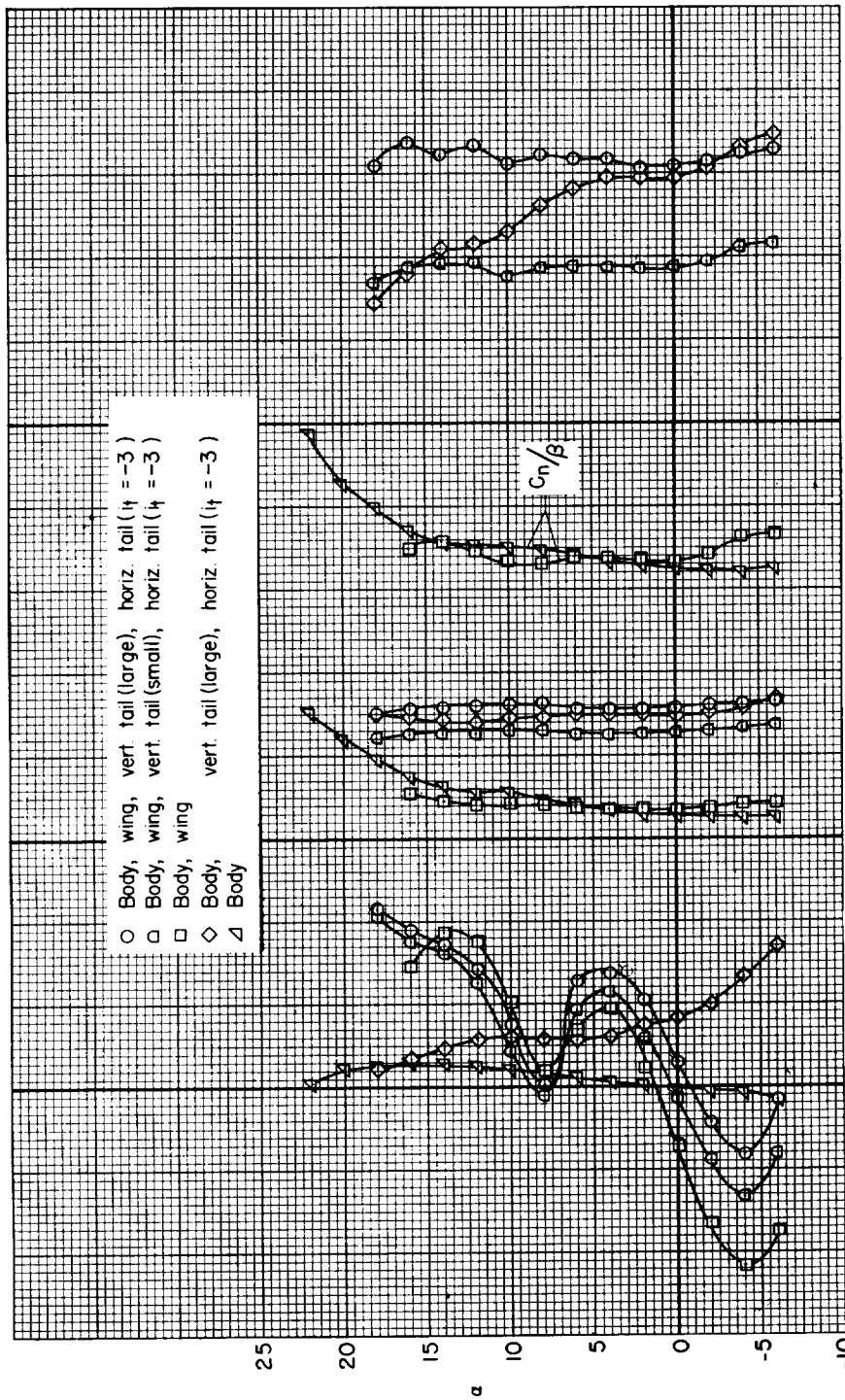

(c) M = 0.90

Figure 12.- Continued.

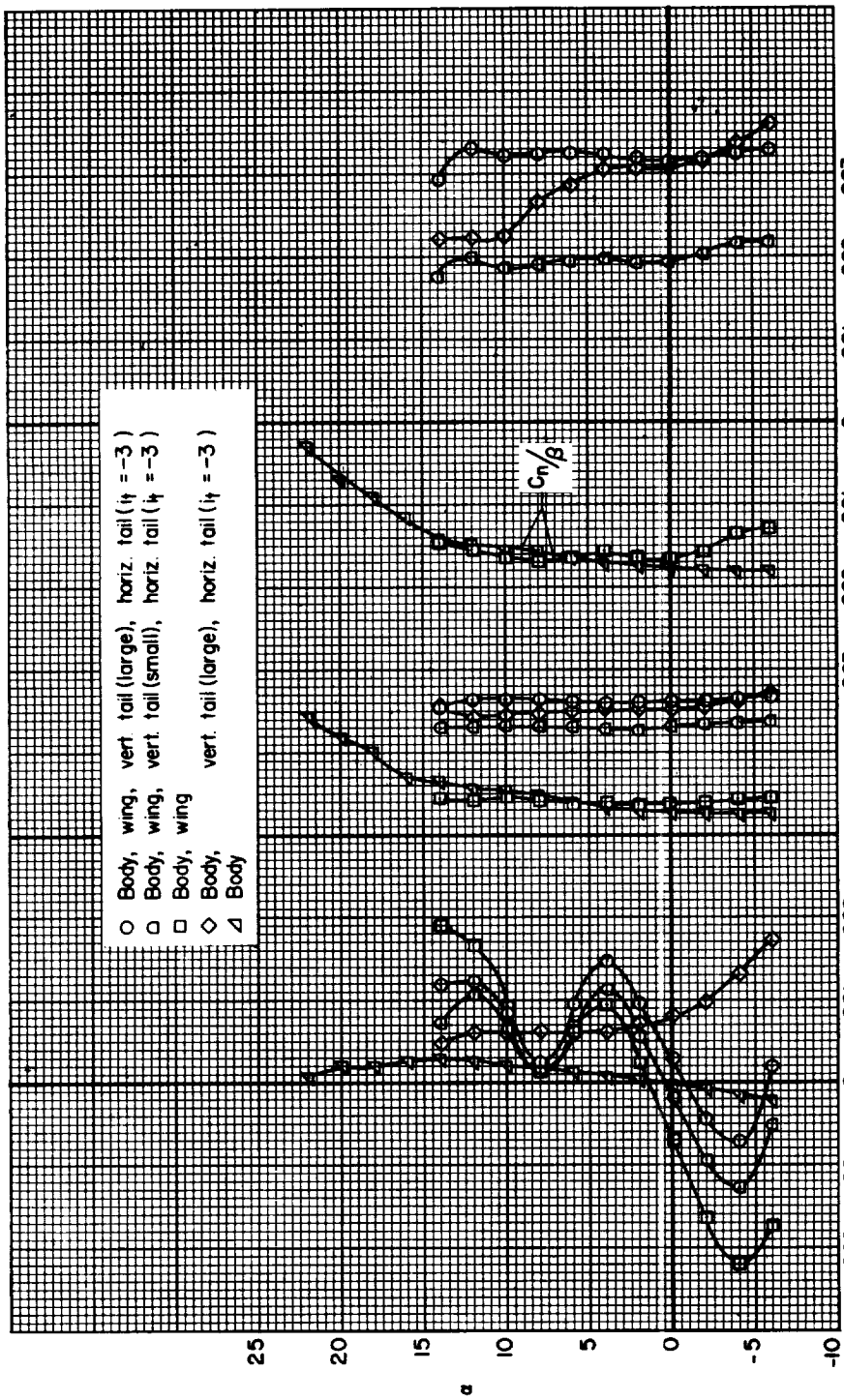

(d) M = 0.92

Figure 12.- Continued.

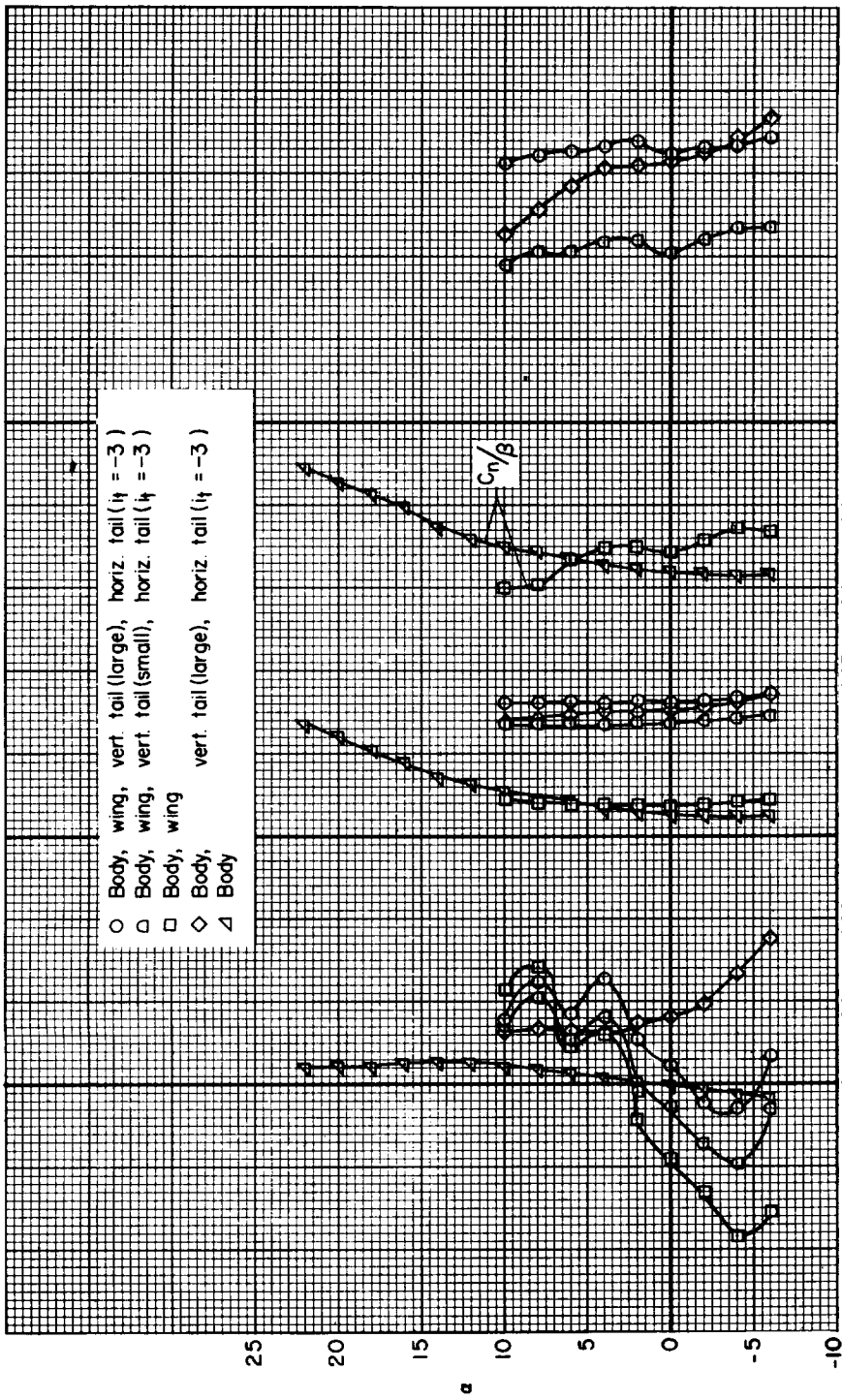

(e) M = 0.94

Figure 12.- Concluded.

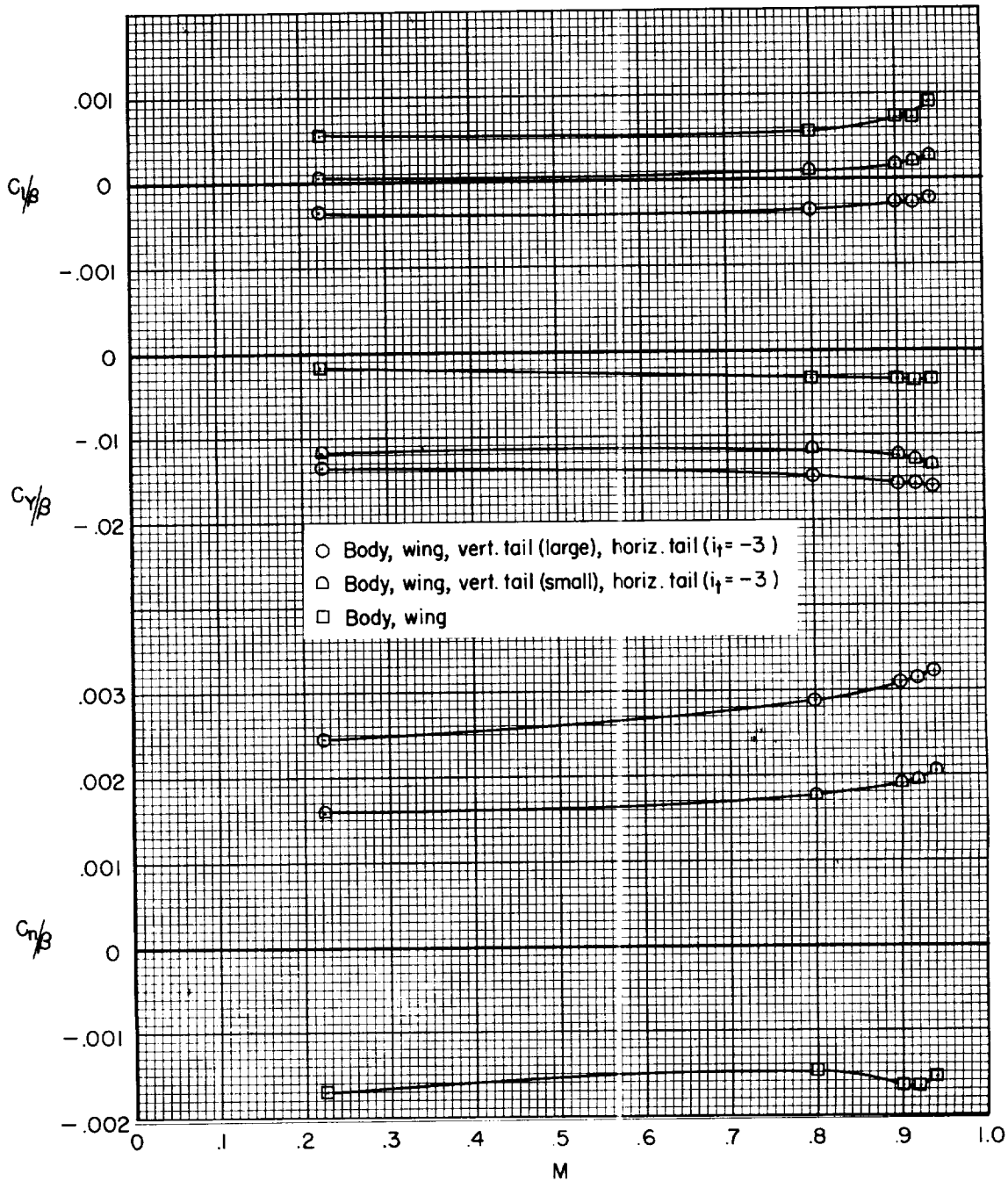

Figure 13.- Variation with Mach number of the lateral-directional derivatives; $\alpha = 0^{\circ}$.

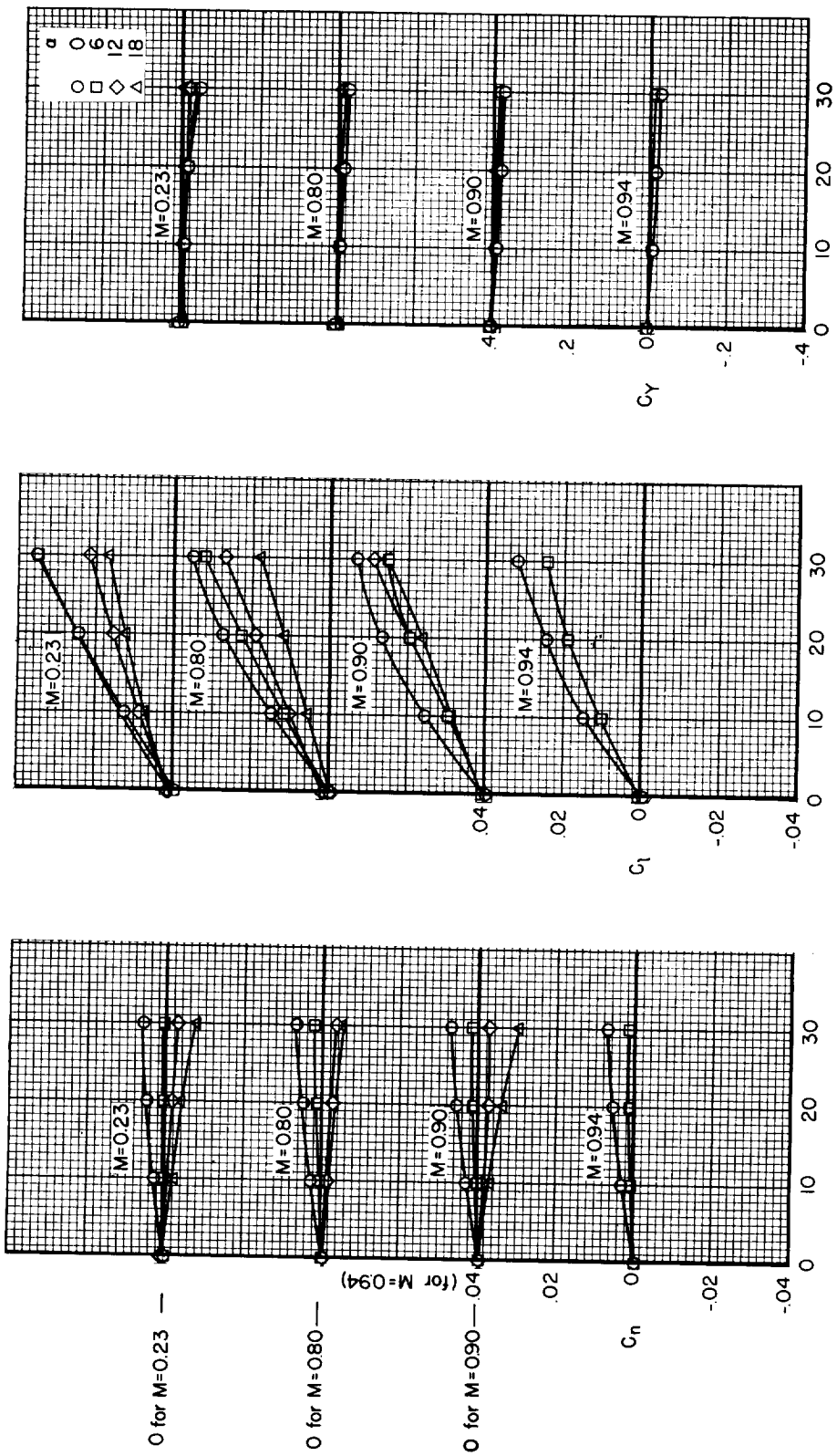

Figure 14.- Variation of yawing-moment, rolling-moment, and side-force coefficients with aileron deflection; $\beta = 0^\circ$.

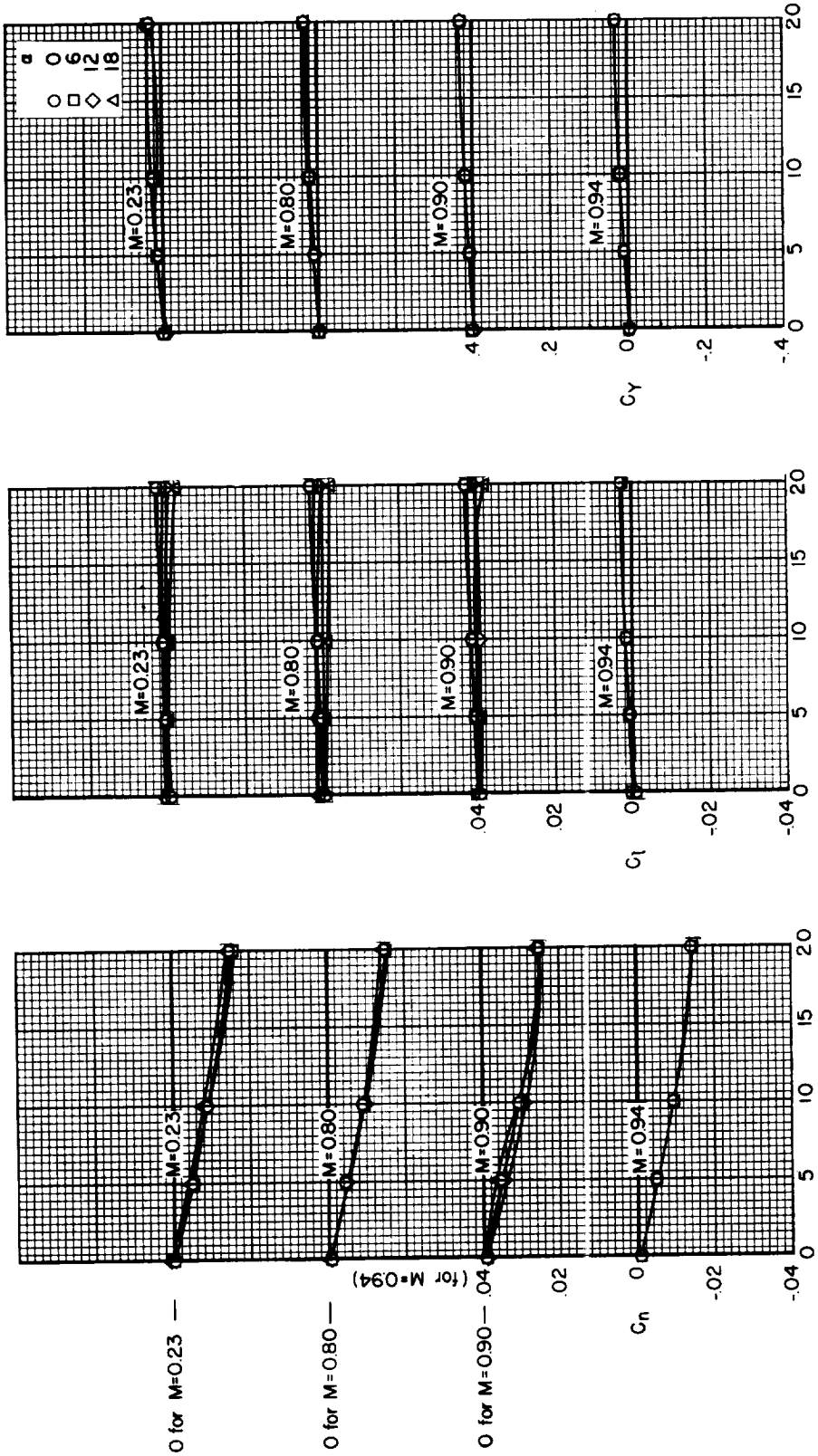

Figure 15.- Variation of yawing-moment, rolling-moment, and side-force coefficients with rudder deflection; $\beta = 0^{\circ}$.

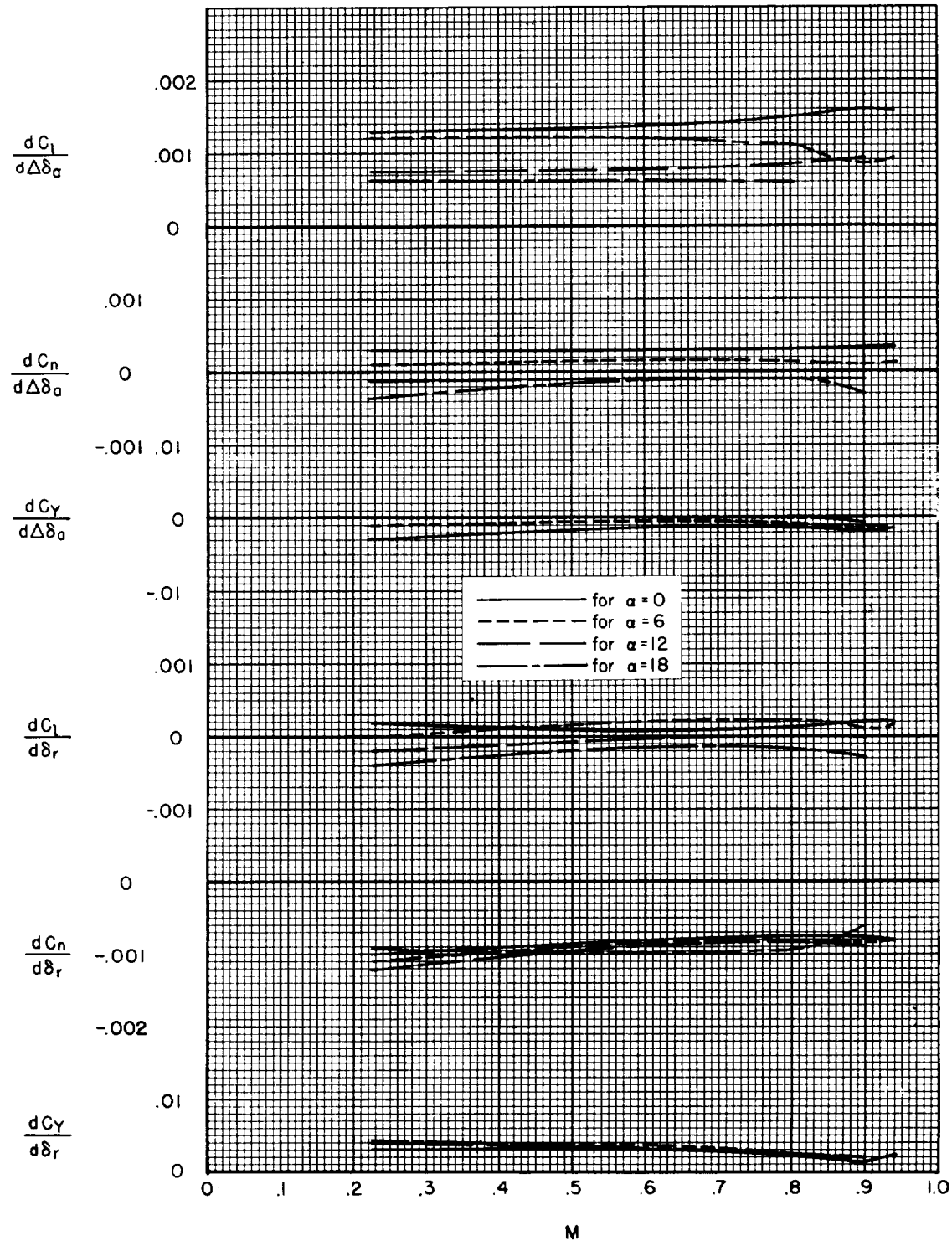

Figure 16.- Variation of control surface effectiveness with Mach number; $\beta = 0^{\circ}$.

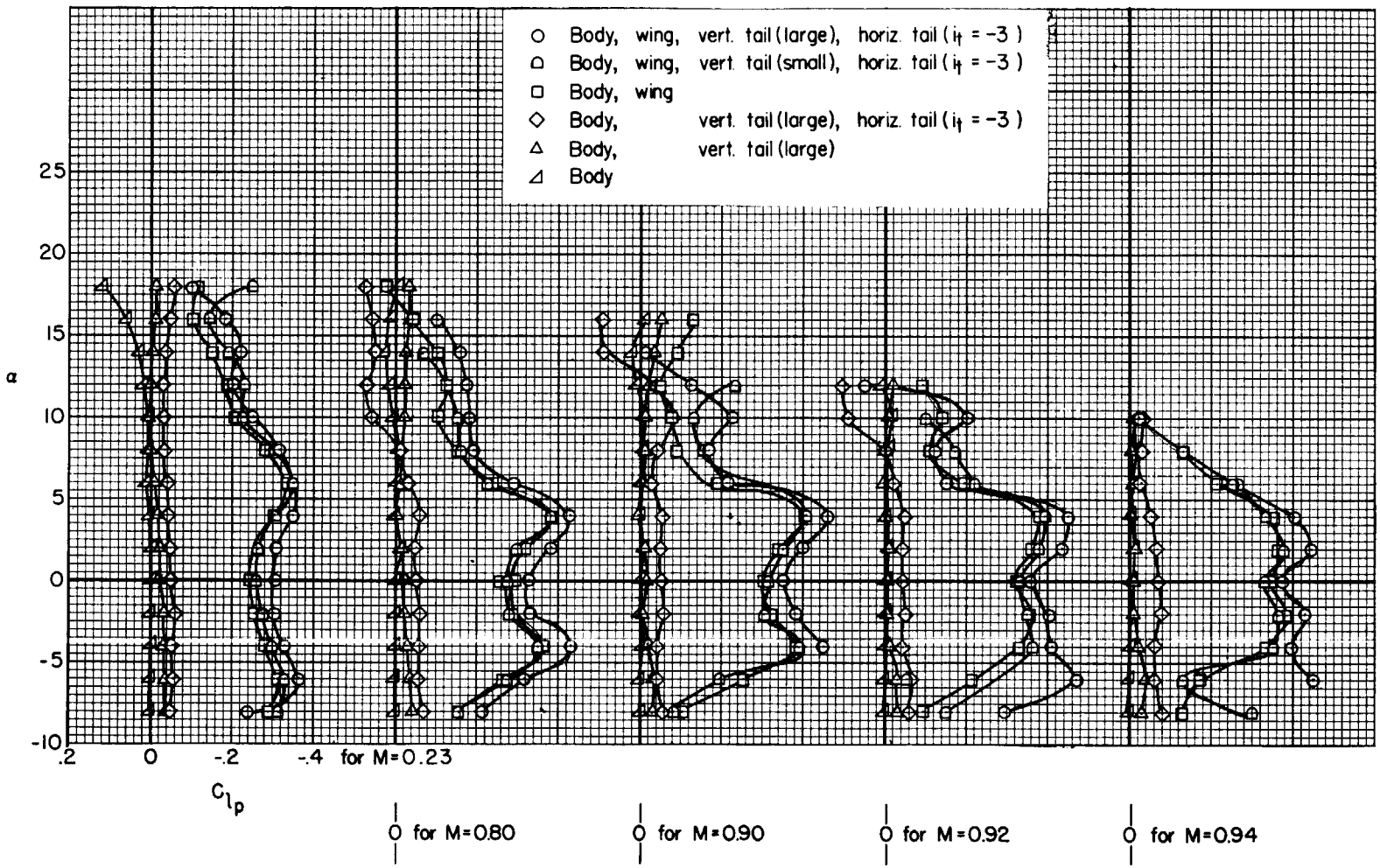

(a) C_{l_p}

Figure 17.- Variation of the lateral-directional dynamic stability derivatives with angle of attack.

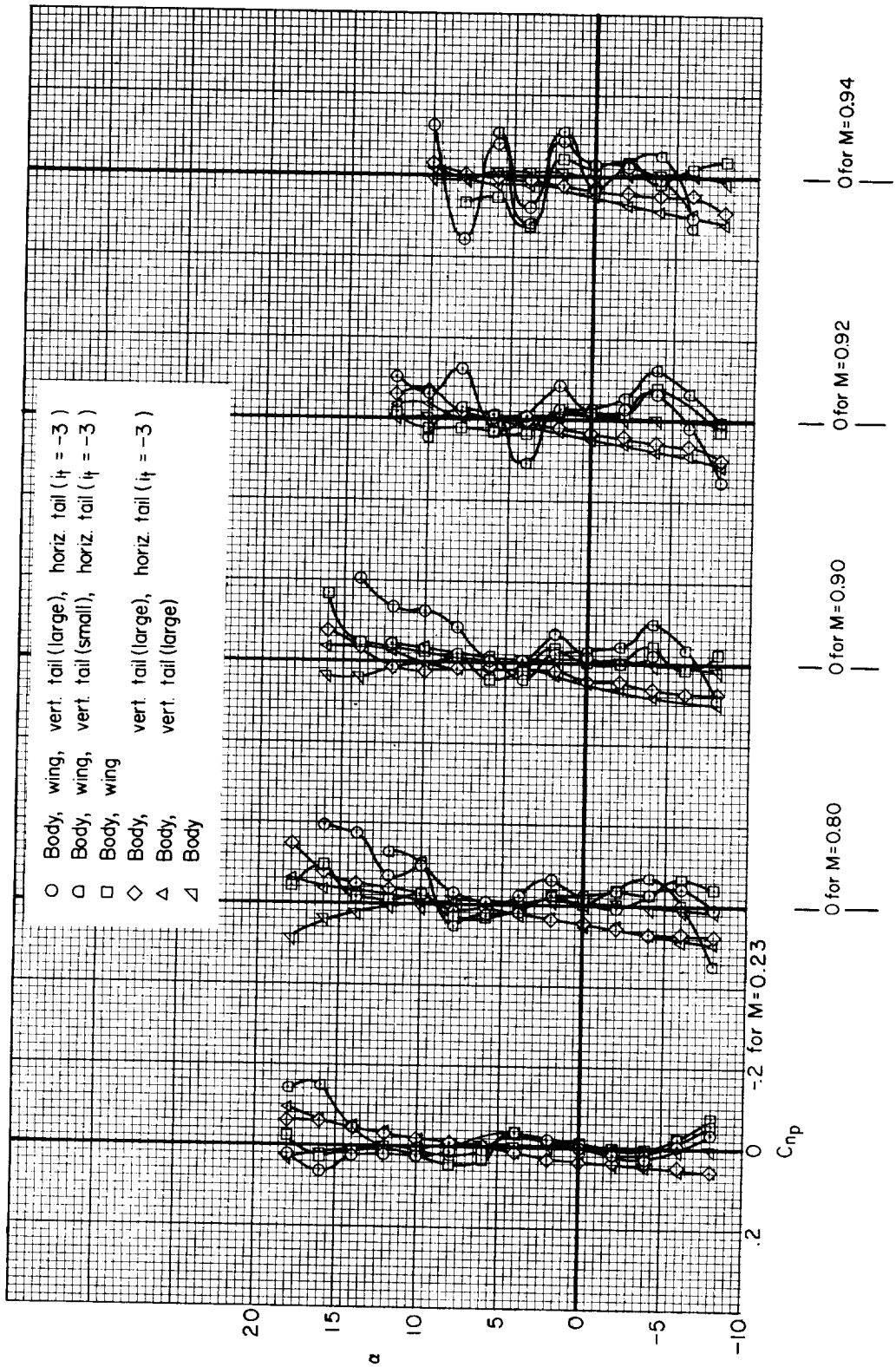

(b) C_{n_p}

Figure 17.- Continued.

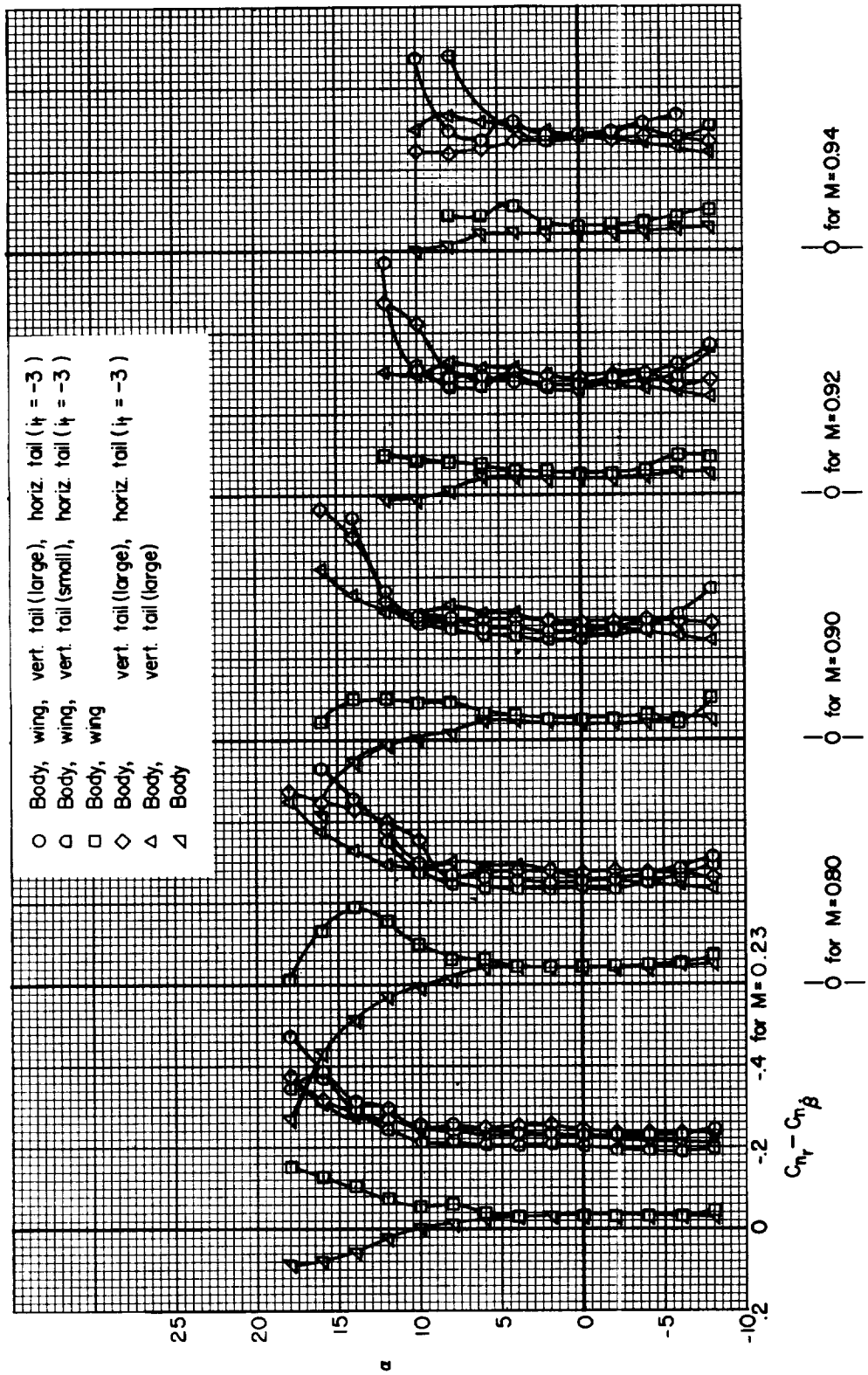

(c) $C_{n_r} - C_{n_{\dot{\beta}}}$

Figure 17.- Continued.

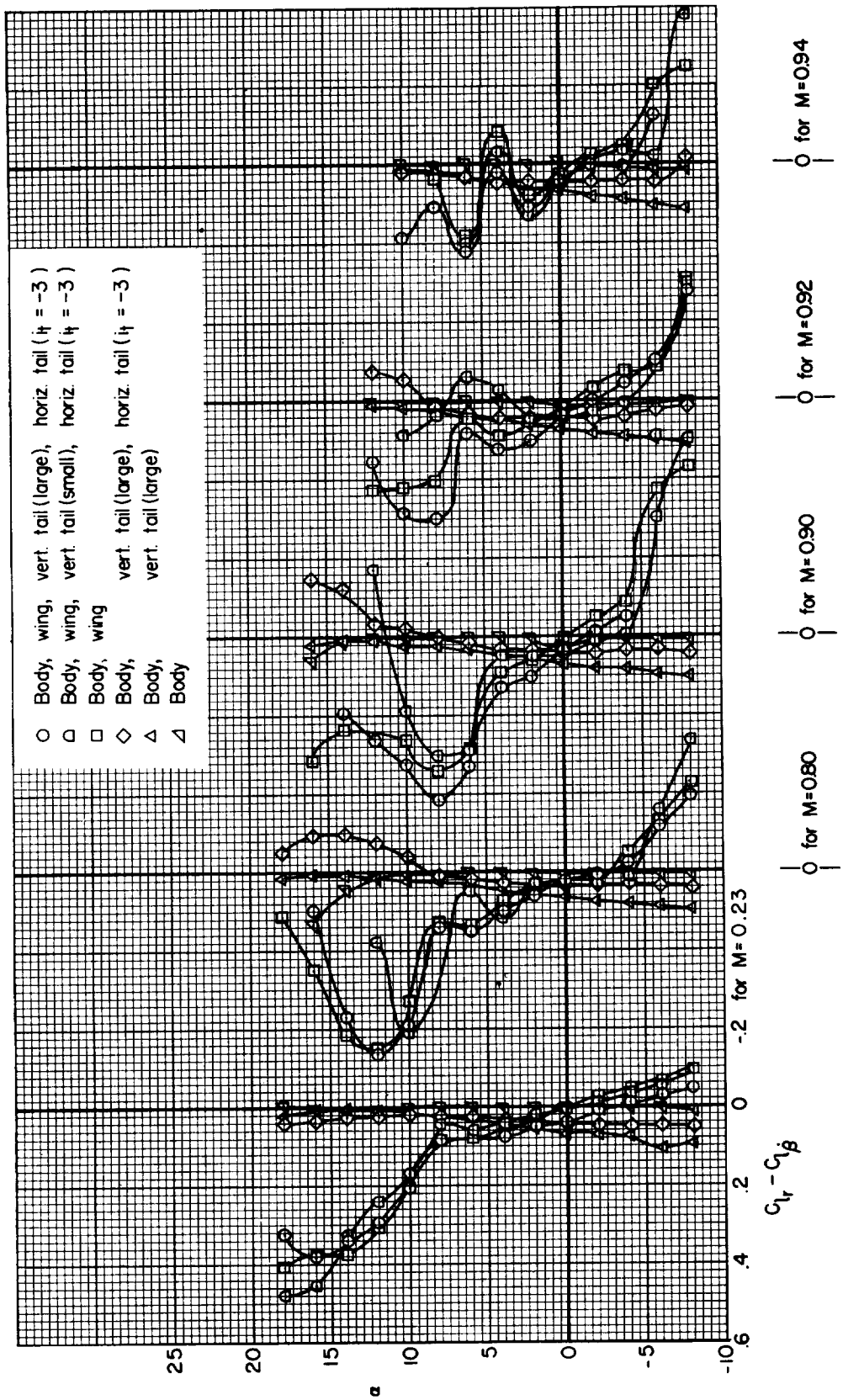

(d) $C_{l_r} - C_{l_{\dot{\beta}}}$

Figure 17.- Concluded.

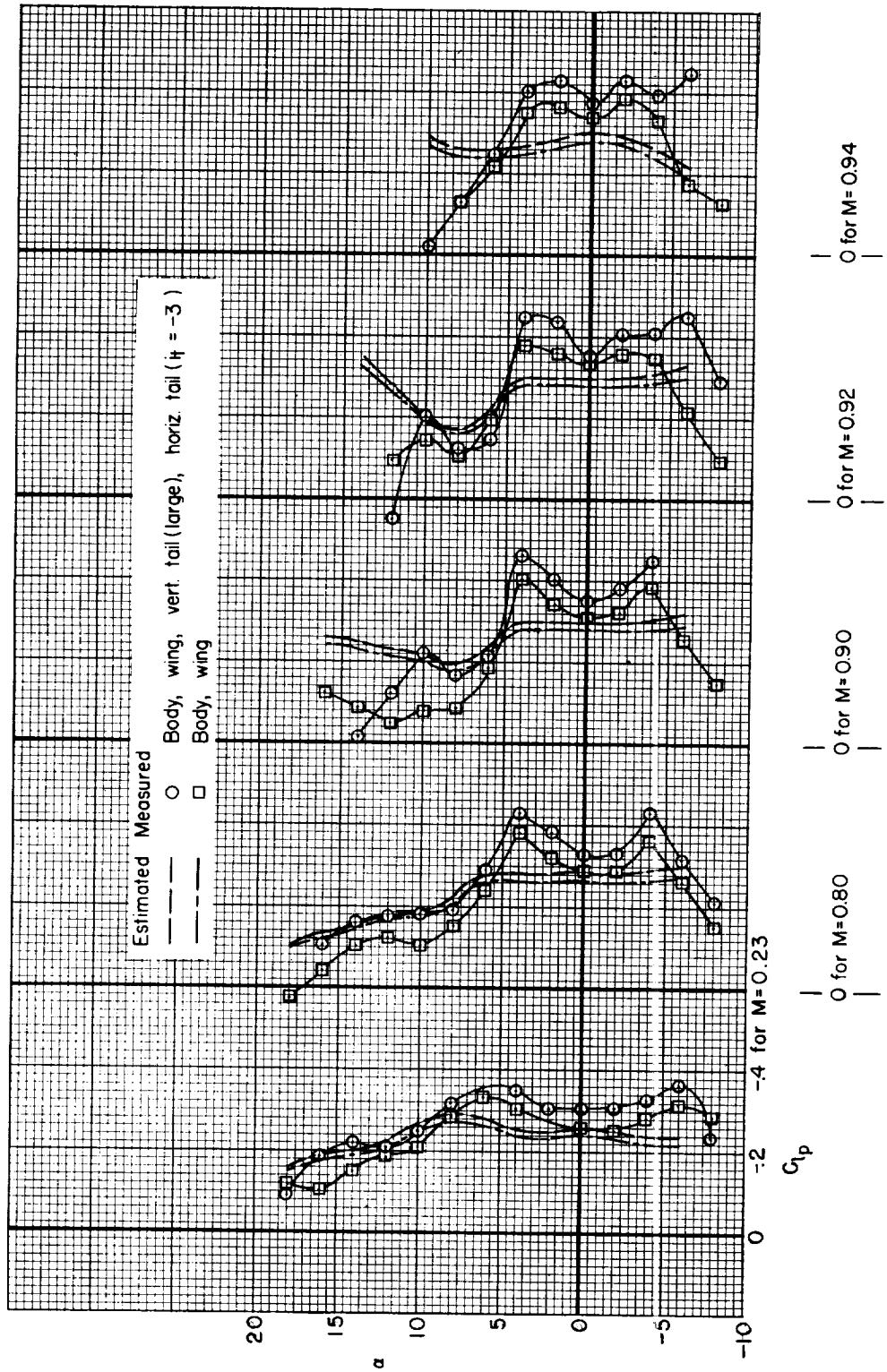

(a) C_{l_p}

Figure 18.- Comparison of measured and estimated values of the lateral-directional dynamic stability derivatives.

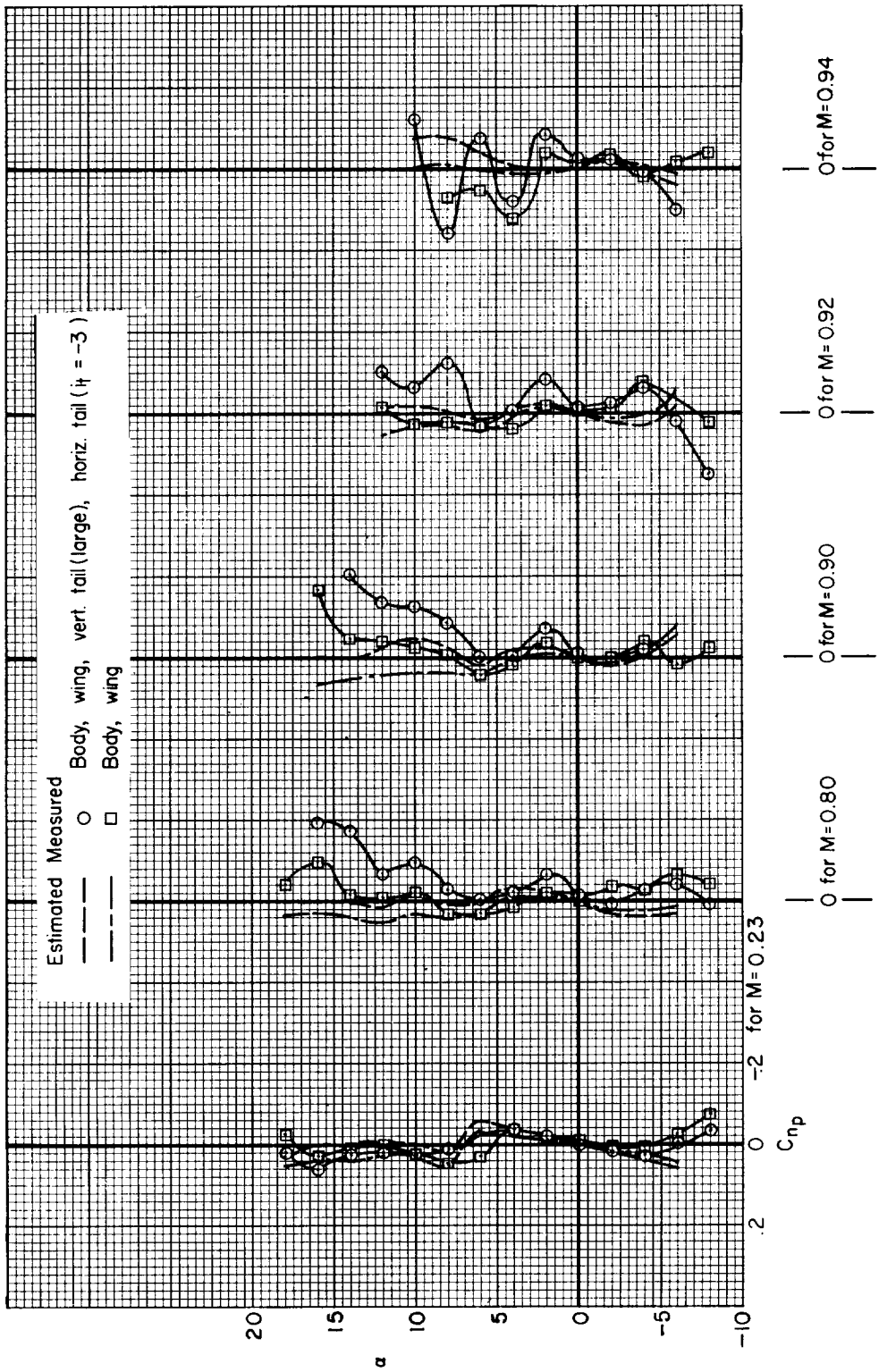

(b) C_{n_p}

Figure 18.- Continued.

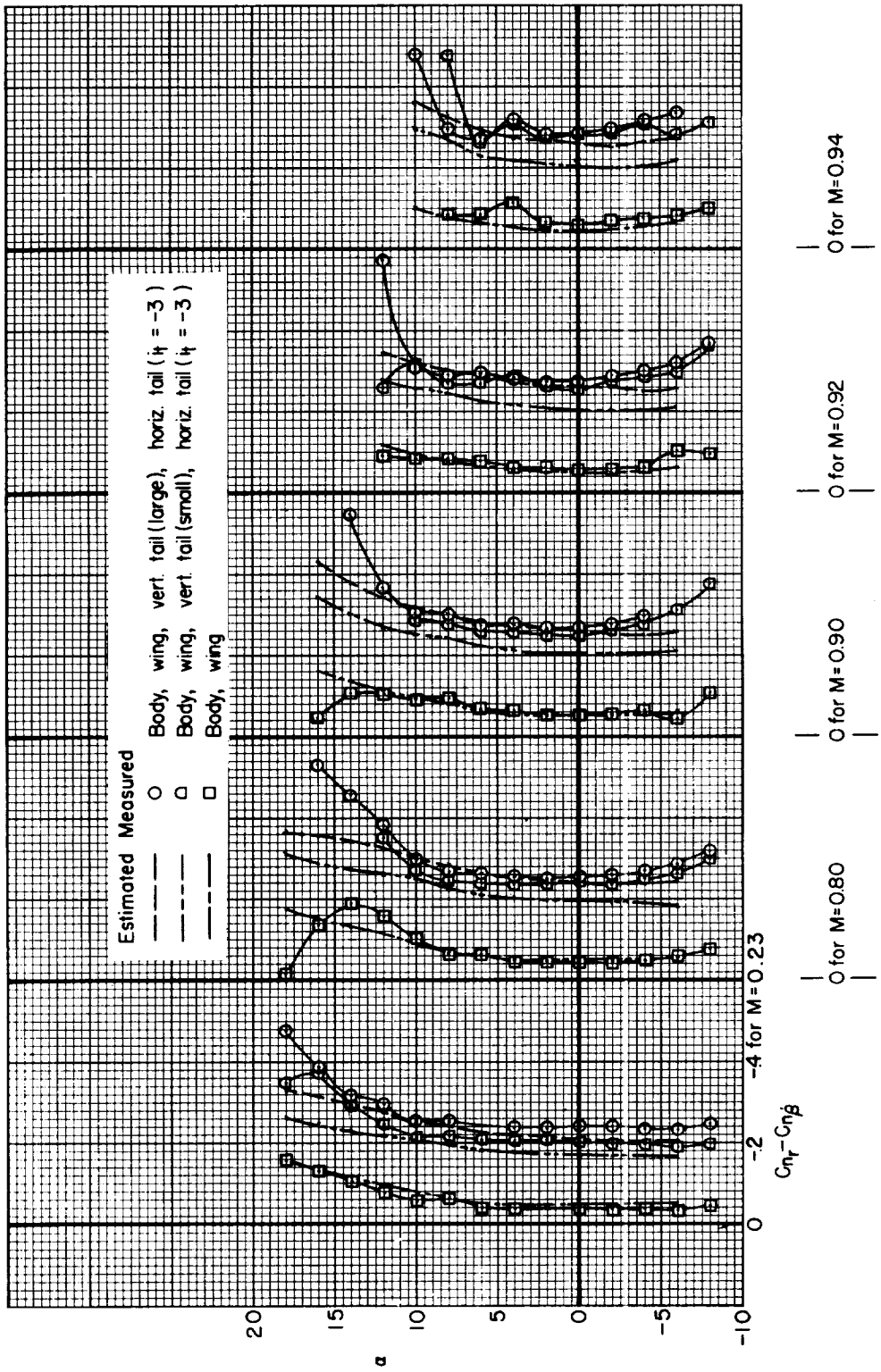

(c) $C_{n_r} - C_{n_{\dot{\beta}}}$

Figure 18.- Concluded.

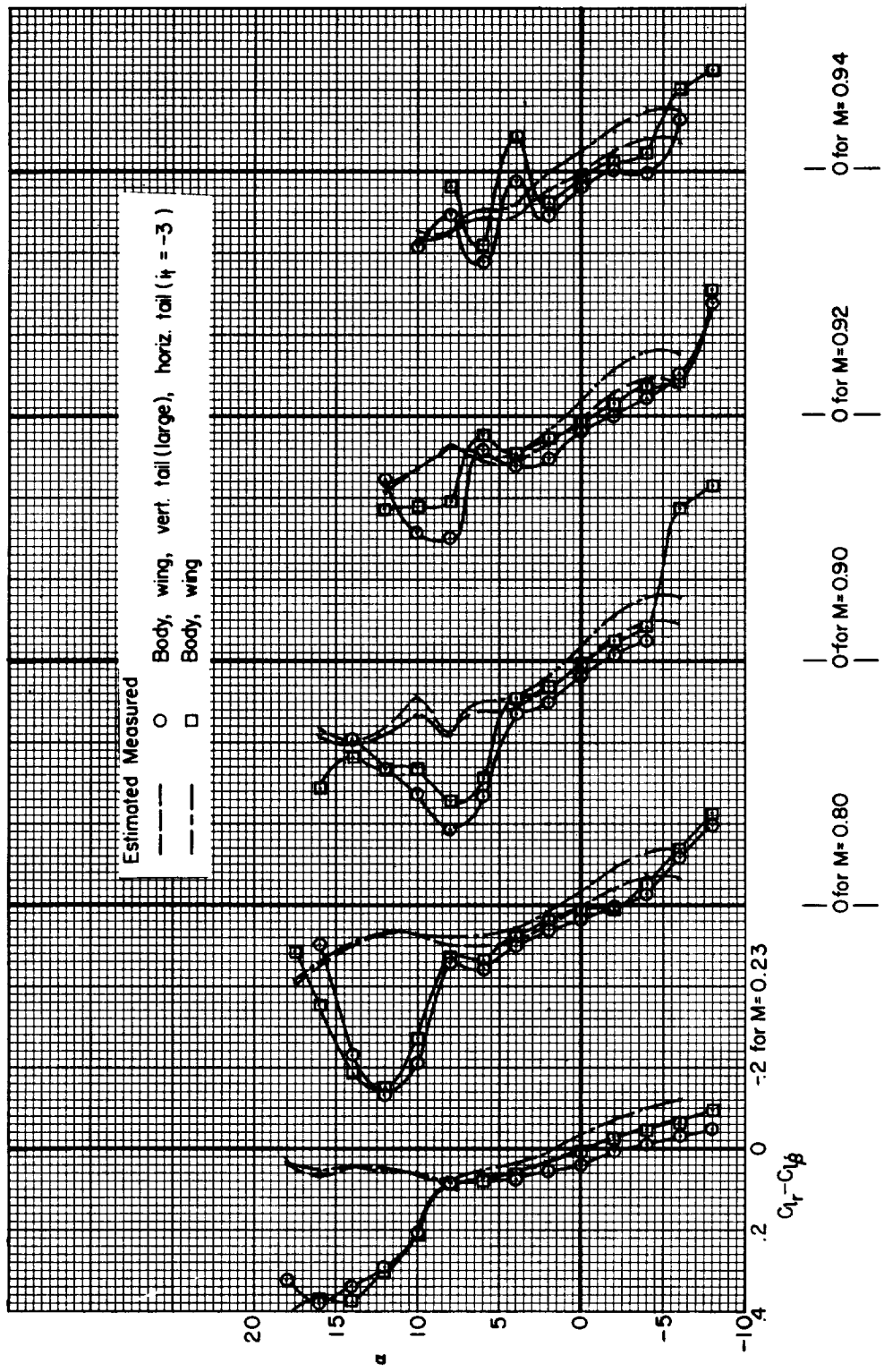

(d) $C_{l_r} - C_{l_{\dot{\beta}}}$

Figure 18.- Concluded.

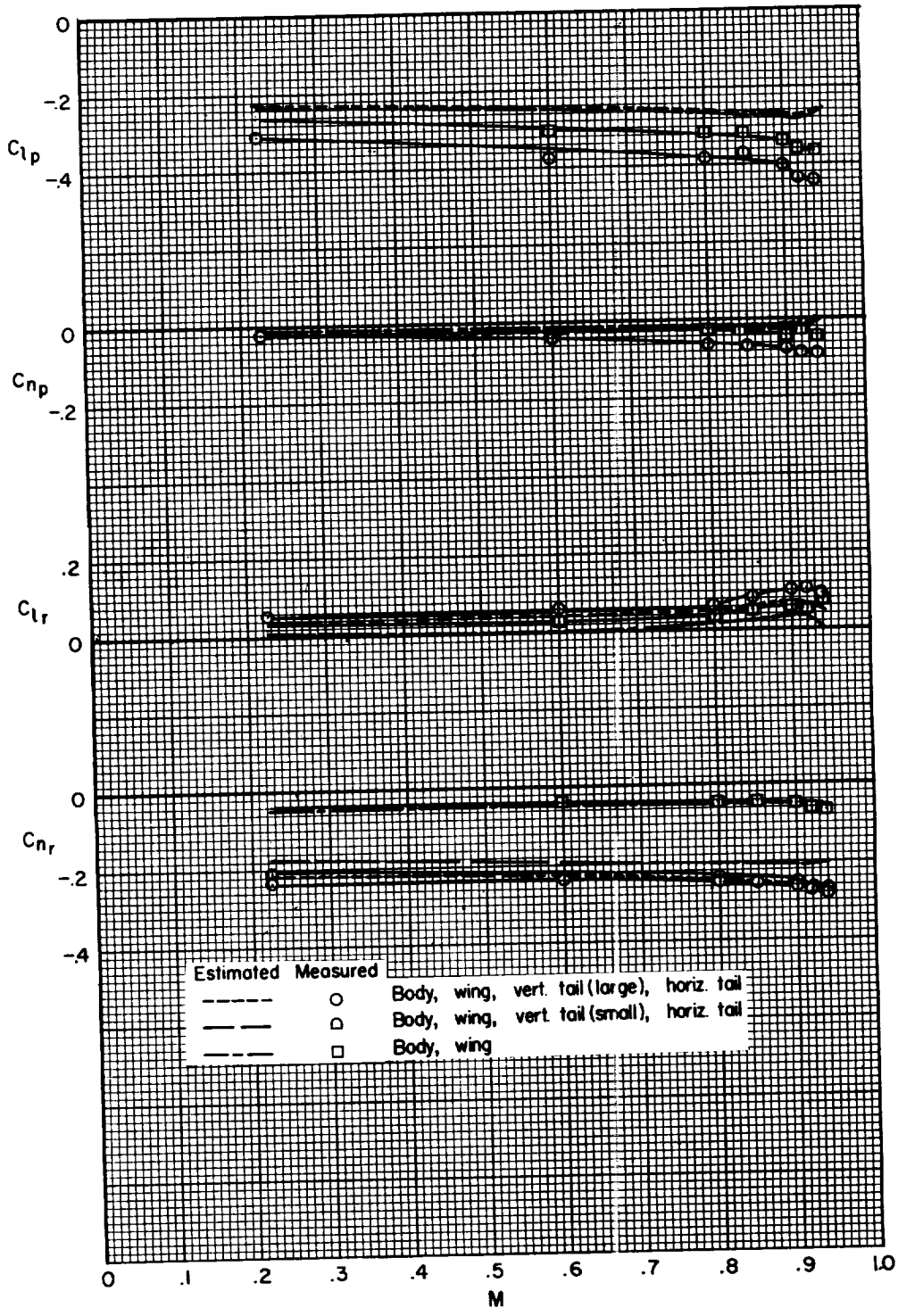

Figure 19.- Variation with Mach number of the lateral-directional dynamic stability derivatives; $\alpha = 2^{o}$.

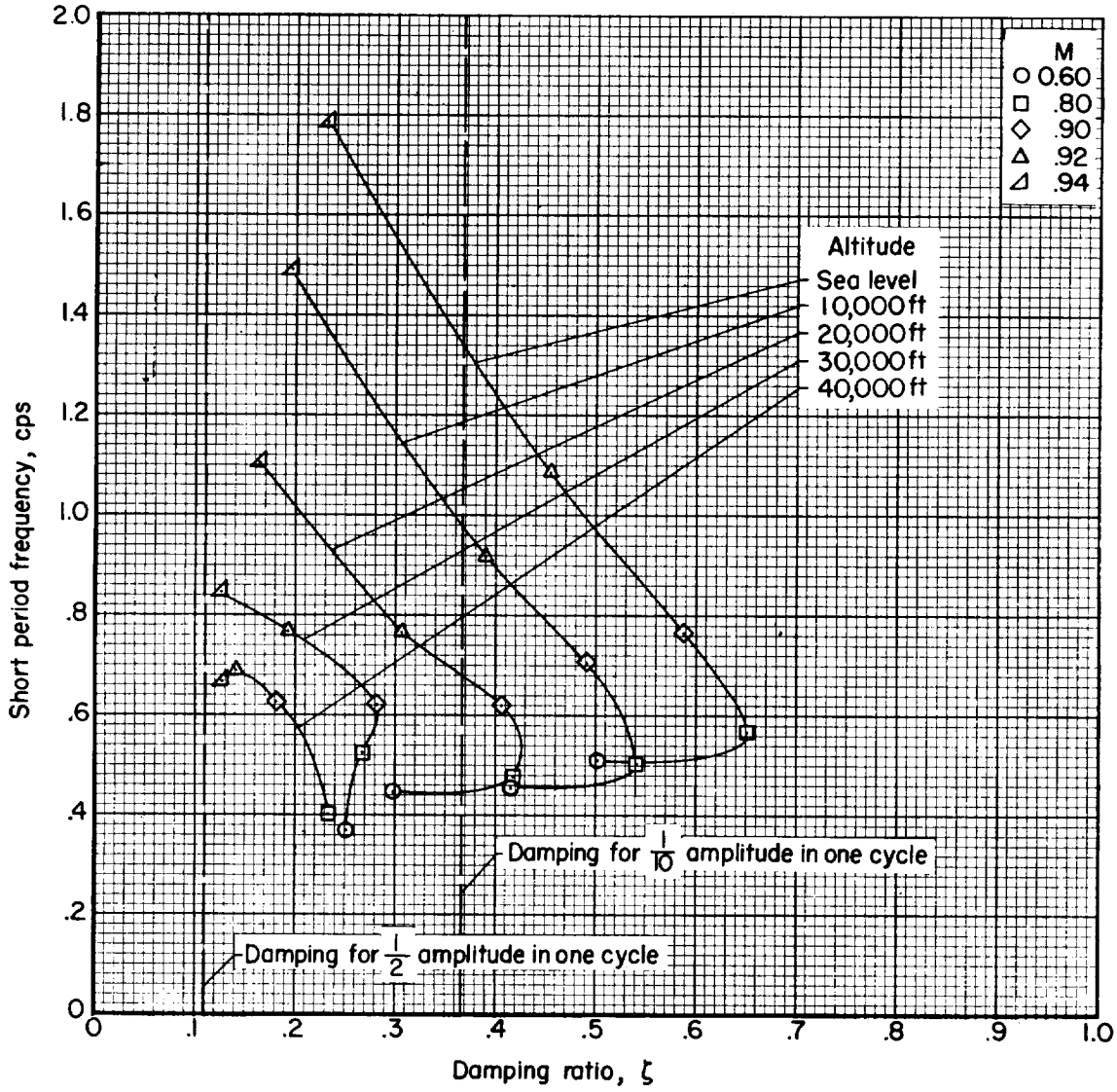

Figure 20.- Longitudinal dynamic stability characteristics of a representative airplane.

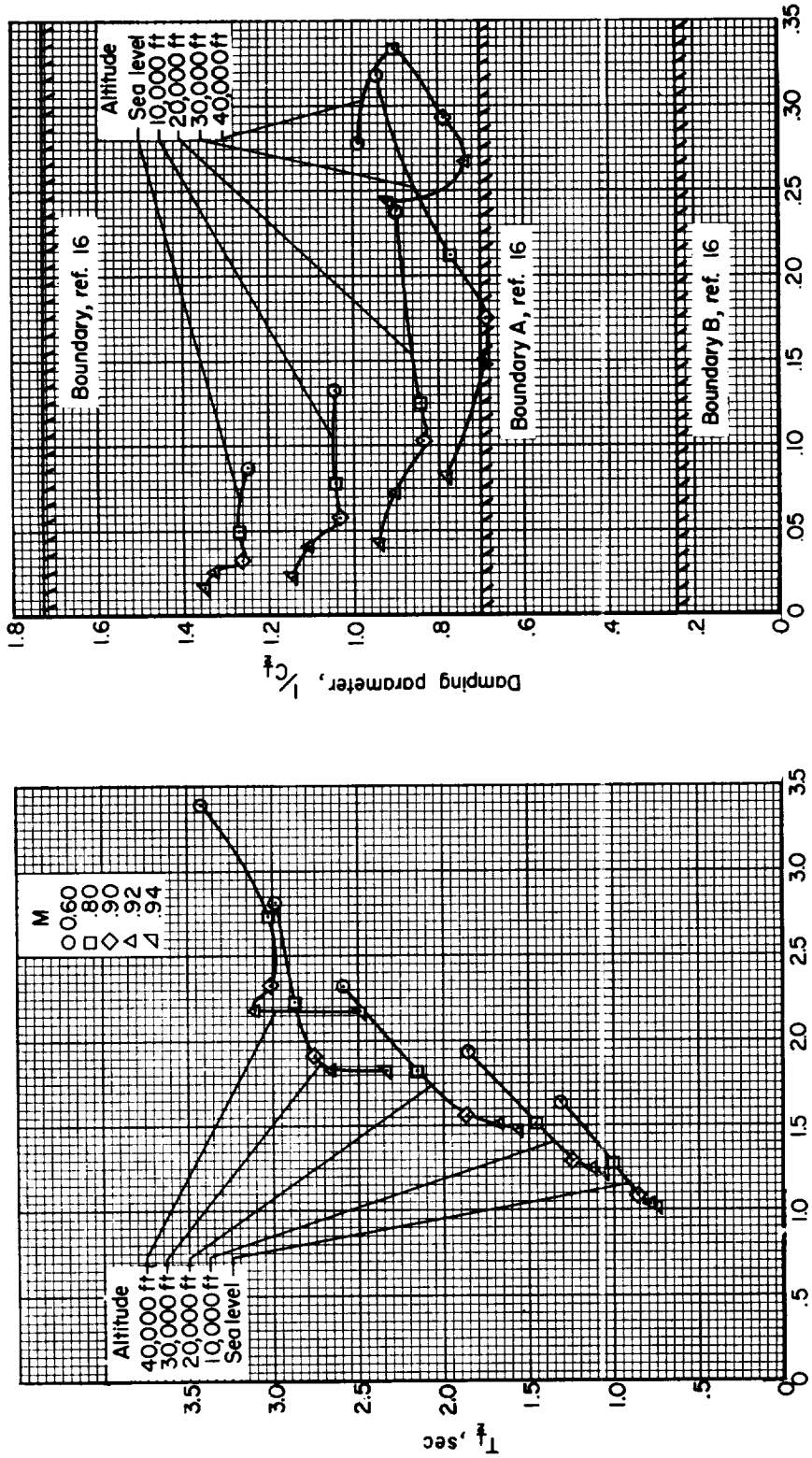

Figure 21.- Lateral-directional dynamic characteristics of a representative airplane.

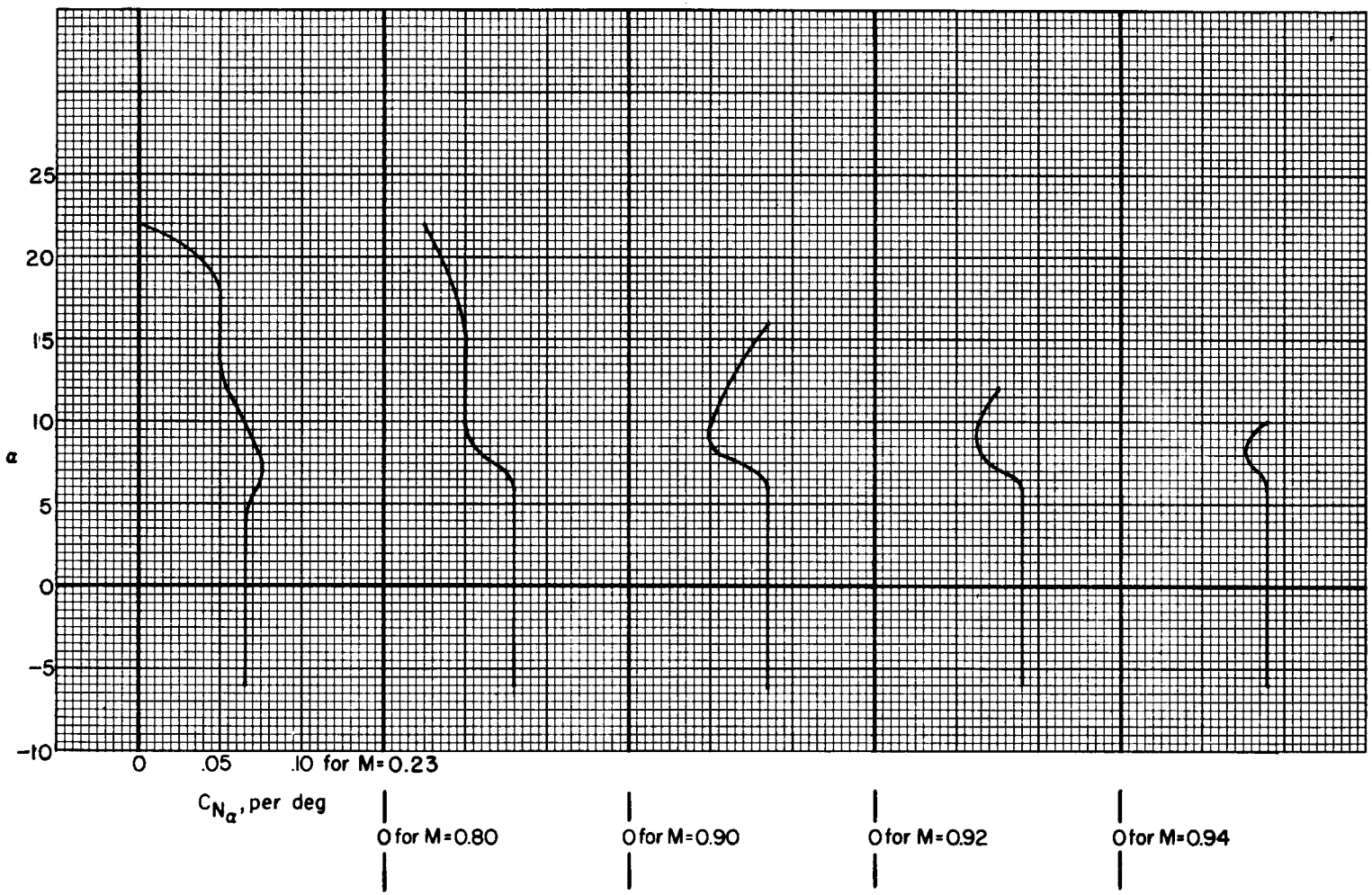

(a) C_{N_α} vs. α

Figure 22.- Static stability derivatives referred to the body system of axes.

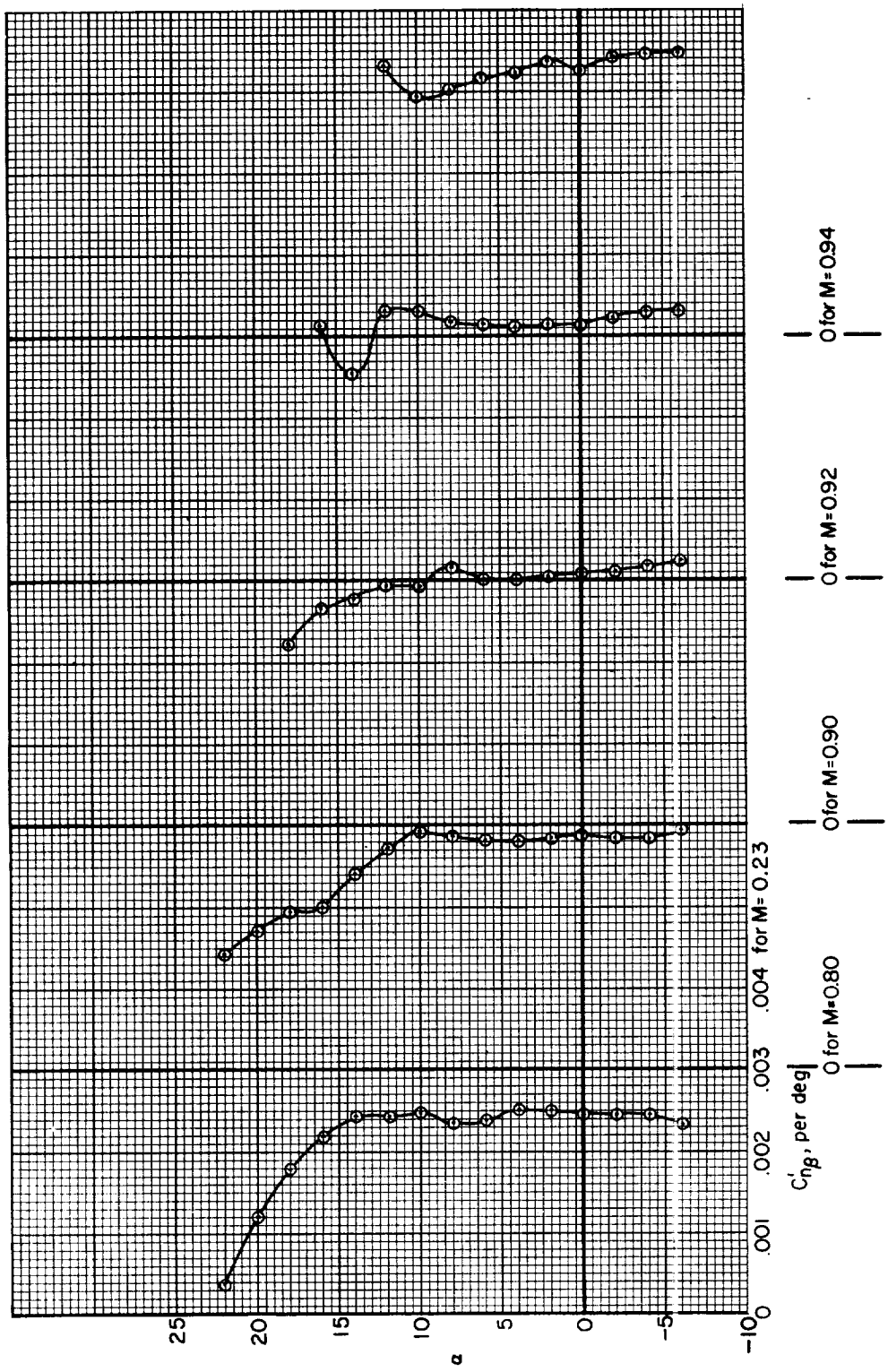

(b) C_{n_β}' vs. α

Figure 22.- Continued.

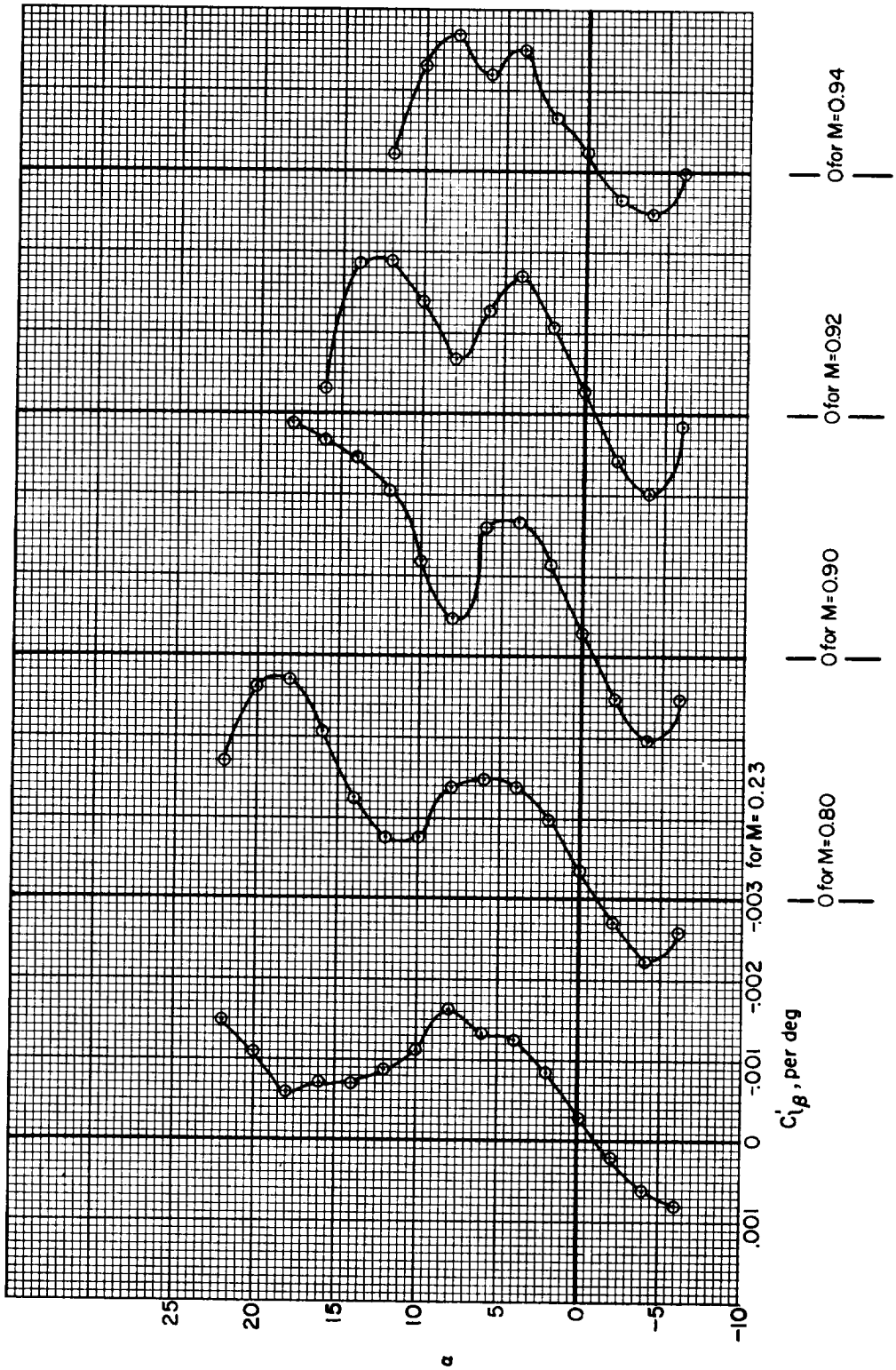

(c) C_{l_β}' vs. α

Figure 22.- Concluded.

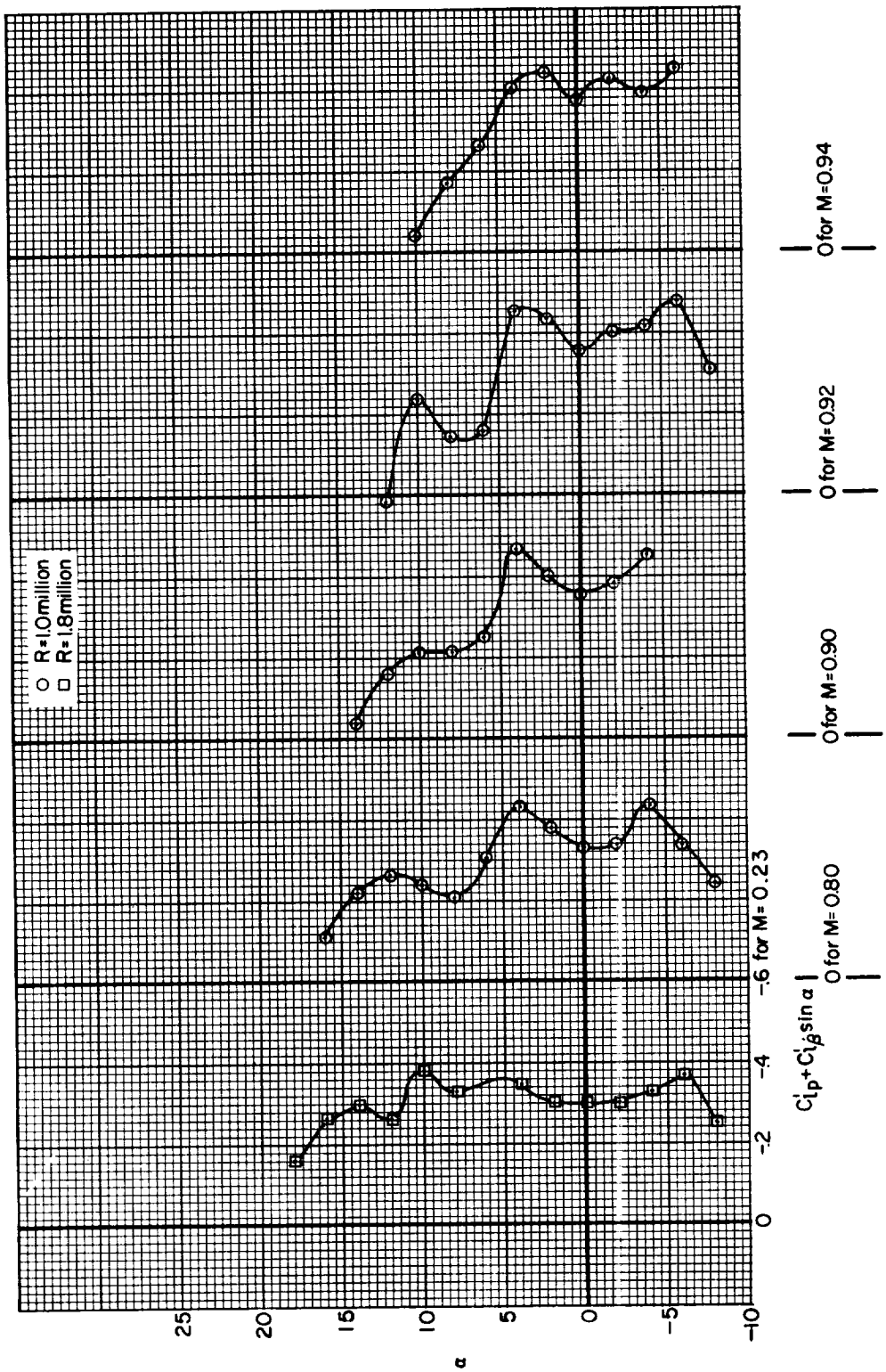

(a) $C_{l_p}' + C_{l_{\dot\beta}}'\sin\alpha$

Figure 23.- The dynamic stability derivatives referred to the body system of axes.

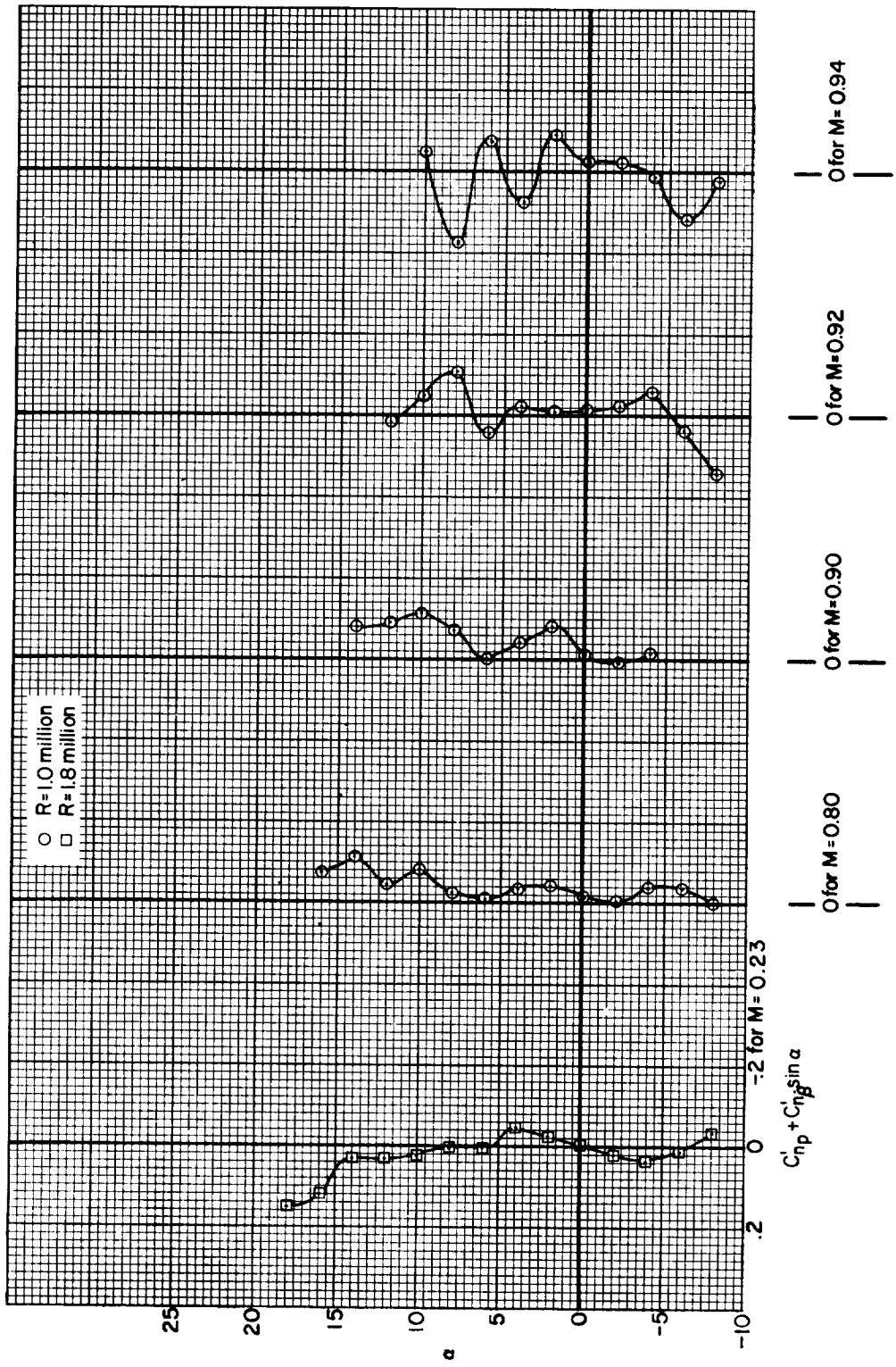

(b) $C_{n_p}' + C_{n_\beta}' \sin \alpha$

Figure 23.- Continued.

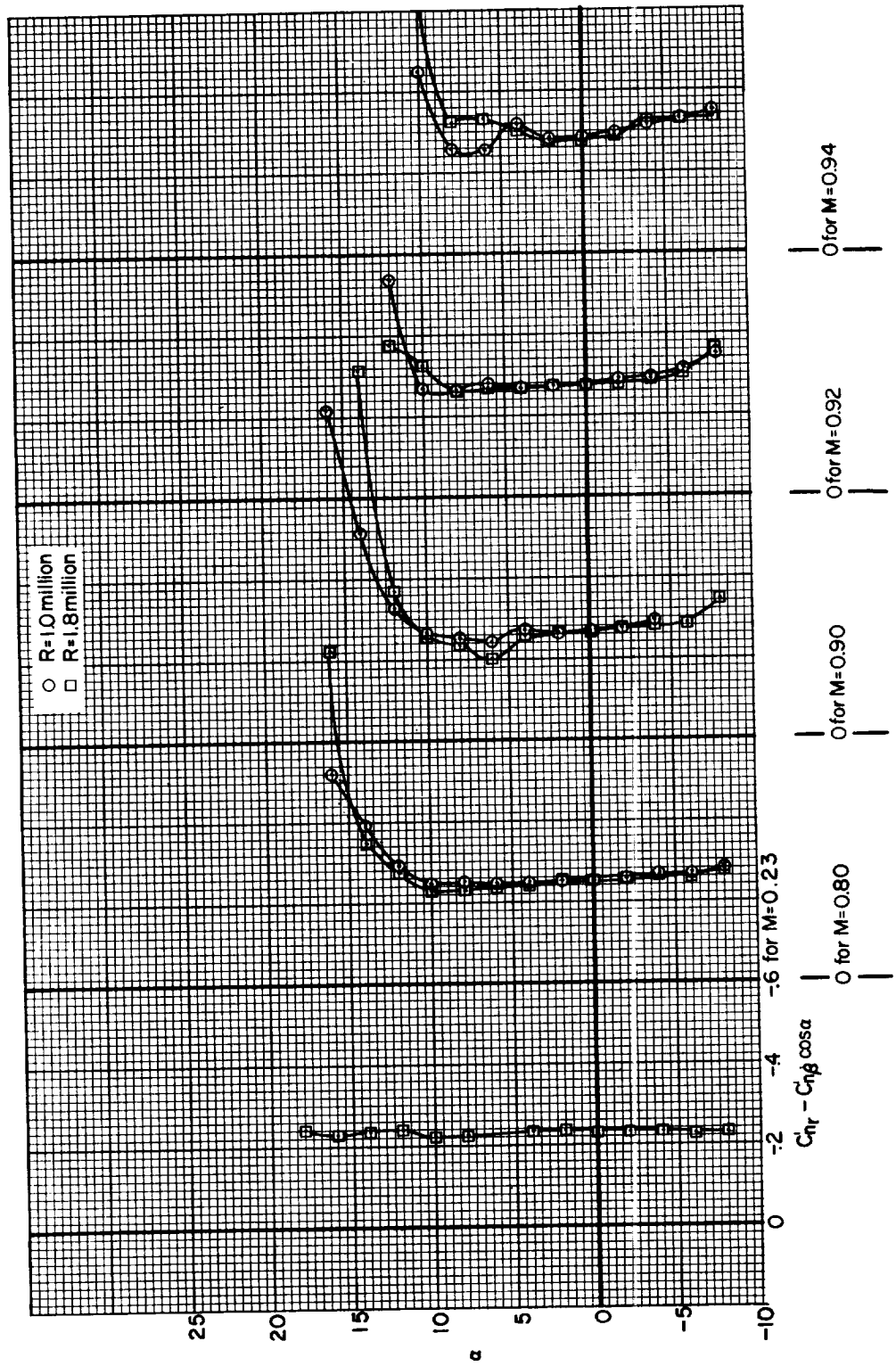

(c) $C_{n_r}' - C_{n_\beta}' \cos\alpha$

Figure 23.- Continued.

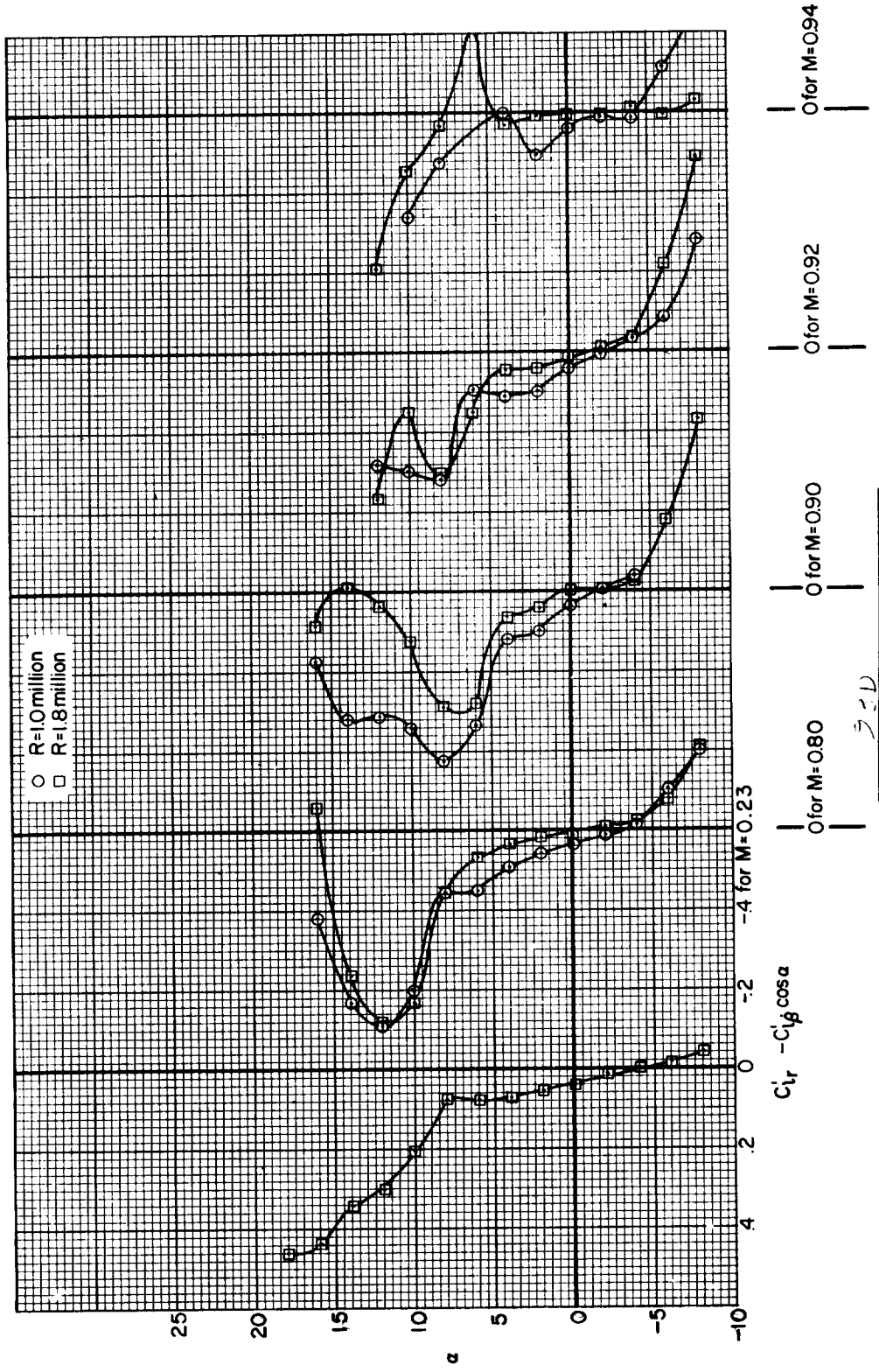

(d) $C_{l_r}' - C_{l_\beta}' \cos \alpha$

Figure 23.- Concluded.